



Reconstituted SNARE-mediated fusion: towards a mechanistic understanding

Dissertation
for the award of the degree
“Doctor of Philosophy” (Ph.D.)
division of Mathematics and Natural Sciences
of the Georg-August-Universität Göttingen

Submitted by
JAVIER MATIAS HERNANDEZ AMEZQUITA
from Antofagasta, Chile

Göttingen 2011



GEORG-AUGUST-UNIVERSITÄT
GÖTTINGEN



MAX-PLANCK-GESELLSCHAFT

GGNB

Göttingen Graduate School for Neurosciences and Molecular Biosciences

Committee members:

Prof. Dr. Reinhard Jahn (referee)

Abteilung Neurobiologie, Max-Planck-Institut für biophysikalische Chemie, Göttingen

Prof. Dr. Markus Wahl (referee)

AG Strukturbiochemie, Institut für Chemie und Biochemie, Freie Universität Berlin

Prof. Dr. Claudia Steinem

Institut für Organische und Biomolekulare Chemie, Georg-August-Universität, Göttingen

Date of the oral examination: 28 March, 2011

Herewith I declare, that I prepared the PhD dissertation entitled
“Reconstituted SNARE-mediated fusion: towards a mechanistic
understanding” on my own and with no other sources and aids than quoted.

Göttingen, February 27, 2011

Acknowledgments

My thanks go to Professor Reinhard Jahn, to whom I am thankful and honored for accepting me in the first place, but I am even more grateful for all these years of mentoring, advice and support.

I am very grateful to Alexander Stein, who was mainly responsible for taking me as a Polymer Chemist and training me to become something closer to a Biochemist. I am not sure if I have succeeded by his standards, but as for me I think I have and I will remain indebted for his generosity and knowledge.

I would like to thank my thesis committee, Professor Markus Wahl and Professor Claudia Steinem, for advice and feedback. I am grateful to the staff of the department of Neurobiology, especially to Gottfried Mieskes for his support for all lab-related matters, and to Barbara Schillings for administrative support, with them I would have been very lost. I am hugely indebted to Ursel Ries for excellent technical support. My thanks go to my collaborators Dietmar Riedel, Anna Cypionka, Elmar Behrmann, Stefan Raunser and Yong-Soo Park, thank you all.

I would like say thanks for all those who I had the opportunity to discuss scientific matters, these included: Professor Erwin Neher, Professor Grubmüller, Dirk Fasshauer, Geert van den Bogaart, Jelger Risselada, Wensi Gao, Esra Demircioglu, Nickias Kienle, Sina Barysch, Ioanna Bethanni, Julia Preobraschenski, Ulf Geumann, Pawel Burkhardt, Nathan Pavlos, and Halenur Yavuz. I apologize if I have missed anyone.

I would like to thank all my colleagues and friends whom I have had the privilege to share a space and time during the last four years here in Germany. You know who you are, I thank you from the very bottom of my heart.

I would like to say a special thank you to Tatyana, for her love and support.

Finally, but not least, I am most grateful to my family, which has a special meaning when a big ocean is in between. To my parents, muchas gracias por todo, por el apoyo y el cariño brindado, los echo mucho de menos. I also wish the best of luck to my sister Fernanda and my brother Ignacio, as they will be expanding their families quite soon. To them and their families, gracias!

The very last people I would like to say thanks are to my grandparents, whom unfortunately are not here anymore, and to them I would like to dedicate this work.

I would like to acknowledge the National Commission for Scientific and Technological Research (CONICYT) of Chile for financial support.

Agradezco el apoyo financiero de la Comisión Nacional para Investigación Científica y Tecnológica (CONICYT), Chile.



Table of Contents

1	Introduction	1
1.1	Basic concepts in membrane fusion and motivation.....	1
1.2	Mechanics of membrane fusion	4
1.2.1	Thermodynamic barriers and models of membrane fusion	4
1.2.2	Supporting evidence for the stalk mechanism.....	8
1.3	Biological vesicle membrane fusion.....	9
1.3.1	Brief historical overview of the role of SNAREs in membrane fusion	10
1.3.2	Biophysical and structural properties of SNARE complexes and their relation to vesicle fusion	12
1.3.3	Intermediates in the assembly pathway of SNAREs	17
1.3.4	Intermediates in SNARE-mediated fusion.....	25
1.4	Reconstitution of SNARE-mediated fusion in liposomes	27
1.4.1	Criteria for fusion.....	28
1.4.2	SNARE-mediated fusion of liposomes	28
1.5	Aims of the study	33
2	Experimental Methods.....	35
2.1	Materials and reagents	35
2.2	Cloning and purification	35
2.2.1	Molecular cloning and constructs.....	35
2.2.2	Expression and purification of SNAREs.....	37
2.2.3	Assembly of SNARE binary complexes.....	40
2.3	Preparation and characterization tools of SNARE-liposomes.....	41
2.3.1	Preparation of liposomes and reconstitution of SNAREs	41
2.3.2	Reconstitution of SNAREs in small liposomes	44
2.3.3	Liposome co-flotation on a density gradient for insertion assessment....	44
2.3.4	Orientation assessment by proteolytic digestion	45
2.3.5	Phosphate determination.....	45
2.4	Fluorescence and light scattering-based methods	45
2.4.1	Fluorescence dequenching for lipid-mixing measurements.....	45
2.4.2	Fluorescence anisotropy for binding and displacement experiments.....	47
2.4.3	Single-particle fluorescence cross-correlation spectroscopy.....	48
2.4.4	Size distribution analysis by FFF-MALLS.....	49
2.5	Other methods	52
2.5.1	SDS-PAGE and Coomassie blue staining	52
2.5.2	Western blot analysis.....	53
2.5.3	Cryo electron microscopy	53
3	Results.....	55
3.1	Characterization and optimization of the reconstitution of SNAREs into large liposomes.....	55
3.1.1	General considerations for detergent-mediated reconstitution	55
3.1.2	Strategy for SNARE reconstitution into large liposomes	58
3.1.3	Orientation and insertion efficiency of reconstituted SNAREs.....	59
3.1.4	Characterization of size distributions of SNARE-liposomes	61
3.1.5	OG removal and phospholipid loss	64
3.2	Biochemical parameters affecting fusion-related properties of large SNARE-liposomes	65
3.2.1	Variations of the Q-SNARE acceptor complex	66

3.2.2	Kinetic influence of ΔN synaptobrevin displacement from stabilized Q-SNARE complexes	71
3.3	Visualization and analysis of putative products and intermediates in the SNARE-mediated fusion pathway.....	76
3.3.1	Ultrastructural identification of docked and hemifused liposomes	77
3.3.2	Hemifusion as an alternative outcome to fusion.....	80
3.3.3	Arrest at the bilayer-bilayer contact stage.....	83
4	Discussion	90
4.1	Reconstitution properties of large SNARE-liposomes	90
4.2	Fusogenic properties of large SNARE-liposomes.....	92
4.3	Bilayer-bilayer contact as an on-pathway intermediate mediated by a partially assembled SNARE complex	97
4.4	Extended hemifusion as a sidetracked off-pathway state.....	100
4.5	Towards a mechanistic understanding of SNARE-mediated fusion	103
5	Conclusion	107
6	Appendix.....	109
7	References	111

Abbreviations

CH	Cholesterol
CMC	Critical micelle concentration
EM	Electron microscopy
FCCS	Fluorescence cross-correlation spectroscopy
FFF	Field flow fractionation
FRET	Förster resonance energy transfer
IMI	Inverted micellar intermediate
l/p	lipid/protein ratio
MALLS	Multi angle laser light scattering
NBD	Nitrobenzoxadiazole
NEM	N-ethylmaleimide
NSF	N-ethylmaleimide-sensitive factor
OG	<i>n</i> -octyl- β -D-glucoside
PC	Phosphatidylcholine
PCR	Polymerase chain reaction
PE	Phosphatidylethanolamine
PS	Phosphatidylserine
RHO	Rhodamine
RRP	Readily releasable pool
SDS-PAGE	Sodium dodecyl sulfate polyacrylamide gel electrophoresis
SN25	SNAP-25
syb	Synaptobrevin
syxFL	Full length syntaxin
syxH3	H3 domain of syntaxin
TMD	Transmembrane domain

Within a cell, membrane fusion constitutes the final step in secretion and cargo transfer between cellular compartments, and is therefore an essential process in cellular trafficking [1, 2]. It is also a means of entry of enveloped viruses and is vital for cell-cell fusion [3, 4]. Biological membrane fusion requires not only energy to overcome the barrier for fusion but also factors that provide spatial and temporal control. Based only on these considerations, it is evident that cells must have evolved intricate mechanisms to provide energy and regulation to the fusion process. Indeed, a few different types of membrane fusion machineries, including their regulatory factors, have evolved and are broadly conserved throughout different species and pathways (figure 1.2).

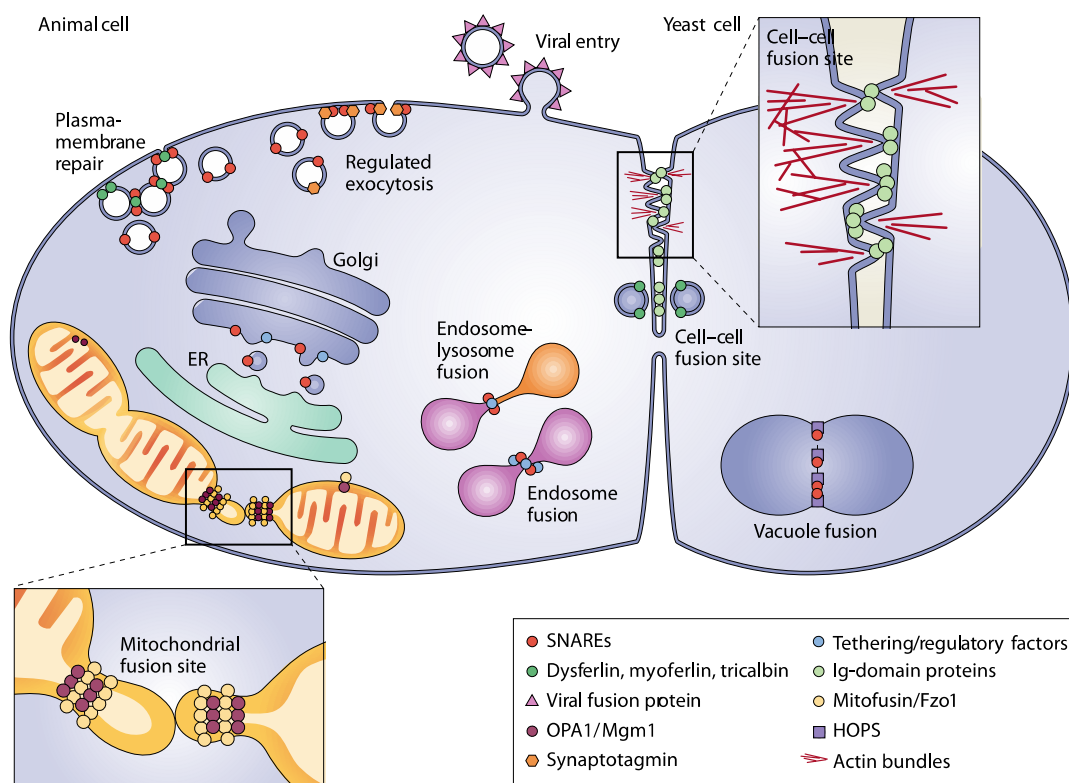


Figure 1.2: The diverse types of membrane fusion reactions in a cell. The SNARE family is responsible for mediating fusion in a number of intracellular and secretory trafficking pathways, including regulated exocytosis (reviewed in [5]), retrograde and anterograde transport in the endoplasmic reticulum (ER) - Golgi pathway (reviewed in [6]), and various fusion reactions in the endosome and lysosome pathways (reviewed in [7]). In yeast, homotypic fusion of vacuoles is mediated by SNAREs and regulated by the HOPS complex (reviewed in [8]). Enveloped viruses have developed three distinct classes of fusion proteins to enter cells or fuse with cellular organelles (reviewed in [4]), whereas cell-cell fusion utilizes a plethora of immunoglobulin (Ig)-like domain proteins and the actin cytoskeleton (reviewed in [9]). Other specific forms of fusion occur in the repair of the plasma membrane (reviewed in [10]) and fusion between mitochondria (reviewed in [11]). Figure taken from [3].

This thesis explores mechanistic aspects of soluble N-ethylmaleimide-sensitive factor attachment protein receptors, or SNAREs, a family of proteins for which a wealth of evidence suggests is the main component of the membrane fusion machinery in cells. A hallmark in the study of how SNAREs work was the successful reconstitution of SNAREs into artificial lipid vesicles, or liposomes, and the employment of assays to show that SNAREs are able to fuse liposomes unaided [12]. Since then, the reconstitution of purified or recombinant SNAREs onto liposomes has become a widely applied approach to investigate not only SNARE function but also the effect of SNARE-interacting proteins on fusion.

An important motivation for this work has been to develop *de novo* a variation of the now classical reconstitution approach. This required initially some basic characterization on the reconstitution of SNAREs onto liposomes, including gaining insights into the mechanism of their insertion. However, an area where considerable effort has been made is in the use of tools or combinations of tools that are not traditionally used in the study of SNARE-mediated fusion. This has been accompanied in some cases with different ways of treating and mechanistically interpreting data obtained from traditional assays, and the result is that the focus of the analysis is not only on SNAREs but also on the liposomes.

This thesis is structured into 7 chapters. In chapter 1 an overview is provided of membrane fusion of artificial model membranes, followed by biological SNARE-mediated fusion and studies involving reconstitution into liposomes. In chapter 2 the methods and experimental techniques used in this work are described, and the main experimental results are presented in chapter 3 with supporting information found in the appendix (chapter 6). The findings of the study are then discussed in chapter 4 within the context of the literature and issues that are currently being debated in the field with the main conclusions described in chapter 5. Finally, all references are compiled in chapter 7.

1.2 Mechanics of membrane fusion

1.2.1 Thermodynamic barriers and models of membrane fusion

The first step for membrane fusion is the bringing together of two lipid bilayers. As membranes approach each other, electrostatic repulsive and attractive forces originating from the membrane surface facilitate or impede their contact, the final result depending on the net effect of these forces and on the energy available to overcome them in the case of stronger repulsive forces. Figure 1.3 illustrates a potential energy landscape as a function of the surface separation of two charged lipid bilayers (dashed line), depicting a reaction coordinate where two energetic barriers must be overcome to bring the membranes together. When bilayers become $\sim 2\text{-}3$ nm apart, a much stronger barrier is encountered consisting of a layer of water molecules which are aligned at the membrane surface (figure 1.3, right). The structuring of water and the hydration forces that mediate it are the final obstacle to allowing the lipid bilayers to establish contact [13].

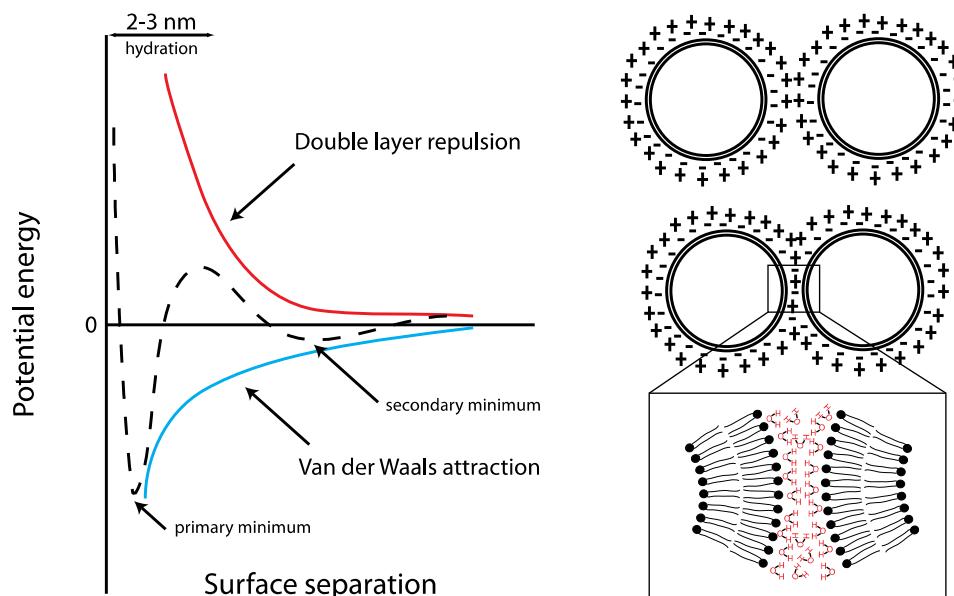


Figure 1.3: Forces experienced by charged lipid bilayers as they are brought into closer contact. Left: potential energy as a function of separation between two charged lipid bilayers depicting repulsion (red) and attractive forces (blue), the sum of which constitute the reaction energy coordinate (dashed line) Right: schematic visualization of barriers for close membrane apposition of two liposomes. Charged phospholipids attract counter ions forming a double ionic layer. As membranes approach and become 2-3 nm of each other, hydration forces dominate electrostatic ones. The structured layer of water molecules aligned at the membrane surface is the last barrier for membrane contact to occur.

Different types of agents are able to mediate fusion of artificial model membranes by overcoming electrostatic and hydration forces. A prime example are divalent cations, most notably Ca^{2+} , which is thought to mediate an anhydrous trans interaction between opposing membranes via a specific interaction with the head group of phosphatidylserine (PS), an acidic phospholipid [14-16]. Polyethylene glycol (PEG) has also been proposed to mediate membrane bilayer fusion of liposomes by dehydrating the inter-bilayer water layer [17].

Although these agents are able to bring two membranes into direct apposition, molecular contact between them is not necessarily sufficient for membrane fusion. This is clearly observed in the case of multivalent cations and DNA-induced aggregation of zwitterionic liposomes, where a tight bilayer-bilayer contact interaction constitutes a stable and final state [18]. Thus, further steps, each with its own energetic barrier, are probably required beyond simple membrane contact in order to fuse membranes. Indeed, in addition to their ability to bring bilayers together, the capacity for both PEG and Ca^{2+} to induce fusion is dependent on membrane curvature, acyl chain unsaturation and temperature, indicating that contact-induced changes to membrane physical properties are needed to mediate fusion [16, 19, 20].

Attempts to understand the molecular mechanism of membrane fusion (i.e. once bilayers have established contact) have been mainly focused on the elucidation and identification of intermediate and transitory states. This has been achieved more notably on two fronts: a theoretical approach based on the principle that membrane fusion proceeds through the lowest possible energy intermediates; and a visual approach, where fusion processes are captured by rapid-freezing and analyzed by electron microscopy for identification of possible intermediate structures. Advances in video recording and optical microscopy have extended this search by allowing the possibility to monitor fusion in real-time without the need to arrest the system, although these approaches are limited by low resolution [21-23] (figure 1.4).

The first studies on fusion intermediates came from freeze-fracture electron microscopy studies, where the observation of “lipid-particles”, small point-like irregularities observed on the membrane surface, were considered to be lipids in inverted hexagonal phases (figure 1.4). These particles were observed during temperature-induced phase transitions, and were further postulated to be prime sites for fusion because of the correlation that liposomes fused near or above the transition temperature [24]. The idea that transformations of lipid phases, in particular hexagonal or inverted micellar phases, constitute intermediary structures in membrane fusion was given considerable theoretical attention by Siegel, who significantly contributed to the development of the inverted micellar intermediate mechanism, or IMI, as it was commonly referred to [25].



Figure 1.4: Experimental attempts at observing membrane fusion intermediates. Top: freeze-fracture electrograph of phosphatidylcholine/phosphatidylethanolamine (PC/PE) liposomes depicting lipid-particles believed to be inverted hexagonal or micellar lipid structures. These protrusions were believed to consist of contact points between fusing bilayers. Fusion was induced by cycles of freezing and thawing. Scale bar: 100 nm. Taken from [26]. Bottom: a frame sequence showing a membrane fusion event between two giant liposomes observed by dark-field microscopy. A melittin concentration gradient was used to induce fusion and liposomes were made from phosphatidylcholine (PC) and phosphatidylglycerol (PG). Scale bar: 5 μm . Taken from [23].

An alternative proposition to IMI theory was developed in parallel by Kozlov and coworkers [27]. By treating membrane monolayers as elastic continuous structures, the model proposes that fusion is initiated by formation of a continuous hourglass-shaped lipid connection between the proximal monolayers of apposed bilayers (figure 1.5). This structure, called a

stalk, is highly symmetric and adopts a bent semi-toroidal shape that expands radially, causing the distal monolayers to establish contact and form a single bilayer separating the aqueous compartments. This state, termed hemifusion because it involves the mixing of outer but not inner leaflet lipids, leads to fusion if the single bilayer ruptures by lateral tension or a structural defect induces the opening of a pore. Alternatively, a pore may open immediately after stalk formation, bypassing the need for an expanded hemifusion diaphragm. Whichever the pathway to pore opening, expansion of the pore completes fusion of both bilayers.

The original stalk mechanism has been further developed by taking into account more specific molecular processes which have lowered the calculation of the free energy of the proposed intermediates, thus making it more plausible that membrane fusion proceeds via this mechanism. This has included taking into account the interstice energy arising from hydrophobic voids present between bent monolayers [28]. Bending and contact of distal monolayers after stalk formation, as well as tilt and splay of hydrocarbon tails, all minimize the cost of formation of voids, resulting in hypothetical fusion intermediates with activation energies which permit more relevant time-scales for biological fusion [29]. Over the years, the modified stalk mechanism of fusion has amply succeeded IMI theory.

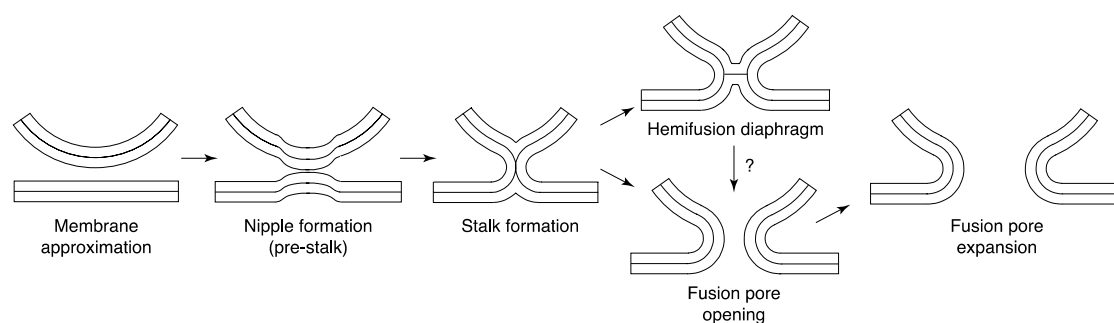


Figure 1.5: The stalk mechanism of membrane fusion. Formation of a stalk is promoted by nipple formation and bending of outer monolayer leaflets. Two pathways for fusion pore opening leading to pore expansion are possible. See text for more details. Modified from [30].

1.2.2 Supporting evidence for the stalk mechanism

Support for the stalk mechanism of membrane fusion is rather scattered and no single study has managed to provide a detailed account depicting its proposed intermediate structures. However, different types of studies have provided insights that are consistent with some of its main features. Many coarse grain and molecular dynamics simulations predict the formation of stalk-like structures as the first transmembrane bridging event for initiation of fusion, although they are not always as symmetrical as commonly conceived [31-33]. The only direct experimental observation of the stalk structure has been reported with x-ray diffraction which was achieved by externally controlling the dehydration state of the inter-bilayer spacing of PC membranes [34]. Another important hallmark of the stalk mechanism is that fusion proceeds via a transient hemifusion state. Here a number of different fusion systems appear to be consistent with hemifusion occurring in model membranes, although it is not always clear if they represent genuine intermediates in the fusion pathway or represent alternative end states [22, 35-40].

Since the stalk theory emphasizes elastic properties of membranes to be crucial for membrane fusion, one way of testing the mechanism is by evaluating the effect of lipids on fusion. Elasticity in this sense refers to the tendency for a lipid within a monolayer to adopt a particular orientation with respect to a flat plane i.e. the curvature of the monolayer surface. This in turn depends on the overall molecular shape of the lipid. Deviations from the spontaneous curvature of the monolayer will raise the energy of the system in a way that is analogous to a spring or elastic which has a natural resting position. The energy (F_{bend}) required for bending of a lipid monolayer to a certain curvature J which has a spontaneous curvature J_s is approximated by the expression [41]:

$$F_{\text{bend}} = \frac{1}{2} A \cdot \kappa \cdot (J - J_s)^2 \quad \text{eq. 1.1}$$

where A is the monolayer surface area and κ the bending modulus (the expression omits the Gaussian curvature contribution to the elastic bending energy [42]).

This expression predicts that lipids with molecular shapes that fit and stabilize the curvature of bent intermediate structures will greatly facilitate their formation (see figure 1.1 in section 1.1), whereas lipids with shapes that deviate from the required geometry will increase the bending energy according to a square power relation. It has been observed that lipids that facilitate monolayer bending favorable for stalk formation enhance hemifusion (i.e. lipids with intrinsic negative curvature such as PE or arachidonic acid), while lipids that make outward bending more difficult inhibit it (lipids with positive intrinsic curvature such as lysophosphatidylcholine, or LPC) [43-46]. Conversely, formation of a fusion pore originating from a hemifusion diaphragm, which requires bending opposite to that needed for stalks, is promoted by lipids such as LPC and inhibited by arachidonic acid [46-48], as predicted by the stalk hypothesis.

Despite the wide application of the stalk mechanism for rationalizing fusion of model and, as will be discussed later, biological membranes, it is important to reiterate that supporting evidence remains largely indirect. This is highlighted by the fact that alternative models have been proposed which are supported by similar criteria that are also consistent with the stalk mechanism. For instance, a mechanism has been observed by Monte Carlo simulation where stalks are formed, but in contrast to the classic stalk mechanism, it does not expand but rather deforms the membrane producing an adjacent hole, bypassing any form of a hemifused state [49].

1.3 Biological vesicle membrane fusion

The pioneering work of Palade and co-workers, based mainly on electron microscopy and cell fractionation procedures, was determining in the establishment of the vesicular transport hypothesis which proposed cellular trafficking and secretory pathways are mediated by vesicles that act as

transport shuttles [50]. The basic principle is that cargo proteins are taken-up by a “budding” vesicle from a sub-cellular donor compartment. This vesicle is transported towards an acceptor compartment, where it docks and then fuses to its membrane, finalizing in cargo release [1].

Over the decades, the level of understanding of this process has gone from the description of the morphology of the organelles and vesicles to the elucidation of the underlying molecular machinery that mediates it. Since this work is focused on the understanding of membrane fusion, this section will begin with a brief overview of the development of the notion that SNAREs are the core molecular machinery of vesicular membrane fusion. This will be followed by an overview of the biophysical and structural properties of SNAREs, and then the assembly stages by which SNAREs are thought to mediate fusion, with a particular focus on neuronal SNAREs that are responsible for fusion of synaptic vesicles and release of neurotransmitters at the synapse. Finally, attempts at reconstituting membrane fusion with liposomes will be reviewed and current issues discussed, and the chapter will end by defining the aims of this study.

1.3.1 Brief historical overview of the role of SNAREs in membrane fusion

Rothman and co-workers provided the first evidence for a specific mammalian protein thought to play a key role in mediating protein trafficking. By using a novel cell-free assay which reproduced protein transport between Golgi stacks [51], N-ethylmaleimide, or NEM, was found to inhibit transport, and a NEM-sensitive factor, or NSF, was predicted to be an essential component of the transport machinery [52]. More direct proof that NSF played an essential role came from its subsequent purification and the observation that it could rescue transport in NEM-treated Golgi membranes [53]. Moreover, morphological evidence suggested that vesicle budding was not affected by NSF inhibition, indicating that NSF acted on a step related to vesicle fusion [54].

A soluble NSF attachment protein, or SNAP, and a membrane-associated receptor for SNAP were later found to be responsible for recruiting NSF to membranes [55, 56]. These three components assembled into a multi-subunit 20S particle that could be dissociated in an ATP-dependent manner and was proposed to constitute the basic fusion machinery of the cell [57]. Identification and purification of membrane SNAP receptors, or SNAREs, was accomplished by using an affinity purification strategy from detergent extracts of bovine brain. Surprising at the time, the SNAREs were identified as pre-synaptic plasma membrane proteins syntaxin (isoforms A and B) and SNAP-25 (synaptosome-associated protein of 25KDa), as well as vesicular membrane protein synaptobrevin [58], proteins which were already known to be implicated in regulated neuronal exocytosis and some of which were known targets of potent neurotoxins that block neurotransmission [59, 60]. Intriguingly, the three SNAREs could also associate with each other in the absence of NSF to form a smaller 7S particle, termed the SNARE complex [61].

Due to their unique location in the synapse, it was initially thought SNAREs could convey the needed specificity in membrane fusion and served as docking factors between membrane compartments. In reference to their likely biochemical pairing, the nomenclature of a vesicle SNARE, or v-SNARE, and a target SNARE, or t-SNARE, was adopted. Noting that, in addition to NSF and SNAP, neuronal syntaxins and synaptobrevin have yeast homologues differentially distributed in vacuoles, Golgi and the endoplasmic reticulum (ER), it was hypothesized that complementary pairing of SNAREs was a universal mechanism for imparting specificity to both regulated and constitutive vesicular membrane fusion. This proposal became known as the SNARE hypothesis [61].

Although the identification and purification of the basic components of what appeared to be a highly conserved fusion apparatus constituted a breakthrough in the understanding of vesicular membrane fusion, many questions remained unanswered with respect to the exact mechanistic role of NSF, SNAP and SNAREs in mediating membrane fusion. According to the

SNARE hypothesis, docking between a vesicle and its target membrane was mediated through an anti-parallel pairing between v and t-SNAREs. However, it was difficult to reconcile this with the findings that *Drosophila* syntaxin mutants and toxin-cleaved synaptobrevin in the giant squid synapse exhibited drastically impaired neurotransmitter release, while docking of vesicles at active zones remained mostly unaffected [62, 63]. Furthermore, the yeast homologues of NSF and SNAP, Sec18p and Sec17p, respectively, were shown to act on a step before docking and were not directly involved in fusion of vacuoles as observed *in vitro* [64].

Further insights on this question came from the direct visualization of SNARE complexes by deep-etch electron microscopy [65]. By tagging the N and C termini of SNAREs, synaptobrevin and syntaxin were observed to form a complex in a parallel orientation and not an anti-parallel configuration as was originally thought. Based on this key finding and taking into account that NSF could disassemble a SNARE complex residing on a single membrane [66], an alternative interpretation on the role of SNAREs was put forward.

In this new model, SNARE assembly was proposed to start *in trans* at the N terminus and “zipper” towards the C terminal direction, providing a molecular-coupled movement that can bring opposed membranes together. The energy released from the assembly process could be used to overcome the barrier for fusion. Once fusion is completed, NSF and SNAP would then disassemble the complex to recycle SNAREs for successive rounds of docking and fusion [65, 67, 68]. The more definitive proof that NSF and SNAP are not directly involved in mediating membrane fusion came from the finding that SNAREs can mediate fusion of liposomes and thus that they constitute the minimal machinery for membrane fusion [12].

1.3.2 Biophysical and structural properties of SNARE complexes and their relation to vesicle fusion

Several lines of evidence support a central role for SNAREs as the molecular engine of both constitutive and regulated membrane fusion, and are routinely referred to as the core or minimal membrane fusion

machinery [5]. The defining feature of SNAREs is their SNARE motifs, amphiphilic portions of 60-70 amino acids that associate with additional motifs to form a SNARE complex. SNARE motifs alone tend to be largely flexible and unstructured, but are highly helical once assembled into a complex [67]. A few SNAREs, such as SNAP-25, contain two SNARE motifs connected by a linker. In addition to SNARE motifs, most SNAREs (but not all) have transmembrane domains or contain post-translational modifications that serve as membrane anchors. They may also contain N-terminal domains that adopt a regulatory function by interacting with additional factors (reviewed in more detail in [5]). Figure 1.6 provides a comparative example of the diversity of SNARE domain topologies.

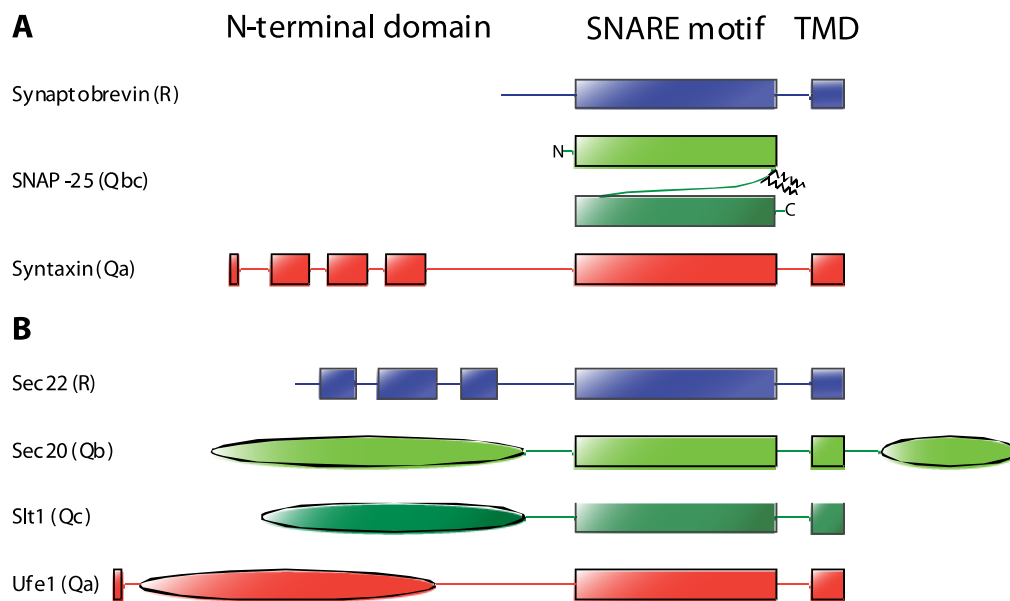


Figure 1.6: Domain structure of a complementary set of SNAREs involved in mammalian regulated neuronal exocytosis (A) and in constitutive retrograde Golgi-ER transport in yeast (B). Despite low sequence similarity and different domain topology, 4 sets of SNARE motifs are needed to form a SNARE complex. SNAP-25 contains two SNARE motifs connected by a linker that is palmitoylated and serve as membrane anchors (ziz-zag lines). Rectangular shapes depict domains for which supporting biochemical, structural and bioinformatics evidence is available, while elliptical shapes denote putative domain regions. Sec20 is a rare case of a possible domain residing in the luminal-orientated side of a membrane. The schematic depiction is approximately to scale. Compiled and adapted from [5, 69-72].

Complexes formed from recombinant neuronal SNAREs lacking transmembrane domains (in the case of synaptobrevin and syntaxin) and palmitoyl side chains (in the case of SNAP-25) are resistant to sodium dodecyl sulfate (SDS) and the proteolytic activity of clostridial neurotoxins, potent

inhibitors of neurosecretion that cleave individual SNAREs [73]. Furthermore, complexes have a high thermal stability, dissociating in the 70-90 °C range [67, 74], and have an even higher stability when transmembrane domains (TMDs) and their connecting linker domains are included [75]. The reason for such high chemical and thermodynamic stability is self-evident upon inspection of the structure [75, 76] (figure 1.7).

The soluble core complex consists of a parallel four-helix bundle held together through side-chains from each of the four helices interacting towards the interior core of the complex. In total, 15 hydrophobic layers contribute to the coil-coiled structure, with each layer forming in accordance to conserved primary-structure alignments. In addition, an ionic layer made up of one arginine (from synaptobrevin) and three glutamines (from syntaxin and one from each SNARE motif of SNAP-25) is located at the center buried inside the interior core of the complex. This central “0” layer is shielded from the surrounding solvent by adjacent hydrophobic layers, enhancing the electrostatic attraction between the helices, and mutations affecting the “0” layer severely disrupt trafficking in vivo [77], an effect which is reminiscent of the importance of this interaction to the stability of the complex. The structures of the distantly related early and late endosomal complexes unveil that these features are highly conserved, despite low sequence homology with neuronal SNAREs [78, 79].

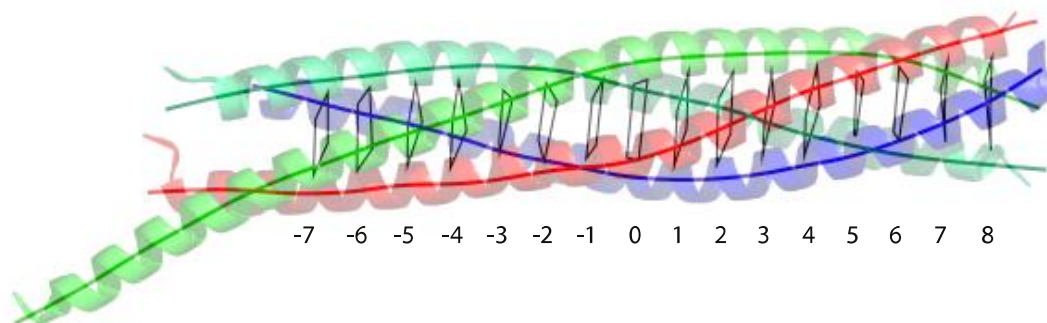


Figure 1.7: Structure of the neuronal SNARE core complex and an overlaid depiction of the backbone of the four-helix bundle with numbered hydrophobic layers and the central ionic “0” layer. Colors correspond to synaptobrevin (blue), syntaxin (red) and SNAP-25 (green). The N-terminal portion of the complex is on the left side. Kindly provided by Dr. Nickias Kienle.

Although the structure of the soluble core SNARE complex is helpful in understanding its thermodynamic stability, the way in which the coiled-coil can mediate fusion is not directly deducible. An intuitive proposal is that SNARE complex assembly initiates in trans at the N-terminal portion and nucleates towards the C-terminus in a zipper-like fashion; however, without knowledge of the structure of the TMD regions and the connecting linkers, there is no definite way to know how changes in free energy produced during SNARE complex formation is coupled to changes at the membrane bilayer.

The recent elucidation of the structure of the neuronal SNARE complex with the linkers and TMDs of synaptobrevin and syntaxin sheds light on this question [75] (figure 1.8). The new structure reveals that the helices from the coiled SNARE motifs are extended throughout the linker and TMDs, and depicts additional side chain interactions between the linker residues of syntaxin and synaptobrevin. These findings are mechanistically important in two ways: 1) the extension of the helices into the membrane provides a continuous rigid structure which is able to mechanically transduce the pulling force generated during SNARE complex nucleation onto the membranes, and 2) the additional interacting side-chains of the linkers ensures zippering can proceed further towards the closely-apposed membranes and may provide extra energy during critical intermediate or transitional states of the membrane merging process.

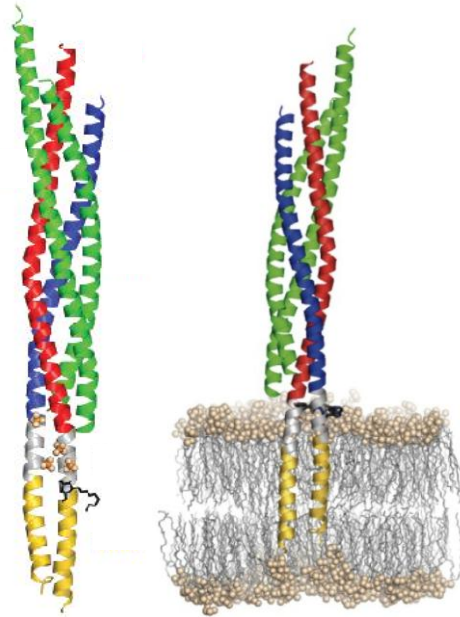


Figure 1.8: Structure of the SNARE complex including linker and TMDs of syntaxin and synaptobrevin. Left: the crystal structure depicting the SNARE motifs (same color coding as from figure 1.7), linkers (light grey) and TMDs (yellow). Sulfate ions are shown as spheres and two glycyglycyglycine molecules are represented by black sticks which are both derived from the crystallization buffer. Right: a simulation depicting how the full-length SNARE complex would reside on a PE membrane. A layer of aromatic residues which provide additional stability to the linkers is portrayed in black. From [75].

Comparative primary sequence analysis of the SNARE motifs involved in distinct trafficking pathways across different species shows that the amino acid composition of the residues forming the central “0” layer is evolutionary conserved and is subject to a requirement of 3 glutamines (Q) and 1 arginine (R). This feature is the biochemical basis for an R and Q classification scheme of SNAREs, with the Q family further subdivided into Qa, Qb and Qc in reference to the neuronal helices of syntaxin (Qa) and SNAP-25 (Qb and Qc) [80, 81]. The 3Q-1R requirement serves as a guide to predict which set of SNAREs would be able to form fusion-competent complexes [81], and *in vivo* mutations that alter the distribution of arginine and glutamine in the central layer can affect secretion in yeast [82, 83].

The vast sequence and structural conservation of the SNARE motifs has functional implications for SNARE pairing interactions. One important ramification is that SNARE complexes can form promiscuously *in vitro*, with non-cognate SNAREs able to substitute for cognate SNAREs of the same subfamily [84, 85]. Non-cognate SNARE complexes are comparable in

thermal stability to cognate SNARE complexes and share similar biochemical properties such as resistance to SDS. Such lack of pairing specificity is incompatible with SNARE-regulated fusion specificity *in vivo* as postulated by the SNARE hypothesis. Moreover, a pronounced hysteresis in the assembly and disassembly of the SNARE complex reveals it is not in a dynamic equilibrium with its monomers, implying that once formed the complex will not spontaneously dissociate within biologically relevant timescales [86]. These observations together suggest that, given their ease of formation and long-lasting stability, assembly of non-cognate SNAREs must be systematically avoided to prevent unspecific vesicular fusion and that additional factors are required to control which SNAREs are able to pair.

1.3.3 Intermediates in the assembly pathway of SNAREs

Understanding of the mechanism of how SNAREs fuse membranes *in vivo* is ultimately linked to the understanding of intermediates in the fusion pathway, both in terms of intermediate states at the membrane level and at the SNARE complex assembly level. As discussed in the previous subsection, the end state of the SNARE assembly pathway is the highly stable coiled-coil four-helix bundle. The fact that four helices are needed for SNARE complex assembly is already an indication of the complexity of the spatial and temporal regulation required for its formation, and it is likely that the process proceeds through a sequence of steps. In fact, the joining of two SNARE motifs into one protein such as SNAP-25 may be seen as an evolutionary strategy to make SNARE assembly more efficient by reducing the number of intermediate steps.

1.3.3.1 Accessibility of SNARE motifs as a first level of assembly

The first level of SNARE assembly occurs at the level of individual SNAREs, specifically at the availability of the SNARE motif for engaging in SNARE complexes (figure 1.9). After a vesicle has fused, SNAREs are found in the fused membrane in a *cis* SNARE complex, and so the complex must be disassembled in order to recycle SNAREs for subsequent rounds of fusion.

This task relies on N-ethylmaleimide-sensitive factor (NSF) and its soluble NSF attachment protein SNAP [66], which were once thought to constitute the fusion machinery (reviewed in section 1.3.1). NSF is a hexameric complex that belongs to the AAA+ family of proteins containing ATPase activity. Using energy from ATP and α -SNAP (one of three different isoforms) as an adaptor for SNARE complex attachment, NSF disentangles the coiled-coil, although how this is done still remains unresolved [65, 87]. Even though NSF and α -SNAP do not directly participate in assembly of SNAREs, their action can be viewed as an essential pre-assembly step since they regenerate the basic “building blocks” for SNARE complex assembly, and they may even act as a correction mechanism by disassembling non-productive or “dead-end” SNARE complexes as suggested by studies from reconstituted fusion of vacuoles in yeast [88].

Once SNAREs are regenerated by NSF/SNAP, SNAREs may be subject to different regulatory mechanisms that can affect their availability to assemble into complexes. In isolated native plasma membrane lawns, neuronal syntaxin and SNAP-25 are present in partially overlapping clusters that are mediated by cholesterol and interactions between SNARE motifs [89, 90]. Nevertheless, at least some of the SNAREs present in these clusters are able to form binary and ternary SNARE complexes with both endogenous and exogenous SNAREs, suggesting syntaxin and SNAP-25 are constitutively active at least with regards to their interactions with partner SNAREs [90, 91]. On the other hand, synaptobrevin has been proposed to be down-regulated in synaptic vesicles by synaptophysin, an abundant transmembrane synaptic vesicle protein, and by interaction of the C-terminal portion of the SNARE motif with its resident membrane which “buries” part of synaptobrevin into the membrane [92, 93]; however, these findings are in contrast to the demonstration that synaptobrevin can readily form ternary complexes in native and artificial membranes [94].

The N-terminal domain of neuronal syntaxin and its homologues (Qa SNAREs) are prime candidates for serving a regulatory function. These

domains form antiparallel three-helix bundles (also referred to as Habc domains) and can fold into the SNARE motif in a “closed” conformation. In exocytic yeast SNAREs, the Habc domain of the syntaxin homologue Sso1p strongly inhibits the formation of binary and ternary complexes due to a stable interaction between Habc and the SNARE motif, and removal of the domain accelerates complex formation by 3 orders of magnitude [95, 96]. In contrast, neuronal syntaxin appears to be in a dynamic equilibrium between the “open” and “closed” forms, which makes it more amenable to interacting with SNARE partners [97].

The balance between “open” and “closed” conformations of syntaxin appears to be controlled by Munc-18, a soluble protein belonging to the conserved SM family of proteins for which genetic evidence implies an essential role for exocytosis in neurons and yeast [98, 99]. The structure of Munc-18 bound to syntaxin reveals an arch-shaped Munc-18 locking the “closed” conformation of syntaxin, indicating that an essential step towards SNARE assembly would require unlocking the Munc-18/syntaxin interaction [100]. Other SM /syntaxin pairs from different trafficking steps appear to interact differently (thoroughly reviewed in [99]), and so the function of SM proteins are perhaps not highly conserved.

However, recent evidence suggests that most, if not all, syntaxins exhibit a second binding interaction through a short peptide at the very N terminus [72]. When the N-peptide is bound to Munc-18, the syntaxin SNARE motif is unable to form a complex with SNAP-25 or synaptobrevin, suggesting the availability of the syntaxin SNARE motif is dependent on Munc-18. Electrophysiological studies in neurons and chromaffin cells support a role of Munc-18 and syntaxin involved in steps upstream of exocytosis (such as vesicle docking), which is consistent with the biochemical evidence implicating Munc-18 acting at the earlier stages of SNARE assembly [101, 102].

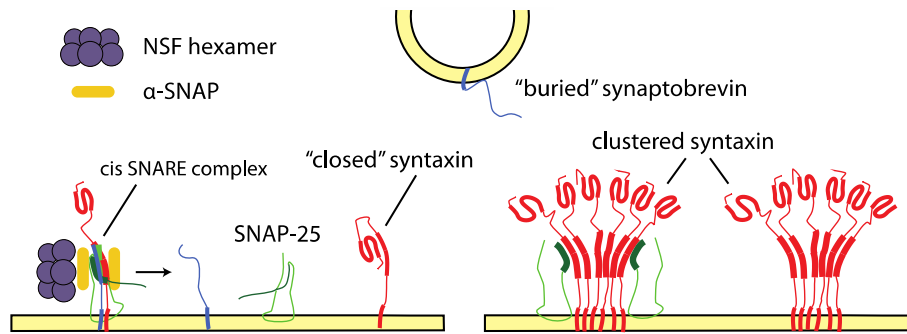


Figure 1.9: Accessibility of SNARE motifs as a first level of SNARE assembly. For assembly, SNARE must make their motifs accessible to complementary partners. Cis SNARE complexes are disassembled by NSF and α -SNAP following ATP hydrolysis, making individual SNAREs freely available. This may be viewed as an essential pre-assembly stage. Endocytosis (not shown) would be required for regeneration of synaptobrevin-containing vesicles. Syntaxin and SNAP-25 tend to cluster, and synaptobrevin may be regulated by its own membrane. See text for further details. Thick lines denote structured regions. Modified from an original figure kindly provided by Dr. Reinhard Jahn.

1.3.3.2 Acceptor complex formation as a second level of assembly

A second level of SNARE assembly is likely to occur at the formation of an acceptor complex consisting of 2 or 3 SNAREs that provide a complementary binding site for a trans SNARE partner (figure 1.10). In vitro, putative acceptor complexes can be identified when a specific topological combination of SNAREs are preformed and enhances full SNARE complex assembly in comparison to the simultaneous mixing of a subset or a full set of SNAREs [103]. In the case of neuronal SNAREs, syntaxin and SNAP-25 form a binary complex in vitro that is required for incorporation of synaptobrevin into a ternary SNARE complex [103, 104]. This is supported by experiments on isolated native plasma membrane lawns, where botulinum neurotoxins C1 and B, which are specific for cleavage of SNAP-25, block the incorporation of synaptobrevin into SNARE complexes and suggests complex formation is dependent on the availability of both syntaxin and SNAP-25, which is consistent with the requirement of an acceptor binary complex [91].

Apart from being a possible additional regulatory step, it is not entirely clear what further advantages the requirement of an intermediate acceptor complex would provide to the entire assembly reaction. It is also not clear whether all acceptor complexes follow a Qabc configuration such as the case of neuronal SNAREs; in fact, in vitro experiments suggest a QabR configuration is required for fusion in the ER-Golgi pathway in yeast [105].

One possibility comes from NMR analysis of the putative acceptor complex of yeast SNAREs Sso1p and Sec9p (the SNAP-25 homologue), which reveals the binary complex is structured at the N terminus but not at the C terminus [106]. It has been proposed that the structured N terminus of the three-helix bundle acceptor complex serves as a high affinity binding site for the nucleation of Snc1p (the synaptobrevin homologue) [107]. Such an arrangement could provide an efficient nucleation template for a trans SNARE complex and drive N to C terminal zippering.

In vitro the three-helix bundle of the syntaxin·SNAP-25 acceptor complex is a transient structure and is in equilibrium with a four-helix bundle where a second syntaxin occupies the position of synaptobrevin in the ternary SNARE complex [67, 104, 108-110]. This 2:1 syntaxin·SNAP-25 complex is probably an off-pathway “dead-end” formed by the tendency for monomeric syntaxin to assemble into oligomers [108, 111], and only slowly disassembles to form an active 1:1 complex with a free synaptobrevin binding site [104]. It is unknown whether the 2:1 complex occurs in native membranes, but if so it would mean that additional factors would be needed to regulate or stabilize the presumed 1:1 syntaxin·SNAP-25 on-pathway acceptor complex.

Interestingly, single-molecule Förster resonance energy transfer (smFRET) analysis of syntaxin·SNAP-25 binary complexes in extremely dilute concentrations, conditions which favor the 1:1 complex side of the equilibrium, reveals a dynamic interchange between three configurations consisting of the SNARE motifs of syntaxin and SNAP-25, and two configurations involving the SNARE motif of syntaxin and either one of the two SNAP-25 SNARE motifs with the other motif unbound [109]. Accessory proteins such as Munc-18 seem to stabilize the 1:1 binary complex in the three-helix bundle configuration, supporting the view that additional factors could play a role in assembling and/or stabilizing an intermediate acceptor complex that leads to full SNARE complex assembly.

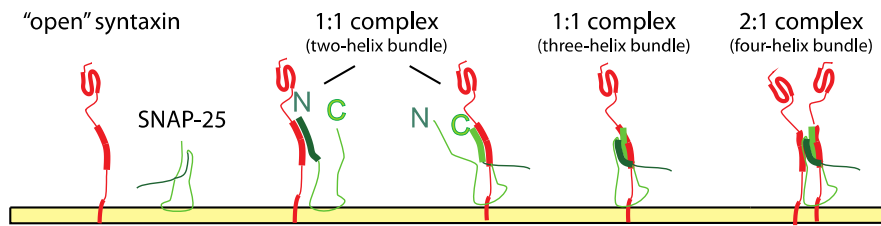


Figure 1.10: Acceptor complex formation as a second level of SNARE assembly. In the case of neuronal Q-SNAREs, the open syntaxin is able to interact dynamically with both SNAP-25 SNARE motifs. The three-helix bundle 1:1 syntaxin:SNAP-25 binary complex is thought to be an on-pathway intermediate for ternary complex assembly, whereas the 2:1 complex, which occurs *in vitro*, is an off-pathway structure. Further details are found in the text. Modified from an original figure kindly provided by Dr. Reinhard Jahn.

1.3.3.3 *Partially zippered SNARE complexes as a third level of assembly in regulated fusion*

The third and final level of SNARE assembly is at the level of intermediate assembly states of the four-helix bundle (figure 1.11). Partially zippered or partially assembled trans four-helix SNARE complexes are difficult to isolate due to their inherently transient nature; any attempt of purification would inevitably lead the complex to adopt the stable *cis* configuration [5]. Thus, evidence for the existence of stable or kinetically trapped intermediate states in the assembly of the four-helix bundle is indirect and has been obtained from electrophysiological data in fast Ca^{2+} -triggered fusion such as the fusion of synaptic vesicles or large dense core vesicles in chromaffin cells.

Perhaps the most compelling of these come from neurotransmitter release from stimulated neuromuscular junctions [112]. When injected with the light chains of tetanus neurotoxin (TeNT) and botulinum neurotoxin B (BoNT/B), the effect of both toxins on release were observed to depend on different stimulation conditions. In particular, the blocking activity of TeNT was highly dependent on continuous high frequency nerve stimulation, whereas BoNT/B could block release at both a high frequency and at no stimulation regimes. Both toxins cleave synaptobrevin at the exact same position, however, TeNT binds at the N terminal part of the synaptobrevin SNARE motif and BoNT/B does so at the C terminus. Since the fully assembled core SNARE complex is resistant to both neurotoxins *in vitro* [73], the interpretation is that synaptobrevin belonging to vesicles in a fusion-ready

state is present in a partially assembled ternary SNARE complex at the N terminus (and hence resistant to TeNT), while the C terminus remains unstructured and exposed to cleavage by BoNT/B. Only when cis SNARE complexes produced after fusion have been disassembled by NSF and SNAP (cycles of which are promoted under high frequency nerve stimulation) is synaptobrevin fully exposed and susceptible to TeNT cleavage [112].

Different populations of vesicles with different functional states are thought to reside at the fusion sites of regulated secretion such as the plasma membrane of neuronal synapses or adrenal chromaffin cells. These have been identified based on different responses to different types of stimuli; for instance, the readily releasable pool (or RRP) of vesicles at the synapse is usually probed by application of a hypertonic saline solution, which triggers exocytosis of fusion-ready, or primed, vesicles [113]. In chromaffin cells, kinetic capacitance profiles measured by the patch-clamp set-up, which reflects the net area increase in plasma membrane produced by fusion, contain two distinct sequential phases referred to as the burst and sustained phases which are triggered by a rapid calcium increase. Studies involving antibody and neurotoxin treatment of cells which alter SNARE-complex assembly differentially affect these two phases and are interpreted as indicating a pool of fusion-ready vesicles (the burst component) and a separate pool which must undergo a priming stage before becoming fusion-ready (the sustained component) [114, 115] (see [116] for a recent review). Together with mutagenic analysis demonstrating that mutations at the C-terminal portion of the SNARE complex affect fusion triggering while N-terminal mutations affect the upstream priming reaction, these studies point out towards the existence of partially assembled SNARE complexes which define the functional state of vesicles [117].

Since SNAREs assembled *in vitro* readily form stable complexes, it quickly becomes apparent that regulatory factors would be required to arrest a SNARE complex at a partially zippered state. Two candidates for this function are synaptotagmin and complexin that are involved in Ca^{2+} -

triggered exocytosis and which have been proposed to play a role in regulating or stabilizing partially assembled SNARE complexes [118].

Synaptotagmin is a vesicular transmembrane protein with two tandem Ca^{2+} -binding C2 domains orientated towards the cytoplasm, and numerous *in vivo* and *in vitro* studies implicate it as the calcium-sensor responsible for triggering fast fusion [119, 120]. Synaptotagmin is able to bind to both acidic phospholipids and SNARE complexes in a Ca^{2+} -dependent manner (reviewed in [30]), and some evidence suggests a coupling between Ca^{2+} -sensing and SNARE-mediated fusion [121, 122]. Synaptotagmin knockouts are generally lethal or severely impair Ca^{2+} -triggered exocytosis, consistent with a role as a positive regulator, but also lead to an increase in spontaneous release, suggesting it may also act as a clamp to control unspecific fusion reactions that are not synchronized or regulated [123, 124]. However, little structural information is available to assess a direct clamping action of synaptotagmin on SNARE complex assembly.

Complexin is a short α -helical peptide that binds to SNARE complexes in between a groove formed by synaptobrevin and syntaxin in an anti-parallel fashion [125]. Like synaptotagmin, electrophysiological data implicate a positive regulatory role in Ca^{2+} -triggered fusion [126] [127] (further discussed and reviewed in [128]), but some mutant studies suggest a negative role in spontaneous release which is supported by *in vitro* reconstituted fusion experiments demonstrating a clamp-like action [129-131]. The molecular origin of this apparent dual role of complexins could be explained by the presence of distinct regions of complexin mediating dual activating and clamping effects that both stabilize SNARE assembly and prevent complete zippering [132-134].

Based on the observation that complexin can be displaced from the SNARE complex by synaptotagmin in a Ca^{2+} -dependent manner, a model has emerged where a partially zippered trans SNARE complex is arrested by the clamping action of complexin, which is released by synaptotagmin upon Ca^{2+} influx and which together cooperate to stimulate or facilitate the final phase

of SNARE complex assembly [134, 135]. Such a synaptotagmin/complexin switch model is mechanistically attractive since a rapid release of a clamp upon a Ca^{2+} signal on an already partially assembled complex could constitute a quick enough sequence of molecular steps to trigger fusion with sub-millisecond kinetics as required for neurotransmitter release. However, structural data depicting a stabilized partially zippered SNARE complex is still required to corroborate the model.

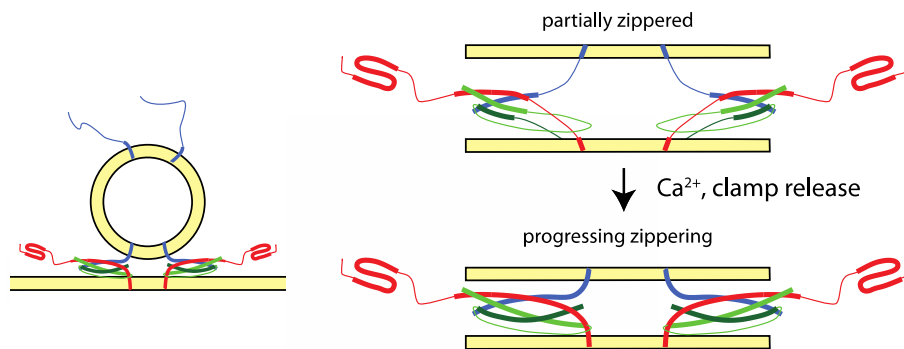


Figure 1.11: Partially zippered SNARE complexes as a third level of assembly implicated in regulated Ca^{2+} -triggered fusion. Trans SNARE complexes may be arrested in a partially assembled or zippered state by regulatory proteins such as synaptotagmin and complexin which could clamp the complex and prevent zippering of the membrane-proximal region of the complex (thick lines denote structured regions of assembly). A switch-like action upon arrival of Ca^{2+} may release the clamp and allow SNARE complexes to complete zippering to a fully assembled state and mediate fusion. Modified from an original figure kindly provided by Dr. Reinhard Jahn.

1.3.4 Intermediates in SNARE-mediated fusion

As discussed in section 1.2.1, fusion of model membranes has been rationalized in terms of the stalk hypothesis, whose central theme is that membrane fusion begins with the formation of a lipidic connection between the proximal monolayer leaflets of opposed bilayers called a stalk. The best understood biological membrane fusion reaction is that mediated by viral fusion proteins [4]. One well-studied case is the fusion protein of Influenza Hemagglutinin (HA). HA proteins belong to the class I viral fusion proteins that contain a single transmembrane domain and, like other fusion proteins of the same class, exhibit an elongated trimeric coiled-coil structure containing fusion peptides that insert into the target membrane [4, 136]. Once activated by low pH, the HA trimer undergoes a conformational change resembling a

hairpin-like structure that brings the opposed membranes closer together to induce fusion.

HA-mediated fusion is impaired and arrested at a hemifusion state when its TMD is replaced by glycosylphosphatidylinositol or is altered by introduction of a point mutation [37, 47, 137], suggesting that the TMD plays a key role in the transition from hemifusion to fusion. Furthermore, low surface density of HA increases the proportion of hemifusion relative to full fusion, indicating hemifusion is likely a metastable intermediate that requires additional energy to proceed to fusion [48]. Fusion is also enhanced when inverted cone-shaped lipids are placed specifically in the inner monolayer leaflet; conversely, cone-shaped non-lamellar lipids inhibit fusion and pore opening [48, 138].

These studies are important in a general sense because they provide evidence indicating biological fusion proceeds via lipidic intermediates, and more specifically because fusion appears to be consistent with the stalk hypothesis. Comparison of activation energies of steps involved in viral fusion, secretion, and fusion of model membranes points towards a common energetic pathway shared among the three processes [139]; however, this is by no means a definitive proof that SNARE-mediated fusion proceeds through the same intermediates.

In vivo, hemifused vesicles at the plasma membrane have been observed using electron tomography [140], and reconstituted SNARE-mediated liposome fusion has been reported to proceed via a hemifusion intermediate as studied by bulk and single particle measurements [141, 142] which can be arrested by complexin [130, 132]. It is not clear, however, whether hemifusion in these systems represent a genuine intermediate or is an alternative outcome to fusion as has been concluded by some [143]. In addition, similar to what has been described in viral fusion, inverted cone-shaped lipids negatively affect the lipid dependency of SNARE-mediated fusion, consistent with stalk-like intermediates in the fusion pathway [144, 145].

Figure 1.12 depicts a model of SNARE-mediated fusion which is based essentially on the stalk mechanism. Although more experimental data is needed to validate the proposed intermediate structures, the model portrays a lipidic fusion pore that is formed by a transition from a trans to a cis conformation of the SNARE complex. The stiff and helical linkers as deduced from the crystal structure (section 1.3.2) are central to this model, where SNAREs are depicted as force transducers acting on the membranes [5].

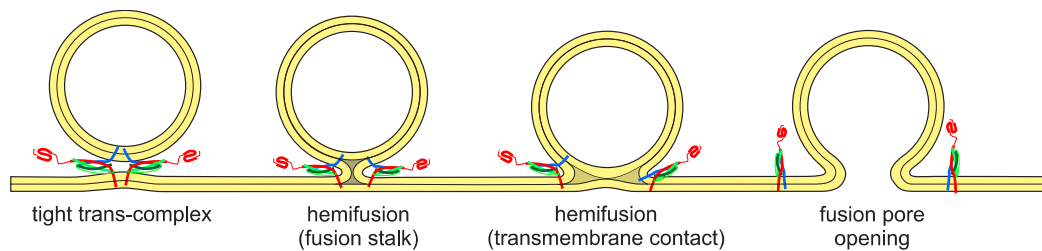


Figure 1.12: Model of SNARE-mediated fusion. Two SNARE complexes are depicted mediating fusion of a vesicle with a planar lipid bilayer. It is not known whether these structures constitute transition states (local maxima) or intermediates (local minima) in the energy landscape of SNARE-mediated fusion. Figure kindly provided by Dr. Reinhard Jahn.

1.4 Reconstitution of SNARE-mediated fusion in liposomes

In the previous sections, the biochemistry of SNAREs has been discussed and reviewed. These properties have been correlated to their function as studied *in vivo*, in particular with regards to neuronal exocytosis. Fusogenic mechanisms and functions attributed to SNAREs based on *in vivo* experiments or from *in vitro* studies involving soluble truncated SNAREs have to ultimately be tested by reconstituting them into model membranes such as liposomes. This brings additional challenges, both experimentally (which lipid compositions to use, how to reconstitute SNAREs, how to measure fusion, etc.) and theoretically (how to interpret assay readouts). However, there are no obvious simple alternative model systems for the reconstitution of SNAREs, and this section will focus on attempted strategies for SNARE-mediated reconstitution and their outcomes.

1.4.1 Criteria for fusion

Fusion between two membranes is indicated by two physical processes: 1) the mixing of the outer and inner leaflet lipids of two bilayers merging into a new bilayer, and 2) the mixing of aqueous or soluble content resulting in a continuous aqueous connection between luminal compartments without exposing the compartments to the exterior solvent. This last requirement is in reference to membrane merging processes that are mediated through rupture and re-sealing, which are inevitably leaky and likely to be biological lethal [146]. In the case of the fusion of two liposomes, an additional criterion for fusion is that the newly fused liposomes must have a larger diameter than the precursor liposomes. Based on these criteria, several types of assays, relying mainly on the use of fluorescence probes and light scattering, have been developed and used for the investigation of fusion of liposomes mediated by different types of agents.

Fluorescence-based lipid-mixing assays have become the standard method for measuring liposome fusion (described in more detail in section 2.4.1), and it is common for fluorescence signals to be treated as “fusion signals”; indeed, the terms “lipid-mixing” and “fusion” are often used interchangeably. This can be misleading, since a thorough establishment of fusion requires a rigorous analysis that takes into account a range of physical criteria as discussed above [30]. Therefore, each study needs to clearly point out what is meant by “fusion” and what are the operational criteria for referring to it.

1.4.2 SNARE-mediated fusion of liposomes

The first studies reporting reconstituted SNARE-mediated fusion of liposomes showed that neuronal and yeast SNAREs are able to induce both lipid and contents-mixing [12, 105, 147]. Fusion is enhanced ~2-fold when the N-terminal Habc domain of syntaxin is cleaved [148], showing that the core SNARE complex is sufficient for fusion and that the Habc domain is inhibitory, although the molecular reason for this effect remains unclear [107].

Extension of the linker connecting the SNARE motif to the TMD by introducing an increasing number of flexible residues progressively diminishes fusion, and it was concluded that this effect was not due to loss of helical structure on the linker but rather to the larger physical separation between SNARE motifs and TMDs [149]. Furthermore, replacing the SNARE TMDs with lipid anchors spanning a single membrane leaflet drastically impairs fusion, but may enhance it if anchors span both leaflets [150]. These findings suggest bringing bilayers closer together is necessary but insufficient for SNARE-mediated liposome fusion, and that TMDs play an active role in the process through interaction of both inner and outer monolayers.

A thorough kinetic analysis of liposome fusion further revealed that the rate of fusion as measured by lipid-mixing is not limited by collision frequency above a certain liposome concentration, indicating that lipid-mixing kinetics is governed by an intrinsic property related to the ability of SNARE complexes to promote fusion [151]. Moreover, cis SNARE complex kinetics is correlated by lipid-mixing kinetics, strengthening the notion that fusion is mediated by the transition of trans complexes into cis complexes [151].

Despite initial progress in the characterization of the fusogenic properties of SNAREs *in vitro*, reported rates of liposome fusion were generally slow, at times taking 1-2 h to complete 2-3 rounds of fusion when 10 rounds was expected from the stoichiometry of the reaction [12, 148]. Purified synaptic vesicles were observed not to fuse with liposomes reconstituted with syntaxin and SNAP-25 unless Ca^{2+} was added, suggesting a calcium-triggered mechanism was required in addition to SNAREs to mediate fusion [152]. One study reported that liposome fusion occurred only when synaptobrevin was activated and released from a negative regulatory interaction with its own membrane, suggesting that synaptobrevin is not constitutively active in a membrane [93]. However, these reports are directly contrary to later findings showing synaptobrevin in native or artificial membranes are able to form

SNARE complexes, and that purified synaptic vesicles constitutively fuse with liposomes in a Ca^{2+} independent manner [94, 153].

An attempt to understand how these contrasting reports on the fusogenic behavior of SNAREs may depend on the SNARE-liposome preparation concluded that the ability of SNAREs to promote lipid-mixing was strongly dependent on the reconstitution method and protein density used, and concluded that previous observations of SNARE-mediated liposome fusion were primarily due to excessively high protein densities aided by the curvature stress of small liposomes [145]. A related study observed that at lower, more realistic densities, neuronal SNAREs can mediate fusion of liposomes only in the presence of PEG, further bringing into question the ability of SNAREs to fuse liposomes and the mechanistic significance of the liposome fusion assay [154].

In light of some these concerns, SNARE-interacting proteins have been proposed to assist SNAREs with mediating liposome fusion, most notably by synaptotagmin [155-157], and more recently by Munc-18 [158, 159]. These proteins have been proposed to enhance fusion either by regulating or promoting SNARE complex formation, or, in the case of synaptotagmin, by destabilizing the membrane in a Ca^{2+} -dependent manner [160, 161]. However, when full-length synaptotagmin is reconstituted, no Ca^{2+} -dependent stimulation is observed, bringing into question the validity of studies reporting enhanced liposome fusion with the soluble domain of synaptotagmin [162]. With few exceptions [163], stimulation of SNARE-mediated liposome fusion by SNARE-interacting proteins is rather modest and so it is unlikely that a key component of the fusion machinery is missing.

One possible reason why reported liposome fusion kinetics has been generally slow was uncovered by considering the kinetics of assembly of the syntaxin-SNAP-25 binary complex. As mentioned in section 1.3.3.2, syntaxin and SNAP-25 can form a binary complex consisting of a three-helix bundle. In vitro, this 1:1 binary complex, however, is a transient intermediate in equilibrium with a 2:1 syntaxin-SNAP-25 complex, which incorporates a

second syntaxin and occupies the binding site for synaptobrevin [104] (figure 1.13 A). Thus, an alternative explanation for slow liposome fusion kinetics is that productive SNARE complex formation is rate-limited by the slow disassembly of the 2:1 complex into an on-pathway 1:1 acceptor complex [104, 107, 151].

To overcome the transient nature of the 1:1 syntaxin·SNAP-25 acceptor complex, a strategy was pursued to stabilize the complex by incorporating a C-terminal fragment of synaptobrevin into its assembly [103]. This Δ N synaptobrevin assembles at the C-terminal region of the syntaxin·SNAP-25 three-helix bundle and prevents the binding of a second syntaxin; however, consistent with the zipper hypothesis, full-length synaptobrevin can still bind at the N terminus of the complex and nucleate toward the C terminus, displacing the Δ N synaptobrevin fragment in the process (figure 1.13 B). This stabilization ensures the availability of a free binding site for synaptobrevin, increases the number of active acceptor complexes and enhances lipid-mixing kinetics by an order of magnitude in comparison to an acceptor complex assembled without the fragment [103]. This result suggests that SNARE-mediated liposome fusion is governed by the underlying kinetics of productive SNARE complex formation, rather than on parameters such the reconstitution method or the physical properties of liposomes.

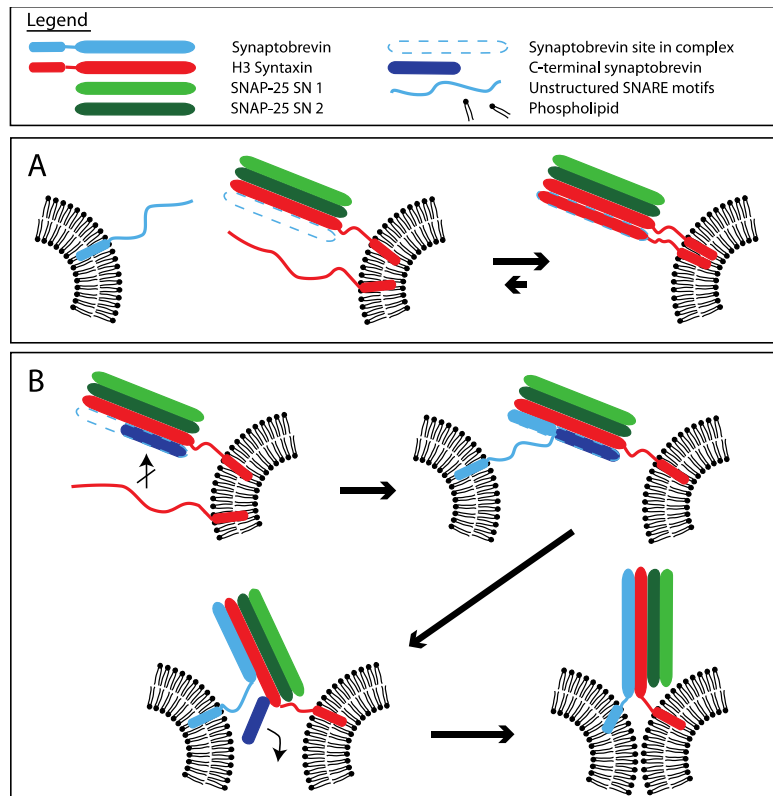


Figure 1.13: Stabilization of a 1:1 syntaxin-SNAP-25 acceptor complex accelerates liposome fusion kinetics. (A) The 1:1 syntaxin-SNAP-25 acceptor complex is in equilibrium with the 2:1 syntaxin-SNAP-25 acceptor complex where a second syntaxin occupies the synaptobrevin-binding site. Liposome fusion kinetics becomes rate-limited by the dissociation of the second syntaxin. (B) A 1:1 syntaxin-SNAP-25 acceptor complex can be stabilized if formed with a C-terminal fragment of synaptobrevin. This fragment prevents binding of a second syntaxin, but still allows binding of an incoming trans full-length synaptobrevin at the N terminus. N to C-terminal assembly eventually displaces the stabilizing synaptobrevin fragment and allows ternary complex formation which is then able to mediate fusion.

Despite the understanding of the importance of stabilizing a Q-SNARE acceptor complex constituted an important step towards elucidating how intermediates in SNARE assembly can lead to faster and more efficient fusion, the concerns raised by the above-mentioned studies regarding the wide variabilities of liposome fusion results using different SNARE-liposome preparations are no less valid. A more recent example of the discrepancies that can result is shown by the observation that Ypt7p, a Rab GTPase which is required for docking in vacuoles in yeast, enhances liposome fusion when vacuolar SNAREs are reconstituted by the direct method but not by the standard method (discussed later in more detail in sections 2.3.1 and 3.1.1). Although an explanation based on the a greater binding capacity of a Ypt7p interacting protein complex towards liposomes prepared by the direct

method was suggested, the lack of a rigorous and complete characterization of the SNARE-liposomes prepared by the two different methods prevents a less ambiguous mechanistic interpretation and does not satisfactorily address the observed discrepancy at the molecular level [164].

A question where much remains to be resolved is how SNARE-mediated fusion is affected by the curvature of the membrane. Although attempts to understand the related question of how SNARE action depends on lipid composition have been made [145, 154, 165], efforts to test the effect of curvature by comparing fusogenic properties of SNAREs when reconstituted on liposomes of different sizes have had limited success [145, 166]. Such a model system would be useful to help clarify certain aspects of SNARE-mediated fusion, for example:

- As would be expected based on the stalk hypothesis, and as has been observed in model membranes, does curvature stress arising from highly curved membranes facilitate SNARE-mediated fusion? Are SNAREs able to fuse liposomes larger than the commonly used size of 40-50 nm?
- Given that the majority of fusion reactions in a cell are asymmetric with respect to membrane size and curvature, can fusion reactions between small liposomes constitute a robust model for studying SNARE-mediated fusion *in vitro*?
- What aspects of SNARE-mediated fusion are different when utilizing larger liposomes? Does the kinetics remain unaffected, or is a higher number of SNARE complexes required in order to fuse them? Do SNARE-interacting proteins work differently or are other aspects revealed about their function when working with less curved membranes, as suggested by recent findings on synaptotagmin [161]?

1.5 Aims of the study

The aim of this study is develop and characterize a robust model system involving large SNARE-liposomes and to explore and gain

mechanistic insights on SNARE-mediated fusion. Although the employment of giant liposomes was an option and has been used in some studies [158, 161], an approach to make SNARE-liposomes only slightly bigger (80-100 nm) was undertaken. According to equation 1.1, a two-fold increase in radius would reduce the energy required for bending four-fold; if curvature does play a role in SNARE-mediated fusion, then large liposomes in this size range should suffice to see a marked difference with the more traditional small liposomes.

An essential part of this study is to first systematically explore aspects of the reconstitution procedure of SNAREs onto larger liposomes; although large SNARE-liposomes have been prepared before [93, 145, 166], a complete and thorough description of their reconstitution parameters remains to be seen. Thus, a significant portion of the Results chapter dwells on this issue.

The remainder of the work is aimed on the fusogenic properties of large SNARE-liposomes and on the use of a complementary set of tools and assays to analyze the fusion process and extract mechanistically meaningful conclusions. The power of the reconstitution approach relies precisely on its conceptual simplicity (which unfortunately does not translate to experimental simplicity) and the ability to add or remove factors from an already minimalist system. Occasionally, the approach is criticized because the conditions of study are inevitably non-physiological; however, it must be remembered that it is only a model whose aim is not to mimic exactly a complex biological reaction, but rather to gain understanding of basic physical principles. Guided by the desire to address some of the questions listed above, this study aims above all to arrive towards a mechanistic understanding of SNARE-mediated fusion that may help resolve or answer questions on how SNAREs mediate fusion *in vivo*.

2 Experimental Methods

2.1 Materials and reagents

Specific chemicals and commercial kits are mentioned in the individual method descriptions and procedures. For standard chemicals such as salts or organic solvents, commercially available chemicals of the highest purity grade were used.

2.2 Cloning and purification

2.2.1 Molecular cloning and constructs

Sequences of recombinant SNARE proteins used in this work were obtained from *Rattus norvegicus* and all except three constructs had been previously cloned into pET28a or pETduet 1 vectors which contain His₆-tags for protein purification (Novagen) (table 2.1). A schematic representation of the SNARE fragments used in this study is depicted in figure 2.1. For the preparation of syntaxin-SNAP-25 complexes stabilized by Δ N synaptobrevin fragments, pETduet 1 vectors were used containing syntaxin 1A 1-288 or 183-288 (referred to as syxFL or syxH3, respectively) and the Δ N synaptobrevin fragment. The procedure for the preparation of the pETduet 1 vector containing syxFL and syb 49-96 is described as an example.

Construct	Amino acid sequence range	Vector	Restriction sites	Reference
Synaptobrevin 2	1-116	pET28a	NdeI/XhoI	[151]
	1-116 (S28C)	pET28a	NdeI/XhoI	[108]
	1-116 (Δ 84)	pET28a	NdeI/XhoI	[94]
	1-96	pET28a	NdeI/XhoI	[151]
	1-96 (S28C)	pET28a	NdeI/XhoI	[108]
	49-96 (T79C)	pET28a	NdeI/XhoI	[167]
Syntaxin 1A	1-288	pET28a	NdeI/XhoI	[151]
	183-288	pET28a	NdeI/XhoI	[151]
SNAP-25A	1-206 (C84,85,90,92S)	pET28a	NdeI/XhoI	[85]
Δ N syb-syxFL complex	Syntaxin 1-288		NcoI/HindIII	
	Synaptobrevin 49-96	pETduet	NdeI/XhoI	this work
Δ N syb-syxH3 complexes	Syntaxin 183-288		NcoI/HindIII	
	Synaptobrevin 45-96	pETduet	NdeI/XhoI	[162]
	Synaptobrevin 49-96	pETduet	NdeI/XhoI	[162]
	Synaptobrevin 53-96	pETduet	NdeI/XhoI	this work
	Synaptobrevin 56-96	pETduet	NdeI/XhoI	this work

Table 2.1: List of SNARE constructs used in this study.

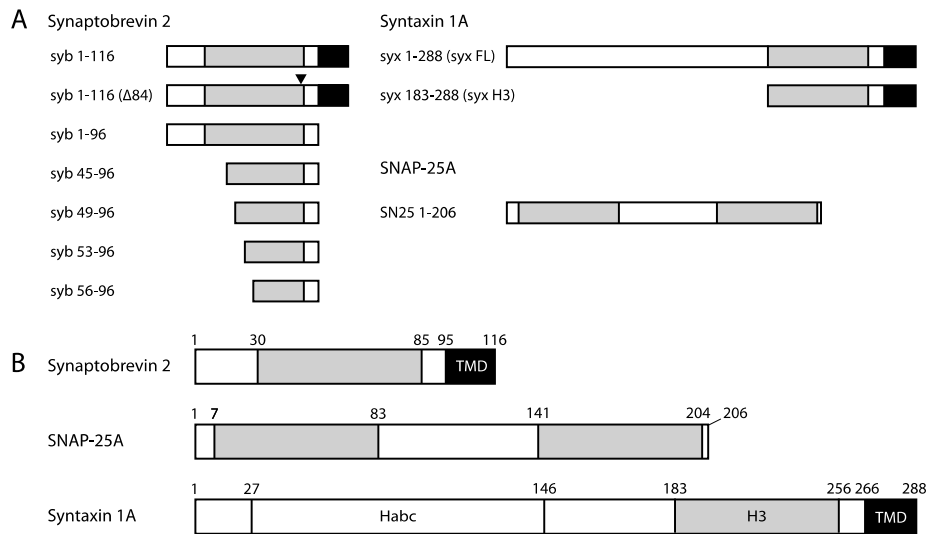


Figure 2.1: Schematic overview of SNARE proteins and fragments used in this study. (A) Comparison of distinct fragments of SNAREs purified. (B) Closer look at the domain structures of the three neuronal SNAREs. Grey areas depict SNARE motifs and black rectangles correspond to transmembrane domains (TMDs). A mutated form of SNAP-25A with cysteines mutated to serines was used in this study. Sizes are approximately to scale.

2.2.1.1 Preparation of syntaxin 1A (1-288) insert

A previously cloned pET28a vector containing syntaxin 1A (1-288) was used as a template for insert amplification by polymerase chain reaction (PCR). Forward and reverse primers containing restriction sequences for Xba I and Hind III, respectively, were selected (Sigma Oligos). In a reaction volume of 50 μ L, template DNA (1 ng) was mixed with forward and reverse primers (1 μ M each) in the presence of pfu polymerase (Promega, 1 unit), pfu buffer (Promega, 1x, 1 μ L) and deoxyribonucleotides (dNTPs) (Fermentas, 2.5 mM of each nucleotide). The PCR reaction program lasted for 2 h and consisted of three steps of 1 min for melting (95 $^{\circ}$ C), annealing (55 $^{\circ}$ C) and elongation (72 $^{\circ}$ C). The amplified insert was separated on an agarose gel (1.5 %), excised and purified with a PCR purification kit (Macherey-Nagel, Nucleospin Extract II). The insert was digested for 2 h at 37 $^{\circ}$ C with Xba I and Hind III (New England Biolabs, 1 μ L) in a total volume of 60 μ L using appropriate buffer and BSA as specified by the manufacturer (New England Biolabs).

2.2.1.2 Preparation of pETduet 1 vector and ligation of insert

A pETduet 1 vector (Novagen, 100 ng μL^{-1} , 10 μL) containing syntaxin 1A (183-288) on molecular clone site 1 and synaptobrevin fragment (49-96) on molecular clone site 2 was digested in a total volume of 60 μL with restriction enzymes Xba I and Hind III (New England Biolabs, 1 μL) in buffer 2 (New England Biolabs, 1x) and BSA (1x) for 2 h at 37 °C. Cleavage of the vector was evaluated by agarose gel (1.5 %) and dephosphorylated with Squid Alkaline Phosphatase (Roche, 1 μL) for 1 h at room temperature. Ligation of the insert (3 μL) and cleaved vector (2 μL) were performed in a total volume of 10 μL with T4 ligase buffer (Fermentas, 1x, 1 μL) and T4 ligase (Fermentas, 1x, 1 μL) (2 h at room temperature). Control reactions contained milliQ water instead of insert.

2.2.1.3 Transformation and clone sequencing

Escherichia coli XL-1-Blue heat shock cells (Stratagene, ~50 μL) were thawed on ice and incubated with ligation product (2-3 μL) or ligation control (2-3 μL) for 30 min. Cells were heat-shocked for 30 s at 42 °C and quickly put on ice. Luria Bertani (LB) media (1 % (w/v) tryptone, 0.5 % (w/v) yeast extract, 1 % (w/v) NaCl, pH 7.0, 1 mL) was added to cells and incubated for 1 h at 37 °C. Cells were plated on ampicillin media and selected colonies grown on LB media (4 mL). Plasmid DNA was purified with NucleoSpin® plasmid purification kit (Macherey-Nagel) and confirmation of cloning was checked by sequencing (MWG Eurofin).

2.2.2 Expression and purification of SNAREs

2.2.2.1 Bacterial transformation

Frozen competent *Escherichia coli* strain BL-21(DE3) (~ 65 μL) was thawed on ice and transferred into an electroporation cuvette. Plasmid DNA (~50 ng) was gently added to cells and electroshocked (Gene Pulser, V= 1.8 kV, R= 200 Ω , C = 25 μF). LB was quickly added (1 mL) and incubated for 45 min at 37°C. Agar plates with the relevant antibiotics were then inoculated and colonies used for overnight bacterial cultures.

2.2.2.2 Expression and extraction procedure for individual SNAREs

Overnight culture (~150 mL) of transformed *E.coli* with a pET28a plasmid encoding the SNARE construct was used to grow a large culture (3-6 L, 3 h, 37 °C). Induction was initiated with isopropyl- β -D-thiogalactoside (IPTG, Formedium, 500 μ M, 3 h at 37 °C). Cultures were then centrifuged at 4000 rpm for 15 min (Beckman J6-MI) and pellets suspended in resuspension buffer (20 mM Tris, 500 mM NaCl, 8 mM imidazole, pH 7.4, ~150 mL) and either frozen at -20 °C for storage or used directly for lysis.

Cells were lysed by adding extraction buffer (20 mM Tris, 500 mM NaCl, 20 mM imidazole, 10 % (w/v) sodium cholate, pH 7.4, ~150 mL) to the resuspended pellet followed by incubation (30 min, room temperature) with lysozyme (AppliChem, 1 mg·mL⁻¹), paramethyl sulphonyl fluoride (1mM), MgCl₂ (1 mM) and DNase I (AppliChem, ~10-20 mg). Treated cells were sonicated (Branson Sonifier, 4 x 40 strokes, large tip, 50% duty cycle at microtip limit) and left at room temperature for 15 min. Urea was added (~6 M) and after an additional 15 min incubation the lysate centrifuged at 16000 G for 30 min (Sorvall, SLA-1500).

Ni-NTA (nitrilotriacetic acid) agarose resin (Qiagen, 10 mL) were added to the lysate supernatant and incubated at 4°C for 2 h with mild shaking. The bead suspension was then loaded onto a column and the flow-through was discarded. Beads were washed (20 mM HEPES, 500 mM NaCl, 20 mM imidazole, pH 7.4, 4 x 50 mL) and eluted (20 mM HEPES, 500 mM, 400 mM imidazole, 4 x 10 mL). Elution fractions were immediately reduced with dithiothreitol (DTT, 10 mM). For SNARE fragments containing TMDs, 2-3 % CHAPS (Affymetrix) was included in the wash and elution buffers.

Protein content of fractions was quickly assessed by Bradford reagent [168] and the most concentrated fractions pooled. Thrombin (Merck, 100 μ L, 1 U· μ L⁻¹, prepared as a 5 mg·mL⁻¹ 50 % (v/v) glycerol stock) was added to cleave the His₆ tag and dialyzed at 4°C over night (MWCO 8 kDa, 20 mM HEPES, 150 mM NaCl, 1 mM DTT, pH 7.4). Dialysis buffer contained 1-2 % CHAPS for SNARE fragments containing TMDs. Expression, extraction,

binding, elution and thrombin cleavage were evaluated by sodium dodecyl sulfate polyacrylamide gel electrophoresis (SDS-PAGE) and Coomassie blue staining.

2.2.2.3 Expression and extraction procedure of binary SNARE complexes

The strategy for purification of binary Q-SNARE complexes stabilized by a C-terminal synaptobrevin fragment is based on the co-expression of the constituent SNAREs. Affinity purification of the complex is mediated by binding to His₆-tagged SNAP-25, resulting in isolation of individual His₆-tagged SNAP-25 and also His₆-tagged SNAP-25 bound to syntaxin and the C-terminal synaptobrevin fragment. For this reason, syntaxin (FL or H3) is cloned into a specific restriction site of pETduet 1 that removes the His₆-tag from the pETduet-1 vector (table 2.1) to avoid double tagging. Excess unbound SNAP-25 is removed in a second step by ion exchange chromatography.

E. coli strain BL-21(DE3) was co-transformed with a pETduet 1 vector containing either syntaxin (FL or H3) and a synaptobrevin fragment (45-96, 49-96, 53-96, 56-96), and with a pET28a vector containing full-length SNAP-25 (without cysteines). Induction was done overnight at 22 °C and extraction was done as described in the previous section. For best yields, elution buffers contained 3 % (w/v) CHAPS. An example of a purification of a binary Q-SNARE complex purified in this way is depicted in figure 2.2.

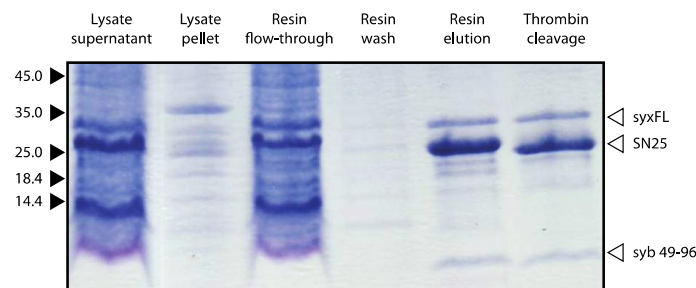


Figure 2.2: Different steps in the extraction and affinity purification of a syb 49-96-stabilized syxFL-SN25 complex (the ΔN syxFL-SN25 complex) as evaluated by SDS-PAGE and Coomassie blue staining. Details of the purification are described in section 2.2.2.2. The thrombin-cleaved eluate was further purified to remove excess SNAP-25.

2.2.2.4 Chromatographic purification of SNAREs and SNARE complexes

SNAREs or SNARE complexes were purified to near homogeneity with ion exchange chromatography on a Äkta system (GE Healthcare) as previously described [151]. After dialysis and cleavage of His₆-tag with thrombin, SNAREs and SNARE complexes were diluted 1:1 with 1-2 % CHAPS to reduce the conductivity to 100 - 150 mS·cm⁻¹. All samples were filtered (0.2 µm, Sartorius) prior to use. Synaptobrevin was purified on a mono-S column (GE Healthcare) and syntaxins, SNAP-25 and all Q-SNARE complexes were purified on a mono-Q column (GE Healthcare). All proteins and complexes were purified in a linear gradient of NaCl (20 mM HEPES, pH 7.4, 1 mM DTT or 0.1 mM tris(2-carboxyethyl)phosphine (TCEP)). Buffers for ion exchange chromatography purification of full-length synaptobrevin contained 34 mM *n*-octyl-β-D-glucoside (OG, Glycon) and buffers for purification of syntaxin and Q-SNARE complexes contained 50 mM OG. Elution of proteins was monitored by absorbance at 280 nm and fractions were collected using an automated fraction collector (GE Healthcare). Fractions were evaluated by SDS-PAGE and Coomassie blue staining and pooled according to purity and band intensity. Concentrations were determined according to absorbance at 280 nm (Nanodrop 1000, Thermo Scientific) using extinction coefficients calculated from the ExPASy proteomics database. Samples were snap-frozen with liquid nitrogen and stored at -80 °C until further use.

2.2.3 Assembly of SNARE binary complexes

Spontaneously formed syntaxin:SNAP-25 binary complexes were assembled from separately purified monomers as described [162]. SNAP-25 was mixed to syxH3 or syxFL in a 2:1 ratio and incubated overnight at 4°C in 50 mM OG. The complex was purified with ion exchange chromatography in 50 mM OG. SDS-PAGE analysis was used to evaluate purity and to confirm that the stoichiometry corresponded to a 2:1 syxH3:SN25 or syxFL:SN25 complex.

2.3 Preparation and characterization tools of SNARE-liposomes

2.3.1 Preparation of liposomes and reconstitution of SNAREs

The composition of liposomes used in this work consisted of cholesterol (CH), phosphatidylcholine (PC), phosphatidylethanolamine (PE), and phosphatidylserine (PS). Small SNARE liposomes were prepared using the co-micellization method as previously described [162]. Large SNARE liposomes were prepared using the “two-step” strategy discussed in more detail in the Results chapter. The procedure for the preparation and reconstitution of large SNARE liposomes, as well as the methods used for their characterization, are described.

2.3.1.1 Preparation of large liposomes by reverse phase evaporation and extrusion

Large unilamellar liposomes were prepared by reverse phase evaporation [169]. Stock solutions of purified lipid extracts from bovine brain (Avanti Polar Lipids) were prepared in 2:1 chloroform:methanol and kept at -20 °C in purged nitrogen sealed vials. Lipid mixes containing the composition PC:PE:PS:CH were combined in the molar ratio 50:20:20:10. The total amount of lipid was calculated based on the final concentration at the end of the preparation procedure (always fixed at 8 mM) and the desired volume of liposomes (0.5 – 2 mL). For labeled liposomes, 1,2-dioleoyl-*sn*-glycero-3-phosphoethanolamine-N-(7-nitro-2-1,3-benzoxadiazol-4-yl), abbreviated NBD-PE, and 1,2-dioleoyl-*sn*-glycero-3-phosphoethanolamine-N-(lissamine rhodamine B sulfonyl), abbreviated RHO-PE, were included in the mix (1.5 % each, Avanti Polar Lipids), with a corresponding 3 % reduction of the unlabeled PE. In some experiments, including those used for chemical reduction by dithionite (Sigma, explained in section 3.3.2), 1,2-dioleoyl-*sn*-glycero-3-phospho-L-serine-N-(7-nitro-2-1,3-benzoxadiazol-4-yl), abbreviated NBD-PS, was used instead of NBD-PE. Unless otherwise noted, labeled liposomes were labeled with the pair NBD-PE/RHO-PE.

Lipids were mixed in a pear-shaped flask (100 mL) previously purged with nitrogen and the solvent removed by a step-wise vacuum pressure decrease from 500 mbar to 20 mbar on a rotatory evaporator set-up (~40 min). The dried lipid film was re-dissolved in diethyl ether (1.5 mL) followed by addition of reconstitution buffer (20 mM HEPES, 150 mM KCl, 1 mM DTT or 0.1 mM TCEP, pH 7.4; 0.5 mL). The resulting two-phase mixture was dispersed with sonication (Branson Sonifier, fine tip, 50% duty cycle at minimum intensity, 3 x 45 s with cooling periods on ice). Removal of diethyl ether from the suspension was achieved by gradually lowering the vacuum pressure (~1 h) to approximately 150 mbar. During the removal a gel phase was formed which coalesced into an aqueous suspension containing multi-lamellar liposomes. The suspension was collected and diluted with an appropriate volume of reconstitution buffer to make the total lipid concentration 8 mM. Liposomes were extruded (Mini-Extruder, Avanti Polar Lipids) using polycarbonate membranes (Avanti Polar Lipids) of pore size 0.4 and 0.1 μm (25 passes each) to give uniformly distributed unilamellar liposomes in the diameter range of 90-130 nm as confirmed by field-flow-fractionation coupled to multi angle laser light scattering (FFF-MALLS, Wyatt Technology Corporation).

2.3.1.2 Reconstitution of SNAREs onto large unilamellar liposomes

Reconstitution of synaptobrevin and Q-SNARE acceptor complexes into liposomes was done by n-octyl- β -D-glucoside (OG)-mediated reconstitution using a modified procedure from Rigaud and co-workers discussed in more detail in the Results chapter [170]. Amounts of liposomes, OG, SNAREs and buffer were calculated so that when all four components were mixed the final total lipid concentration was 4 mM. Approximately 10-20 % of lipids were lost during membrane extrusion and so it was assumed that the starting total lipid concentration was 6 mM. An OG stock of 300 mM was used and the concentration of OG in the mixture was calculated in order to make the final molar ratio between the excess detergent above the critical micelle concentration (CMC, 17 mM for OG) and the total lipid concentration

equal to 1.5 – 2 (see equation 3.1 in the Results chapter). The detergent concentration present in the SNARE OG solution was taken into account in the calculation, therefore, the exact amount of OG and reconstitution buffer to be added depended on the concentration of the purified SNAREs, the lipid/protein ratio of the liposomes and the desired volume of SNARE liposomes (between 250 and 500 μL). The sequence of addition to the liposomes consisted of reconstitution buffer, followed by OG and then SNAREs. Table 2.2 provides an example depicting the information needed for preparation of synaptobrevin liposomes.

Input values for preparation of syb large liposomes	
MW of OG (g/mol)	292.4
CMC of OG (mM)	17.0
(total detergent-CMC)/lipid ratio (R-value)	1.5
Concentration of OG stock (mM)	300
Concentration of syb stock (μM)	77
Concentration of OG in protein stock (mM)	34
Total volume of OG/SNARE/lipid mixture (μL)	350
lipid:protein ratio	500
Concentration of liposome stock (total lipid, mM)	6.0
Final concentration of lipid (mM)	4.0
Output values	
Volume of lipid to be added (μL)	233.3 (1)
Final concentration of syb in mixture (μM)	8.0
Volume of protein to be added (μL)	36.4 (4)
Final concentration of OG in mixture (mM)	23.0
OG amount to be added (μmol)	8.05
OG derived from protein stock (μmol)	1.24
Volume of OG stock to add (μL)	22.7 (3)
Extra buffer to add to make total volume (μL)	57.6 (2)

Table 2.2: Example of input parameters required for preparation of large syb liposomes and the amounts needed to add to the mixture. In grey are the calculated volumes of the four reagents and the sequence of addition is denoted in brackets. See text for further details.

As soon as OG/SNAREs/lipids were mixed, detergent was removed by overnight dialysis at room temperature in reconstitution buffer with SM-2 Bio-Beads (Bio Rad, $2 \text{ g}\cdot\text{L}^{-1}$) followed by a second dialysis (3-6 h) using Slide-A-Lyzer dialysis cassettes of molecular weight cut-off of 2 kDa and 10 kDa, respectively (Thermo Scientific). The size distribution of all large SNARE-liposomes used in this study was measured by FFF-MALLS and considered to

be an important quality control for SNARE-liposome preparation. Size distributions of SNARE-liposomes remained essentially unchanged after 11 days when stored on ice.

2.3.2 Reconstitution of SNAREs onto small liposomes

SNAREs were reconstituted according to the co-micellization method with detergent removed by size-exclusion chromatography on a SMART system (Amersham Biosciences) using a PC 3.2/10 Fast Desalting column (GE Healthcare) as described with slight modifications [103]. The lipid composition of the lipid mixes was PC:PE:PS:CH combined in the molar ratio 50:20:20:10, while for labeled liposomes 1.5 % (n/n) 1,2-dioleoyl-*sn*-glycero-3-phospho-L-serine-N-(7-nitro-2-1,3-benzoxadiazol-4-yl), or NBD-PS, and 1.5 % (n/n) 1,2-dioleoyl-*sn*-glycero-3-phosphoethanolamine-N-(lissamine rhodamine B sulfonyl), or RHO-PE, was included in the lipid mixture that was accompanied with a corresponding reduction in PS and PE. For this protocol SNAREs that had been purified in 1 % (w/v) CHAPS-containing buffer during ion exchange chromatography were used and the reconstitution buffer consisted of the same buffer used for the reconstitution of large SNARE liposomes. Lipid/protein ratios of SNARE-liposomes prepared in this way are denoted in the figure legend.

2.3.3 Liposome co-flotation on a density gradient for insertion assessment

SNARE liposomes (50 μ L) were mixed with Nycodenz (Axis Shield, 80 %, 50 μ L) in a centrifuge insert with a maximum capacity of 250 μ L. A second Nycodenz layer (30 %, 50 μ L) was gently applied followed by another layer of reconstitution buffer (50 μ L). The density gradient was centrifuged with a Beckman TL-ultracentrifuge (TLS55 rotor, 48,000 rpm, 4 $^{\circ}$ C, 1.5 h). Upon completion, 20 μ L aliquots (10 x) were carefully taken from the top of the gradient and analyzed by SDS-PAGE or western blot.

2.3.4 Orientation assessment by proteolytic digestion

Orientation assessment of SNAREs reconstituted on large liposomes was done essentially as described with minor modifications [94]. The principle of assessment is based on the accessibility of membrane-inserted transmembrane proteins to a protein-cleaving enzyme. Proteins inserted with inside-out orientation are protected from degradation while proteins with correct right side-out will be exposed to proteolytic enzymes and be degraded. By comparing the amount of cleaved protein to the protein content of an untreated sample, an estimate of the correctly orientated protein can be made.

Proteolytic digestion reactions were performed in 50 μL volumes in reconstitution buffer. Tetanus toxin light chain pET28a vector was used for expression and purified on a mono-Q column using identical procedures as described in sections 2.2.2.2 and 2.2.2.4. Synaptobrevin liposomes (30 μL) were incubated with tetanus toxin light chain (11.2 μM) and Q-SNARE complex liposomes were incubated with trypsin (Sigma, 0.1 $\text{mg}\cdot\text{mL}^{-1}$) at 37 $^{\circ}\text{C}$ for 2 h in the presence or absence of 0.3 % (w/v) Triton X-100 (Sigma). A control reaction with reconstitution buffer instead of tetanus toxin or trypsin was also done. Synaptobrevin-containing samples were analyzed with SDS-PAGE followed by visualization with Coomassie Blue staining, and Q-SNARE complex-containing samples were analyzed by Western blot and detected with monoclonal antibody for SNAP-25 (Synaptic Systems, CI 71.1).

2.3.5 Phosphate determination

Phospholipid content quantification of liposomes was performed by Ursel Ries by phosphorus determination using an acidic digestion procedure and spectroscopic measurement as described [171].

2.4 Fluorescence and light scattering-based methods

2.4.1 Fluorescence dequenching for lipid-mixing measurements

The most common method for investigating the ability of SNAREs to mediate liposome fusion has been a lipid-mixing assay based on the dilution

of a pair of fluorophore-labeled lipids which undergo Förster resonance energy transfer, or FRET [172, 173]. In this assay, a FRET donor and an acceptor are located on one population of liposomes (for example, containing an R-SNARE), and are mixed to another population of unlabeled liposomes (for example, containing the required set of Q-SNAREs). Upon fusion, the labeled lipids become diluted with unlabeled lipids and the average distance between the dyes is increased, resulting in a dequenching of the FRET donor. This process can be monitored by measuring the increase of fluorescence of the donor dye or alternatively the decrease of fluorescence of the acceptor dye (figure 2.3).

In this study, lipid-mixing kinetics was monitored with the FRET pair Rhodamine (RHO) and Nitrobenzoxadiazole (NBD) as previously described [103, 162]. Liposome fusion reactions were performed and measured in either a Fluorolog 3 (Model FL322) or a Fluoromax 2 spectrometer equipped with a magnetic stirrer and a temperature controller (Jobin Yvon). Data was acquired with the software provided by the manufacturer. Excitation and emission wavelengths were 460 nm and 538 nm, respectively, and unless otherwise stated, reactions were performed at 30 °C in cuvette volumes of 1.2 mL. Typically synaptobrevin was reconstituted in NBD/RHO-labeled liposomes, exceptions are noted in the figures. Reactions were started by mixing SNARE-liposomes (10-20 μ L) in reconstitution buffer and were terminated by adding reduced Triton X-100 (Sigma, 0.02%). Dequenching signals were normalized to the maximum fluorescence produced by detergent solubilization and lipid-mixing curves were plotted as a percentage of the maximum fluorescence (figure 2.3). For control reactions, soluble synaptobrevin (1-96, 2-4 μ M) was pre-incubated with labeled liposomes (~5 min) before initiation of fusion.

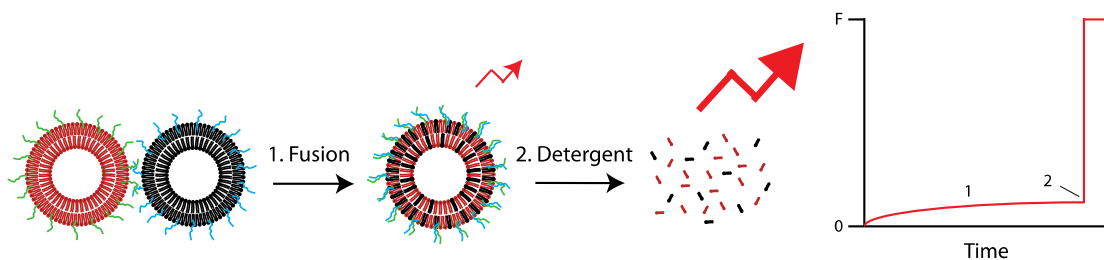


Figure 2.3: Schematic representation of the lipid-mixing “dequenching” assay depicting the increase of fluorescence of the donor dye as the FRET dye pair become “diluted” upon fusion with an unlabeled liposome. The solubilization of liposomes with detergent. Lipid-mixing curves were normalized to the maximum fluorescence F measured after solubilization.

2.4.2 Fluorescence anisotropy for binding and displacement experiments

Fluorescence anisotropy of a fluorophore is a measure of the polarization of emission when excited with polarized light. When the rate of emission is comparable to the rate of the rotational diffusion of the fluorophore, anisotropy values change according to factors that alter their diffusional properties, such as an increase in viscosity. When fluorophores are chemically linked to a protein, fluorescence anisotropy reflect the local conformational motion of the labeled residue, and can be used to probe for changes such as complex formation or dissociation of a labeled protein [174].

Anisotropy (r) is a ratiometric quantity and is empirically measured according to the expression:

$$r = \frac{I_{VV} - GI_{VH}}{I_{VV} + 2GI_{VH}} \quad \text{eq. 2.1}$$

where I_{VV} and I_{VH} are the fluorescence intensities of the vertically and horizontally polarized emissions of the fluorophore when excited with vertically polarized light, respectively. G is an instrumental correction factor that takes into account the differences in sensitivity of the detection system between vertically and horizontally polarized emitted light and can be measured according to:

$$G = \frac{I_{HV}}{I_{HH}} \quad \text{eq. 2.2}$$

Anisotropy measurements were carried out in a Fluorolog 3 (Model FL322, Jobin Yvon) with in-built polarizers and data was collected with the manufacturer's software with the integration time set at 2 s. Unless stated otherwise, all experiments were done in a total volume of 1.2 mL at 30 °C. All SNAREs and SNARE complexes with the desired cysteine mutations used for anisotropy experiments in this study were a kind gift from Dr. Alexander Stein and were labeled with an Alexa Fluor 488 C₅-maleimide derivative (Invitrogen, abbreviated Alexa488 or A488) according to previously described procedures [104]. Excitation and emission wavelengths were 488 nm and 520 nm. Concentrations and conditions for each experiment are described in the figure legends and G factors (equation 2.2) were measured for every set of experiments.

2.4.3 Single-particle fluorescence cross-correlation spectroscopy

Single particle analysis of fluorescence cross-correlation spectroscopy in combination with FRET allows discriminating between docking and fusion of SNARE-liposomes [175]. R and Q-SNARE liposomes are separately labeled with a FRET pair of dyes and their fluorescence are recorded as they diffuse through the detection volume of a confocal microscope equipped with a two-detection system. Diffusion of single undocked liposomes is recorded as fluorescence bursts (figure 2.4, left). When two liposomes dock or fuse, their fluorescence bursts become synchronized and their signal is said to be cross-correlated (figure 2.4, middle and right). However, fusion can be differentiated from docking since in fused liposomes the dyes undergo FRET which can be detected by changes in dye intensity or changes in fluorescence lifetime.

Details of the set-up and experimental procedures are found elsewhere and measurements were made by Dr. Anna Cypionka [175]. Large SNARE-liposomes were prepared as described in sections 2.3.1.1 and 2.3.1.2 except liposomes for reconstituted synaptobrevin contained Texas Red-phosphatidylethanolamine and Q-SNARE acceptor complexes contained

Oregon Green-phosphatidylethanolamine (both at 1.5 % (n/n) from Molecular Probes).

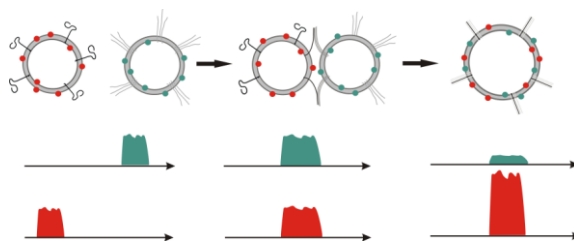


Figure 2.4: Schematic illustration of discrimination between liposome docking and fusion by concurrent analysis of FRET and fluorescence cross-correlation spectroscopy (FCCS). Figure kindly provided by Dr. Anna Cypionka.

2.4.4 Size distribution analysis by FFF-MALLS

2.4.4.1 Principle of separation by FFF and size determination by MALLS

Field-flow-fractionation (FFF) is an analytical method designed for the physical separation of macromolecules [176]. The principle behind the fractionation is based on the differential diffusion of particles of different sizes when exposed to two perpendicular flows. Particles are injected into one end of a thin trapezoidal-shaped channel ($\sim 350 \mu\text{m}$ thick) formed by a closed upper plate and a porous bottom plate (figure 2.5). A semi-permeable membrane is placed on this porous plate so that particles stay within the channel. An external pump is used to run an aqueous flow parallel to the channel (called the channel flow), which exerts a horizontal force on the particles and whose velocity vector profile is parabolic, with the flow being greatest at the center. At the same time, a valve is opened at the bottom of the channel that allows liquid to leave through the porous plate, establishing a second perpendicular flow to the channel flow (called the cross flow). This flow exerts a second vertical force on the particles in the direction of the membrane.

The accumulation of particles at the membrane establishes a concentration gradient that is counterbalanced by diffusion. Smaller particles have a greater diffusion coefficient than larger ones, and will therefore “push back” against the cross flow further than larger particles. An equilibrium is established when cross-flow and gradient diffusion forces cancel each other,

with smaller particles moving closer to the center where they experience a faster horizontal channel flow. Thus, in contrast to other separation methods such as size exclusion chromatography, in FFF smaller particles are eluted first from the channel.

When FFF is coupled to a light scattering detector, the size of the fractionated sample can be determined and a size distribution constructed by taking into account the different fractionation bins [177]. Multi-angle laser light scattering, more classically known as static light scattering, measures the intensity of scattered light from macromolecules at different scattering angles. The intensity of the scattered light as a function of angle can be fitted by different types of geometric models from which a size or structure parameter can be obtained, usually a radius or the molecular weight. Furthermore, the intensity of scattered light at one angle (usually 90°) can be used to calculate the number of particles within a given fractionated bin. By combining the size and the number of particles of that given size, FFF-MALLS allows determining the relative size distribution of an entire ensemble of particles [177, 178].

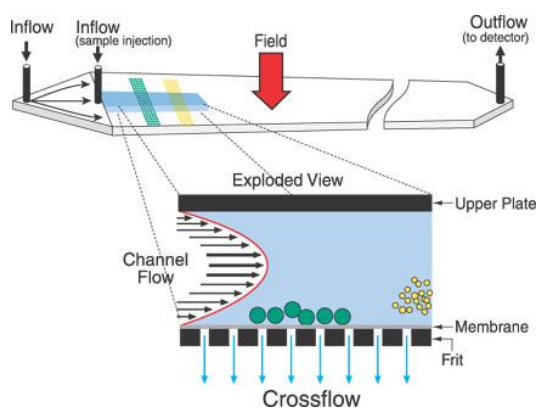


Figure 2.5: Schematic representation of a field-flow-fractionation channel. See text for details. Image obtained from the website of Wyatt Technology Corporation (<http://www.wyatt.com>).

2.4.4.2 Set-up and procedure for size distribution determination of liposomes

Size distributions of liposomes determined by FFF-MALLS were obtained using an Eclipse 2 set-up (Wyatt Technology Corporation). The FFF separation chamber was assembled with a membrane of molecular-weight cut-off 10 kDa and with a spacer of 350 μm . The chamber was connected to a

high-pressure liquid chromatography (HPLC) pump connected to a degasser and an auto-sampler (Agilent). Buffer (20 mM HEPES, 150 mM KCl, pH 7.4, 0.02 % NaN₃) was filtered with a 0.1 μM regenerated cellulose filter (Sartorius). The separation procedure was optimized with a 0.1 μM extruded liposome and the sequence program consisted of elution (1 min), focus (1 min), sample injection (1 min), focus (2 min) and elution with a cross-flow gradient lasting 40 min. The channel flow, focus flow and injection flow were 1, 3 and 0.1 mL·min⁻¹, respectively. The cross-flow consisted of a linear gradient from 0.5 to 0 mL·min⁻¹. For individual SNARE-liposomes, samples were diluted ~1:10 and 30 μL injected. For the size distribution determination of liposomes in fusion reactions, ~150-180 μL samples were taken from the reaction and injected.

Light scattering data was measured with a DAWN[®] EOS 18-angle light scattering detector (laser wavelength: 690.0 nm, Wyatt Technology Corporation) and raw data was collected and processed using the manufacturer's Astra software. Angle-dependent light scattering values were fitted with the coated sphere model (real refractive index = 1.33, coating refractive index = 1.45, and coating thickness = 4 nm). This fit assumed liposomes were perfectly symmetrical spheres with a bilayer membrane thickness of 4 nm and refractive index 1.45. With this input the software calculated the relative number (N) of liposomes as a function of the geometric radius (r) defined by a coated sphere model. This function N(r) was exported from the software and plotted using the Origin software package (Optilab).

For size distribution determination of samples obtained from fusion reactions, N(r) was converted into a relative weight size distribution W(r) and the x axis name was changed to "equivalent geometric radius". This change in name is to remind that liposomes do not necessarily satisfy the criteria of a sphere, since liposomes in a docked or hemifused state are present during the course of the reaction. In this case, a pair of docked liposomes or a hemifused liposome is treated as a hypothetical sphere with geometric radius r that would elute from the FFF chamber with the same retention time as that of the

docked or hemifused liposome. To convert $N(r)$ to $W(r)$, the following relationship was used:

$$\frac{W(r)}{N(r)} = M(r) \quad \text{eq. 2.3}$$

where $M(r)$ is the molecular weight of a liposome with geometric radius r . M can be estimated by the following expression [178]:

$$M = \frac{4\pi}{3}(R_o^3 - R_i^3)N_A\rho_b \quad \text{eq. 2.4}$$

where R_o is the outer liposome diameter (which is also equal to the geometric radius r), R_i the inner liposome diameter, N_A is Avogadro's number and ρ_b the lipid bilayer mass density. Assuming the bilayer thickness was 4 nm and using the approximation of $\rho_b = 1 \text{ g}\cdot\text{cm}^3$, equations 2.3 and 2.4 were used to convert the relative number distribution of $N(r)$ to the relative weight distribution $W(r)$.

The reason for converting to weight distributions to depict size changes in fusion reactions was because fusion reduces the number of liposomes in an ensemble, introducing a complication when normalizing and therefore directly comparing unfused with fused samples. A way around this is by converting to distributions in terms of the relative distribution of the weight of liposomes, since the lipid mass is approximately conserved during the duration of an ensemble fusion reaction.

2.5 Other methods

2.5.1 SDS-PAGE and Coomassie blue staining

Polyacrylamide gels were prepared with 10 % acrylamide as described [179]. After electrophoresis gels were stained with Coomassie Brilliant Blue R250 (Fluka, 0.2 % (w/v)) in methanol (50 % (v/v)), acetic acid (10 % (v/v)) for 30-40 min. Destaining was achieved by first incubating for 5 min in

ethanol (50 % (v/v)) and acetic acid (10 % (v/v)) followed by several hours of incubation in ethanol (10 %, (v/v)) and acetic acid (5 %, (v/v)).

2.5.2 Western blot analysis

After sample separation with polyacrylamide gel electrophoresis, gels were electroblotted onto nitrocellulose membranes as described [180]. Blots were blocked with a 5 % milk powder solution (5 % (w/v), 20 mL) and incubated for 1 h at room temperature. The membrane was refilled with milk powder solution (10 mL) and antibody added (1 h at room temperature). In this work, monoclonal antibodies for synaptobrevin II (Synaptic Systems, 69.1, diluted 10000:1) and SNAP-25 (Synaptic Systems, 71.1, diluted 1000:1) were used. Milk solution was decanted and washed three times for 5 min with “blocking” solution (20 mM Tris, 150 mM KCl, pH 7.5, 0.1 % (v/v) Tween 20 (Sigma)). The membrane was refilled with milk powder solution (10 mL) and incubated with horseradish peroxidase (HRP)-conjugated secondary anti-mouse antibody (diluted 5000:1) for 1 h at room temperature. Solutions were decanted and washed three times for 5 min with “blocking” solution and blotted proteins were visualized with a Western Lightning Ultra chemiluminescence kit according to the manufacturer’s instruction (Perkin Elmer).

2.5.3 Cryo electron microscopy

Electron microscopy of liposomes visualized with negative staining was done as described previously [162] and was performed by Dr. Dietmar Riedel. Cryo electron microscopy was done with controlled sample vitrification via plunge-freezing using Vitrobot™ and imaged as described [153].

For statistical analysis and for imaging of synaptobrevin mutant liposomes, Elmar Behrmann performed measurements. Samples were frozen in vitrified ice at defined time-points. Liposome mixtures (5 μ L) were applied to a freshly glow-discharged holey carbon grid (Quantifoil R2/1 copper 400 mesh) overlaid with a continuous carbon film. Grids were blotted manually

in a chamber with 95 % humidity at room temperature using a Gatan Cryoplunge3. Blotting time was between 10 and 14 seconds. Grids were then stored in liquid nitrogen-gas phase until analysis.

Liposomes were imaged with a JEOL JEM-3200FSC electron microscope at an acceleration voltage of 200 kV operated at liquid nitrogen temperature. An in-column omega energy filter was used to improve the image contrast by zero-loss filtering (15 eV slit width). Images were taken at a nominal magnification of 40000 and recorded on a 8.192 x 8.192 pixel TemCam-F816 (TVIPS).

3 Results

3.1 Characterization and optimization of the reconstitution of SNAREs onto large liposomes

The reconstitution of transmembrane proteins in artificial model membranes has been a subject of extensive study. Pioneering work on the reconstitution of transmembrane proteins by Racker, followed later by Rigaud, has laid much of the empirical foundations for subsequent reconstitution studies (thoroughly reviewed in [170, 181]). Methods for the reconstitution of membrane proteins include organic solvent and mechanical-based procedures; however, due to issues relating to the preservation of the native state of transmembrane proteins, the most widely used method is detergent-mediated reconstitution. This section will focus on how the strategy for the reconstitution of SNAREs on large liposomes was pursued and on the different parameters looked at for its optimization.

3.1.1 General considerations for detergent-mediated reconstitution

Two mechanistically distinct strategies can be discerned for reconstitution of transmembrane proteins. The co-micellization method (referred sometimes as the “standard” method owing to its widespread application) involves the dissolution of purified transmembrane proteins in a mixture of detergent and excess phospholipids, resulting in protein-detergent-phospholipid and detergent-phospholipid micelles. Initial removal of the detergent leads to the coalescence of both types of micelles, with further detergent depletion driving the protein to take part of the micellar-to-lamellar transition and spontaneously inserting into the forming bilayer. In the direct reconstitution method (also known as the “step-by-step” method) preformed liposomes are exposed to a critical amount of detergent followed by a micellar solution of protein [182]. At appropriate conditions, progressive removal of detergent results in direct insertion of transmembrane protein into detergent-

doped membrane bilayers. A third and hybrid mechanism at detergent concentrations intermediate of those needed for direct reconstitution and reconstitution via co-micellization is also observed and contains features from both mechanisms.

The mechanisms by which transmembrane proteins are reconstituted have been rationalized as part of a 3-stage model where the critical parameter is the relative amount of detergent above the critical micelle concentration (CMC) to the total lipid content (figure 3.1). This ratio, denoted R , is formalized by the expression [170]:

$$\frac{[D_{\text{total}}] - [D_{\text{water}}]}{[\text{lipid}]} = R \quad \text{eq. 3.1}$$

where $[D_{\text{total}}]$ and $[D_{\text{water}}]$ are the total detergent concentration and the detergent concentration in the water phase, respectively. In detergent/ lipid mixtures, $[D_{\text{water}}]$ is the number with most uncertainty, but is approximated by $[D_{\text{cmc}}]$.

For reconstitution by co-micellization, excess amounts of detergent are used for total solubilization (i.e. high R -values) while in direct reconstitution only non-solubilizing amounts of detergent sufficient for saturating liposomes are added (i.e. low R -values, referred to as the onset of solubilization [183]). At detergent levels in between those required for the onset and total solubilization, detergent micelles will partially and gradually solubilize liposomes and give rise to a two-phase system consisting of liposomes and micelles (called a “coexistence” phase [184]). Irrespective of at which stage the lipid/ detergent aggregates are found in, a key assumption and an integral part of the 3-stage reconstitution model is that liposome formation after detergent removal mirrors the opposite process that occurs during liposome solubilization [181]. Thus, knowledge of the different phases of the chosen liposome/ detergent mixtures is an important prerequisite to predict how the protein will be reconstituted.

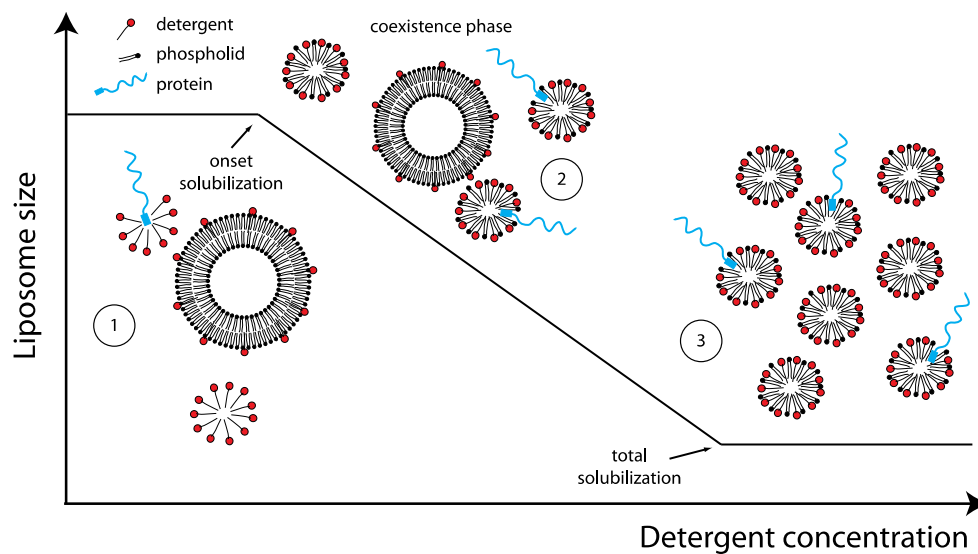


Figure 3.1: Detergent-mediated reconstitution of transmembrane proteins and schematic of the 3-stage model depicting the effect of the detergent concentration on the insertion mechanism and the size of the liposomes. (1) Above the critical micelle concentration (CMC) of a detergent, a transmembrane protein (blue) can be spontaneously and directly inserted into a liposome at or very near the onset of solubilization. Proteins inserted in this way will adopt the preferred right side-out orientation. (2) At detergent concentrations above the onset of solubilization, the detergent micelles begin to solubilize lipid bilayers, forming mixed detergent/phospholipid/protein micelles. These micelles act like delivery shuttles that fuse with the lipid-bilayer resulting in insertion of the transmembrane protein. The orientation of a protein inserted in this way is not asymmetric and may depend on the interactions between the protein and the membrane. (3) At total solubilization conditions, all liposomes are solubilized and their lipids present in mixed micelles. This co-micellization results usually in randomly-orientated transmembrane proteins once detergent is removed and liposomes are reformed. Adapted and modified from [170].

Before deciding on a reconstitution strategy for preparing large SNARE-liposomes, it was imperative to define what properties of a SNARE-liposome are most suitable for mechanistic studies. The first and most evident requirement is that SNARE-liposomes must be unilamellar and in the 80-500 nm range, preferably exhibiting a narrow size distribution. Second, the insertion efficiency must be close to 100 %, an important criterion for quantitative studies, for example, when investigating fusion kinetics of proteoliposomes containing different SNARE-density. Third, the orientation of the SNAREs should be preferentially asymmetric and in the right side-out direction, since SNAREs with their cytosolic domain pointing towards the interior of the liposomes would be inaccessible for SNARE complex formation. Finally, the method must contain some degree of repeatability both in terms

of the three previous criteria but also in terms of losses in phospholipids and SNAREs during the reconstitution procedure.

3.1.2 Strategy for SNARE reconstitution into large liposomes

Considering the above-mentioned criteria for large SNARE-liposomes, a strategy based on using the direct reconstitution method with *n*-octyl- β -D-glucoside as the detergent (hereby denoted OG) was pursued. The main reason for this was the better mechanistic prospects for preparing large SNARE-liposomes with optimal properties for fusion studies. This nonionic detergent is reportedly one of few that have been rigorously shown to reconstitute transmembrane proteins via the direct reconstitution mechanism, in contrast to detergents such as cholate and Triton X-100 [182].

Table 3.1 lists studies that have employed OG as the detergent for reconstituting neuronal SNAREs along with some of the reconstitution conditions and properties of SNARE-liposomes. To compare reconstitution conditions, R-values were calculated based on the OG and the total lipid concentrations used during the phospholipid/OG mixing step (regardless of whether the initial state of the lipids consisted of dried films or preformed liposomes). Even though all these studies used OG for the reconstitution of SNAREs, the properties of the resulting SNARE-liposomes were varied and seemed to depend on the OG concentration used. For instance, at comicellization conditions (i.e. high R-values), SNARE-liposomes were predominantly small (40-50 nm), while in one study that used conditions apt for direct reconstitution (i.e. low R-values) SNARE-liposomes were \sim 100 nm [145]. Furthermore, it is worthwhile to note that even in separate studies using identical solubilization conditions and lipid composition, considerable differences were observed with respect to orientation and insertion efficiencies [12, 154].

Due to the variable properties of SNARE-liposomes reconstituted by OG and following the suggestions by Rigaud and co-workers [170], a *de novo* procedure was undertaken to systematically explore the reconstitution behavior of SNARE-liposomes as a function of the R-value. Based on this

approach, SNARE-liposomes were characterized according to size, SNARE orientation and insertion efficiency at different OG concentrations.

Study	R-value	Size	Orientation	Insertion efficiency	Detergent removal	Lipid composition	Comments
[12]	R = 5.7	45 ± 15 nm by EM	70-80 %	10-40 %	Dilution followed by dialysis	POPC/DOPS (85/15)	Phospholipid loss: 50-80 %; standard
[154]	~R = 0.1	40-50 nm by DLS	100 %	N/A	Dialysis	DOPC/DOPE/SM/CH/DOPS (32:25:15:20:8)	-
[164]	R = 0.2-0.3	114 ± 3 nm by EM	N/A	N/A	Dialysis	Complex mixture of 8 lipids	Density gradient purification
[145]	R = 1.1 R = 5.7	40-100 nm by DLS	80-90 %	80-90 %	BioBeads & dialysis	POPC/DOPS (85/15)	Standard & direct method
[93]	N/A	~100 nm by EM	N/A	N/A	BioBeads & dialysis	POPC/DOPS (85/15)	Additional centrifugation step

Table 3.1: Some published reconstitution conditions for the OG-mediated reconstitution of neuronal SNARE-into liposomes. For studies where R-values were not explicitly mentioned, the CMC of OG was assumed to be 17 mM. Key: EM = electron microscopy; DLS = dynamic light scattering; POPC = palmitoyl oleoyl phosphatidylcholine; DOPS = dioleoyl phosphatidylserine; DOPE = dioleoyl phosphatidylethanolamine; SM = sphingomyelin; CH = cholesterol.

3.1.3 Orientation and insertion efficiency of reconstituted SNAREs

The first characterization of the orientation and insertion efficiency of large SNARE-liposomes was done with synaptobrevin (syb). For this, syb was purified in an OG solution and added to preformed liposomes together with appropriate amounts of additional OG. Four different R-values close to the onset of solubilization, including values corresponding to OG concentration below the CMC (~17 mM), were chosen to explore the orientation and insertion behavior around this point (figure 3.2).

In conditions below the CMC and near it ($R \approx -1$ and 0 , respectively) all syb was accessible to proteolytic cleavage by tetanus toxin (figure 3.2, left). However, more than 90 % of syb was found towards the bottom of the Nycodenz density gradient, while liposomes, observed as a turbid colorless layer, were at the top, indicating that in these conditions syb was not reconstituted and was probably present in aggregates (figure 3.2, right). Meanwhile, at higher R-values syb was found to increasingly co-float with liposomes at the top of the gradient, an effect that was concurrently followed with some syb (~40-50 %) being inaccessible to tetanus toxin in the absence of Triton X-100. These findings together suggest that syb is optimally inserted

into liposomes at an R-value of at least 1 and do so with no preference for a particular orientation.

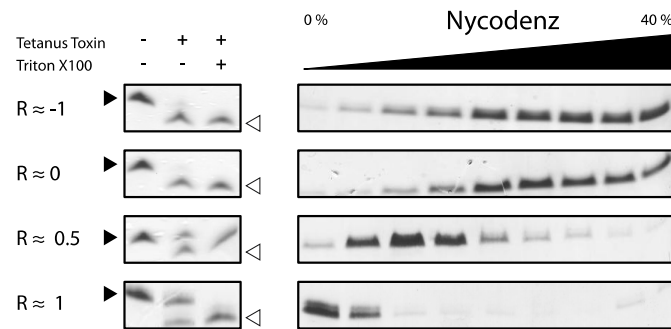


Figure 3.2: Orientation and insertion efficiency of syb incubated with large liposomes and OG at different R-values. Left: syb/liposome mixtures (nominal l/p of 200:1) were incubated with OG at the indicated R-values followed by dialysis. Mixtures were treated with tetanus toxin in the absence or presence of Triton X-100 and analyzed by SDS-PAGE for protein orientation. Filled arrowheads indicate the position of intact syb while open arrowheads correspond to cleaved product. Right: the same syb/liposome mixtures were separated by centrifugation on a Nycodenz gradient. Liposomes were observed in the top $\sim 40 \mu\text{L}$ and aliquoted fractions ($20 \mu\text{L}$) were analyzed by SDS-PAGE. Total lipid concentration was $\sim 6 \text{ mM}$ and dialysis was done with molecular weight cut-off 10 kDa .

Based on the results for the reconstitution of syb, a similar strategy for the characterization of the reconstitution of a Q-SNARE acceptor complex was attempted. Given that there are different types of Q-SNARE complexes, the 1:1 syntaxin SNAP-25 complex stabilized by a ΔN syb 49-96 fragment (hereby referred to as the ΔN syxH3-SN25 complex) was first studied as a model for other types (looked at later in more detail in section 3.2.1).

The ΔN syxH3-SN25 complex was first reconstituted at $R \approx 1$ (figure 3.3). Western blot analysis of the aliquoted fractions of the Nycodenz gradient revealed that the complex also co-floated with the liposomes, albeit over a wider range of densities than syb. However, incubation of the ΔN syxH3-SN25-liposome mixtures with trypsin suggested that the complex was reconstituted with an evident preference for right side-out orientation.

Further experiments confirmed the distinct reconstitution patterns of ΔN syxH3-SN25 and syb in large liposomes. Reconstitution of ΔN syxH3-SN25 at higher R-values did not considerably change the density profile as shown in figure 3.3, suggesting that OG-mediated reconstitution results in ΔN syxH3-SN25-liposomes that are less homogenous than syb. Furthermore, there was some variability in the extent of ΔN syxH3-SN25

complex digestion by trypsin in the absence of Triton X-100, but a consensus value of $\sim 90\%$ of ΔN syxH3-SN25 having the correct inside-out orientation was found to be a reasonable estimate (see appendix 6.1).

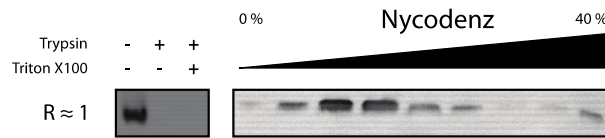


Figure 3.3: Orientation and insertion efficiency of ΔN syxH3-SN25 complex liposomes. Left: a ΔN syxH3-SN25/liposome mixture (nominal 1/p of 200:1) was incubated with OG at $R \approx 1$ followed by dialysis. The resulting mixture was treated with trypsin in the absence or presence of Triton X-100 and analyzed by Western blot and detection of SNAP-25 (CL 71.1). Right: the same ΔN syxH3-SN25/liposome mixture was floated on a Nycodenz gradient, aliquoted (20 μ L fractions) and analyzed by Western blot and detection of SNAP-25 (CL 71.1). Liposomes were observed to float predominantly in the top ~ 80 μ L of the gradient (from left). The total lipid concentration was ~ 4 mM and dialysis was done using a membrane of molecular weight cut-off 10 kDa.

3.1.4 Characterization of size distributions of SNARE-liposomes

To gain insights on how liposome size varies with different reconstitution conditions, all liposomes depicted in figures 3.2 and 3.3 were analyzed by field-flow-fractionation coupled to multi-angle laser light scattering (FFF-MALLS). As described in section 2.4.4, FFF-MALLS measures the relative number size distribution. The number size distribution of syb liposomes prepared at different R-values was compared to the size distribution of the original template liposomes (figure 3.4). This comparison revealed that at all tested conditions the size distribution shifted towards lower sizes. Interestingly, as R was increased from -1 to 1, liposomes with sizes at the higher end of the distribution became progressively depleted, resulting in an accumulation of liposomes with smaller diameters. This effect culminated with syb liposomes prepared at $R \approx 1$ adopting a narrower size distribution than the original template liposomes with $\sim 80\%$ of liposomes adopting geometric diameters between 70 and 120 nm.

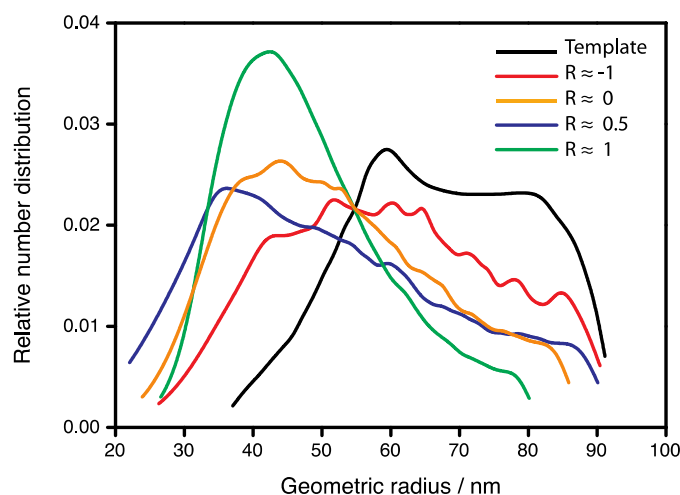


Figure 3.4: Size distributions of syb liposomes reconstituted with OG at indicated R-values compared to the original template distribution. Distributions were obtained by FFF-MALLS. Nominal lipid/protein ratio (l/p) was 200:1 for all syb liposomes.

The size distribution of ΔN syxH3-SN25 complex liposomes at nominal lipid/protein (l/p) of 200:1, on the other hand, exhibited a substantial increase in size compared to the template liposome size distribution (figure 3.5). However, increasing the l/p to 500:1 and 1000:1 resulted in size distributions resembling those of syb liposomes with their characteristic shift towards smaller sizes. This tendency for a broader size distribution at higher ΔN syxH3-SN25 density may reflect difficulties with precipitation of the complex at elevated concentrations or a higher propensity for SNARE-liposomes to fuse unspecifically during detergent removal.

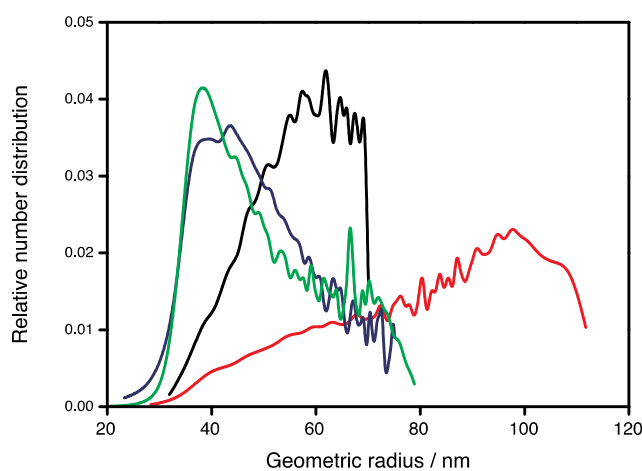


Figure 3.5: Size distributions of ΔN syxH3-SN25 complex liposomes at different SNARE densities obtained by FFF-MALLS. Template liposomes (black) are portrayed together with ΔN syxH3-SN25 liposomes of nominal l/p of 200:1 (red), 500:1 (blue) and 1000:1 (green). All reconstitutions were done at $R \approx 1$.

In this study, more than 500 SNARE-liposomes were prepared and characterized by FFF-MALLS. Although it is impractical to depict all of the size distributions here, a few general trends regarding the relationship between size and reconstitution conditions were found:

- For a given R-value greater than 1, the size distribution of all syb-liposomes reconstituted with OG was mostly invariant to lipid-protein ratio (l/p) and always had smaller average diameters with narrower size distributions than the template liposomes.
- For a given R-value between 1 and 2.5, ΔN syxH3-SN25 complex liposomes with l/p below 500:1 resulted in broader size distributions with a substantial proportion of liposomes adopting much larger diameters than the template. However, in a few cases these effects were minor. Above 500:1 size distributions became narrower and shifted towards smaller diameters until $\sim 1500:1$ when distributions converged and became independent of the density.
- As the R-value increased from 1 to 2.5, the size distribution of syb liposomes shifted towards larger sizes. At $R \approx 3$, size distributions exhibited a sudden and drastic shift towards large liposomes in the range of 150-300 nm.
- For R-values between 1 and 2, the size distribution of ΔN syxH3-SN25 complex liposomes changed somewhat unpredictably; either they were shifted towards smaller diameters or they appeared in the same range as that of the template. Reconstitutions at $R > 2$ were not attempted. In general, the effect of changing the l/p ratio in the range 200:1 to 500:1 had a greater effect on the distribution than the R-value.
- The repeatability of the size distributions of syb liposomes prepared from different template preparations was significantly better than that of ΔN syxH3-SN25 complex liposomes, probably due to the greater

sensitivity of the latter towards changes in l/p originating from uncertainty in the total lipid concentration of each preparation.

Importantly, regardless of the specific reconstitution conditions, size distributions of all SNARE-liposomes prepared in this way were almost always (>98 %) large, with distributions starting with liposomes with 70 nm diameters. The size of these large liposomes is graphically compared with that of liposomes prepared according to the co-micellization method more commonly used (figure 3.6).

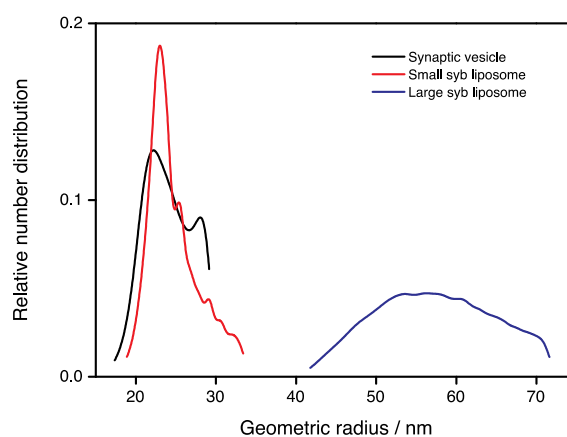


Figure 3.6: Examples of size distributions of syb liposomes prepared in this study. The size distribution of purified synaptic vesicles from rat brain (kindly provided by Dr. Nathan Pavlos) is shown as a reference. Distribution areas were arbitrarily normalized to 1.

3.1.5 OG removal and phospholipid loss

Another studied parameter was the procedure for removing OG from SNARE/lipid/OG mixtures. Detergent removal was initially based on dialysis using a membrane of molecular weight cut-off (MWCO) of 10 kDa. Electron microscopy imaging of OG-free template liposomes and dialyzed OG-associated liposomes did not reveal signs of detergent micelles, suggesting the dialysis procedure was effective (figure 3.7).

Phosphate analysis, however, revealed ~40 % of lipid contents were lost during this procedure (figure 3.8). Furthermore, the extent of the loss was not repeatable even among SNARE-liposomes prepared simultaneously. To overcome this, overnight dialysis was tried first with a MWCO of 2 kDa

followed by a second dialysis step using a MWCO of 10 kDa to ensure efficient removal of residual amounts of detergent. As shown in figure 3.8, this strategy reduced the lipid loss to ~20 % and allowed much more repeatable preparations. Electron microscopic analysis confirmed that this procedure was also effective in removing OG micelles and was therefore used for all subsequent experiments.

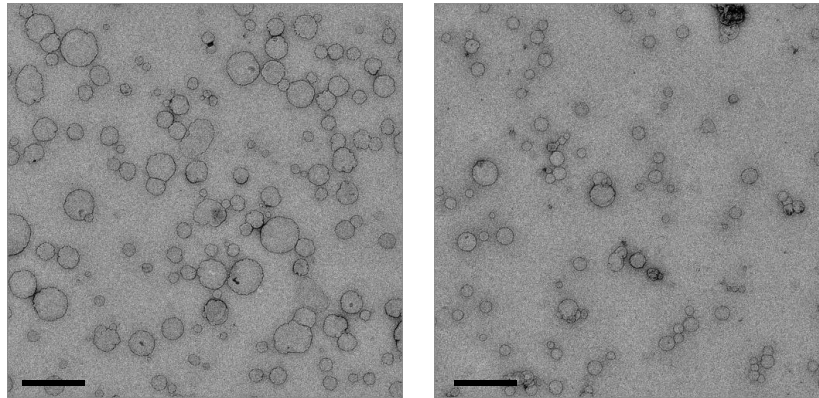


Figure 3.7: Negative staining electron microscopy of large unilamellar liposomes before (left) and after (right) incubation with OG and dialysis with a membrane of molecular weight cut-off 10 kDa. Bar: 500 nm. Images taken by Dr. Dietmar Riedel.

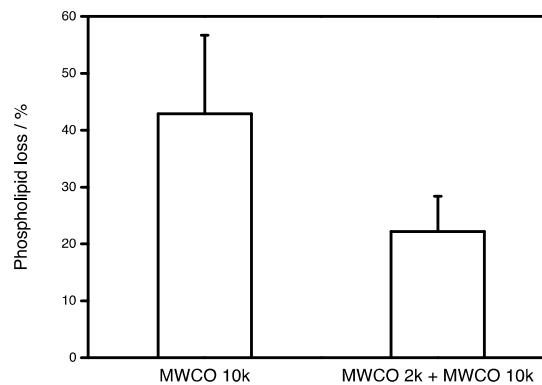


Figure 3.8: Quantification and comparison of phospholipid loss of SNARE/liposome/OG mixtures after overnight dialysis with a membrane of molecular weight cut-off (MWCO) 10 kDa (left) and 2 kDa followed by a second dialysis step (~3-6 h) with MWCO 10 kDa (right). In the former case the losses of 5 preparations were averaged while in the latter 9 preparations were taken into account. A combination of both R and Q-SNARE liposomes prepared on different days was used to better reflect the day-to-day variability of both procedures. Losses were calculated based on the phospholipid content of the extruded template liposomes prior to reconstitution.

3.2 Biochemical parameters affecting fusion-related properties of large SNARE-liposomes

As discussed in section 1.4.1, two essential criteria for membrane fusion of liposomes is the ability of lipids from both membranes to mix giving

rise to a new liposome with a larger size. Lipid-mixing has arguably become the most common way to study SNARE-mediated fusion of liposomes, while the importance of characterizing size changes has more recently been noted, although rarely have both processes been combined to elucidate mechanistic questions.

Throughout this section, the ability of SNAREs to mediate lipid-mixing of large liposomes is assessed using labeled phospholipids with the FRET pair NBD and Rhodamine in the dequenching mode (see section 2.4.1 for details). This is complemented with size distribution data obtained by FFF-MALLS (section 2.4.4), adding a new angle to the study of SNARE-mediated fusion of liposomes. By further correlating these with anisotropy-based binding assays, the first insights on the requirements and conditions for SNAREs to fuse large liposomes will be obtained.

3.2.1 Variations of the Q-SNARE acceptor complex

There are multiple ways in which reconstituted SNARE-mediated fusion has been studied and reported. A critical variable is the type of Q-SNARE acceptor complex used and how it is reconstituted. As reviewed in section 1.4.2, lipid-mixing between small SNARE-liposomes is dramatically accelerated only when a Q-SNARE acceptor complex is pre-assembled in the presence of syb 49-96 [103]. This ΔN syb fragment locks the syntaxin·SNAP-25 binary complex into a stable 1:1 configuration and prevents the formation of a “dead end” 2:1 complex, which are unavailable for trans SNARE complex formation. The tendency for the syntaxin·SNAP-25 complex to adopt a 2:1 configuration *in vitro* can explain why most reconstituted studies until then had only reported moderate fusion kinetics (hour time-scale), although this explanation is not universally accepted and continues to be controversial.

Another variable concerning the type Q-SNARE complex is the Habc domain of syntaxin. This N-terminal domain is essential for the availability of the SNARE motif of syntaxin and is regulated via its interaction with SM proteins (discussed in section 1.3.3.1). Exclusion of this domain from the Q-

SNARE complex accelerates lipid-mixing 2-3 fold [148], and some studies thereafter have employed the N-terminally truncated version of the syntaxin-SNAP-25 acceptor complex.

In order to establish how these biochemical parameters affect fusogenic properties of large liposomes, four different Q-SNARE complexes were assembled. These included the syb 49-96 stabilized complex containing N-terminally truncated syntaxin (abbreviated as the “ Δ N syxH3-SN25” complex), as well as the complex assembled without the Δ N syb fragment denoted simply as the “syxH3-SN25 complex”. Additionally, complexes with full-length syntaxin containing the Habc domain were assembled with and without stabilization by syb 49-96 (“ Δ N syxFL-SN25 complex” and “syxFL-SN25 complex”, respectively).

The four Q-SNARE complexes were reconstituted into large liposomes at an intermediate density (nominal l/p ~500:1) and mixed with syb RHO/NBD-labeled liposomes. A sustained increase in NBD fluorescence was exhibited by the Δ N syxH3-SN25 and the Δ N syxFL-SN25 complexes but not by syxH3-SN25 and syxFL-SN25 liposomes (figure 3.9). Furthermore, lipid-mixing stimulation by Δ N syxH3-SN25 was approximately twice as much as that mediated by the Δ N syxFL-SN25 complex. However, evaluation of the insertion efficiency of both complexes revealed that ~30-40 % of the Δ N syxFL-SN25 complex was not reconstituted (figure 3.9, right). Apart from this difference, the disparities in lipid-mixing kinetics between all other complexes cannot be explained by differences in SNARE orientation and insertion efficiency.

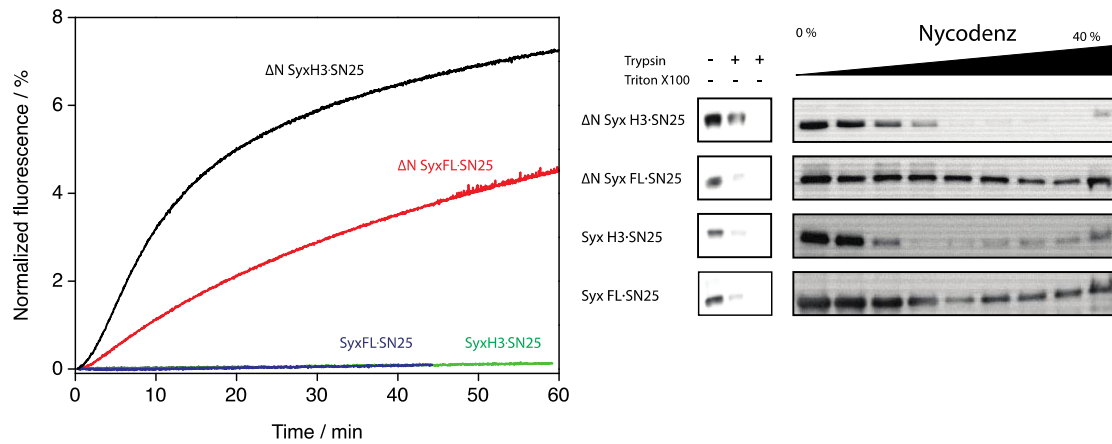


Figure 3.9: Effect of the type of Q-SNARE complex on SNARE-mediated lipid-mixing of large liposomes. Left: syb RHO/NBD liposomes (10 μ L) of nominal l/p \sim 500:1 were mixed with four different Q-SNARE complex liposomes as (15 μ L). Corrected l/p ratios for these proteoliposomes were 700:1 (black), 750:1 (red), 500:1 (blue) and 950:1 (green). Right: Nycodenz density gradient co-floatation and trypsin digestion analysis of Q-SNARE liposomes evaluated by SDS-PAGE and western blot analysis. Blots were immunostained for detection of SNAP-25 (CI 71.1, Synaptic Systems).

To evaluate whether lipid-mixing activities correlated with changes in liposome size, the size distribution of the four reactions was determined by FFF-MALLS after 60 min of incubation (figure 3.10). In addition, the size distributions of control reactions containing excess syb 1-96 were determined as both a control and a reference for evaluating the proportion of liposomes that increased in size. Weight distribution analysis revealed that both stabilized ΔN syxH3-SN25 and ΔN syxFL-SN25 complexes induced significant changes to the size distribution, while the distributions of the reactions with syxH3-SN25 and syxFL-SN25 were practically indistinguishable from controls.

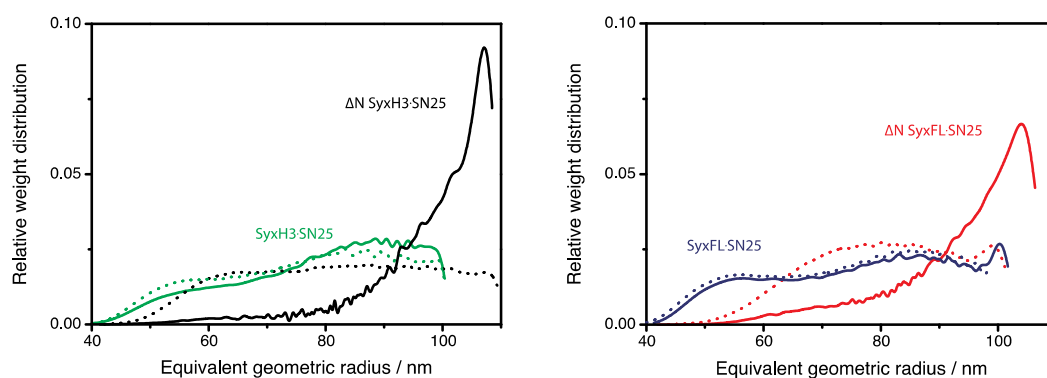


Figure 3.10: Weight size distributions of different liposome fusion reactions mediated by four different Q-SNARE acceptor complexes. The Q-SNARE complexes are the same as those depicted in figure 3.9, including the concentrations used. Distributions in solid line are the size distributions after 1 h of reaction, while those in dot representation are the control and reference distributions obtained by adding syb 1-96 (2 μ M).

Having looked into the ability of the four complexes to affect two important indicators of fusion, the syb binding ability of the four Q-SNARE complexes was assessed in order to determine whether it correlated with lipid-mixing and size increase behaviors. For this a cysteine mutant of the cytosolic domain of syb (1-96) was labeled on position 28 with an Alexa488 fluorophore (abbreviated syb 1-96^{C28Alexa488}) and mixed with the four different Q-SNARE complex liposomes. The increase in anisotropy revealed that ΔN syxH3-SN25 and ΔN syxFL-SN25 complexes exhibited syb binding kinetics with a time constant of $t_{1/2} \approx 7$ s (figure 3.11), while addition of syxH3-SN25 and syxFL-SN25 liposomes to syb 1-96^{C28Alexa488} had only a marginal effect on anisotropy and only slowly increased over a 1 h period (not shown).

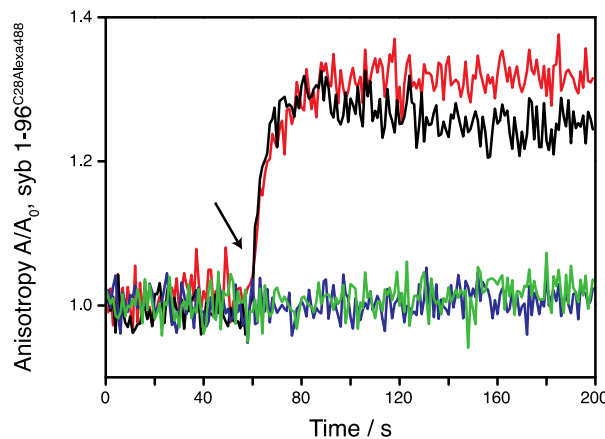


Figure 3.11: Syb binding kinetics on four different types of Q-SNARE complex liposomes measured by anisotropy. The same ΔN syxH3-SN25 (black), ΔN syxFL-SN25 (red), syxH3-SN25 (green) and syxFL-SN25 (blue) liposomes from figure 3.9 (15 μ L, total Q-SNARE complex concentration ~ 75 nM) were added to syb^{C28Alexa488} (~ 200 nM, marked by an arrow, see text for further details). The increase in anisotropy (A) relative to the initial anisotropy (A_0) is shown.

These results show that stabilization of the Q-SNARE acceptor complex is a basic requirement for lipid-mixing and further emphasizes the need to use ΔN syb as a means of bypassing unavailable Q-SNARE acceptor complexes. Still, it is worthy to make note that the inclusion of the Habc domain on the stabilized acceptor complex slows down lipid-mixing kinetics, which could be

partly explained by the lower efficiency of insertion of Habc-containing Q-SNARE complexes.

To quantitatively evaluate the effect of the Habc domain on lipid-mixing kinetics, Alexa488-labeled full-length syb (syb 1-116^{C28Alexa488}) was reconstituted into large liposomes. The increase in anisotropy after mixing with Q-SNARE liposomes reflects the formation of SNARE complexes during liposome fusion, showing that ΔN syxH3-SN25 complex liposomes formed approximately twice as many SNARE complexes as ΔN syxFL-SN25 liposomes (figure 3.12, left). These same Q-SNARE liposomes were then added to syb RHO/NBD liposomes and their lipid-mixing profiles normalized to the SNARE complex formation traces, yielding a relative quantitative parameter reflecting the amount of lipid-mixing contributed by each SNARE complex formed (figure 3.12, right). Combined with all other observations in this section, this analysis suggests that the Habc domain of syntaxin does in fact have an intrinsic inhibitory effect on the ability for SNAREs to mediate lipid-mixing despite identical syb binding kinetics (figure 3.11).

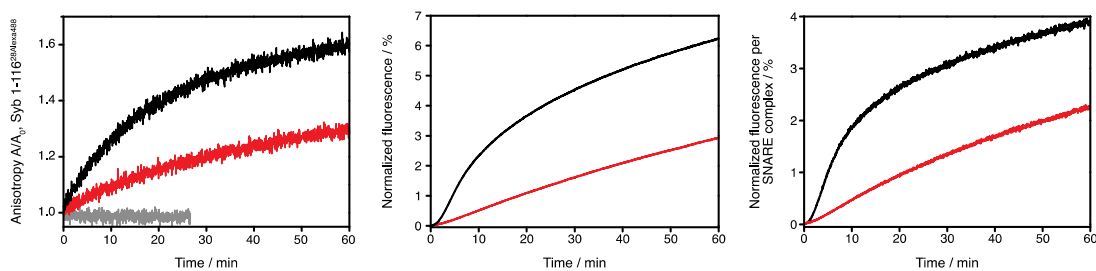


Figure 3.12: Comparative kinetics of SNARE complex formation and lipid-mixing during a liposome fusion reaction between syb liposomes and stabilized Q-SNARE complex liposomes without (ΔN syxH3-SN25) or with (ΔN syxFL-SN25) the Habc domain of syntaxin. Left: syb 1-116 labeled at position 28 with an Alexa488 fluorophore was reconstituted in unlabeled large liposomes (10 μ L) and mixed with 15 μ L of ΔN syxH3-SN25 (black) and ΔN syxFL-SN25 (red) liposomes (1/p = 500:1). The increase in anisotropy was inhibited in the presence of unlabeled syb 1-96 (~ 2 μ M, grey). Center: lipid-mixing kinetics of the same Q-SNARE liposomes used on the left added to syb RHO/NBD liposomes of 1/p = 500:1. Right: calculation of lipid-mixing on a per SNARE complex basis calculated by normalizing the lipid-mixing traces (center) by the corresponding anisotropy traces (left).

3.2.2 Kinetic influence of ΔN synaptobrevin displacement from stabilized Q-SNARE complexes

A prominent feature of the lipid-mixing profile of a fusion reaction mediated by stabilized Q-SNARE acceptor complexes is an initial delay in the beginning of fusion (see for example figures 3.9). This delay is accentuated in large SNARE-liposomes as their SNARE density is progressively decreased (figure 3.13, see also appendix 6.2 and 6.3), imparting the lipid-mixing traces with a characteristic sigmoidal shape comprising two parts: an initial lag phase lasting ~ 2 -3 min where a build-up of the instantaneous rate of lipid-mixing occurs, followed by a longer plateau phase where the instantaneous rate monotonically approaches zero.

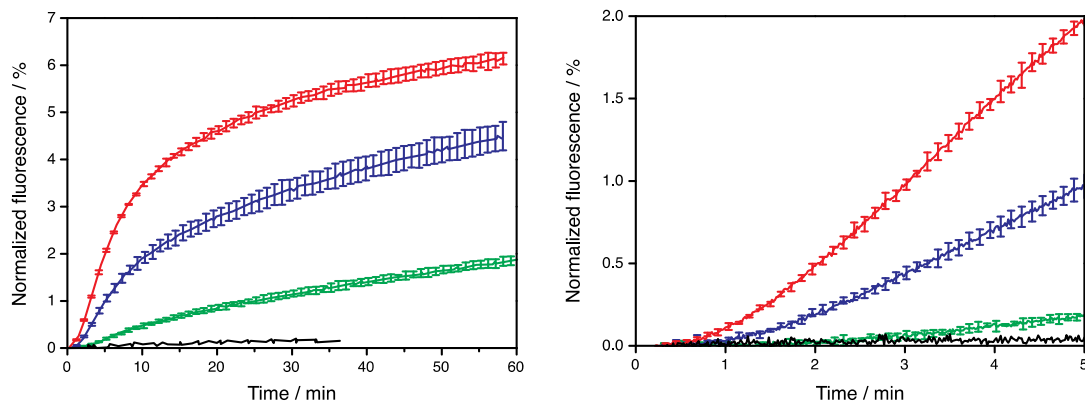


Figure 3.13: Lipid-mixing kinetics of large SNARE-liposomes at varying SNARE density. Left: syb RHO/NBD liposomes (10 μ L) were mixed with ΔN syxH3-SN25 complex liposomes (10 μ L) with nominal l/p of 250:1 (red), 500:1 (blue) and 1500:1 (green). Syb 1-96 (2 μ M) was added to the reaction mixture of l/p 250:1 (black), with similar inhibition observed at lower densities (not shown). Estimates of actual l/p which takes into account phospholipid losses and SNARE orientation were 450:1 (red), 1050:1 (blue), 2950:1 (green) for synaptobrevin and 300:1 (red), 600:1 (blue) and 1750:1 (green) for ΔN syxH3-SN25 complex liposomes. Right: close-up of the first 5 min of lipid-mixing depicting the extended lag phase as SNARE density is decreased.

Sigmoidal-like kinetic profiles such as these are typically indicative of hidden steps that precede the biochemical step that is being measured; in this case, membrane merging. Two scenarios are conceived that could result in a delay in lipid-mixing and give rise to a lag phase: 1) trans SNARE complex formation does not begin immediately upon mixing of R and Q-SNARE liposomes but instead exhibits a retardation in the recruitment of parallel R and Q SNAREs which delays the onset of fusion or 2) the prevalence of a

long-lived transient docking state mediated by trans SNARE complex formation but preceding membrane fusion.

To evaluate the first scenario, syb 1-116^{C28Alexa488} was reconstituted into large liposomes and added to ΔN syxH3-SN25 complex liposomes. Anisotropy of syb 1-116^{C28Alexa488} increased immediately after mixing, indicating that trans SNARE complex formation begins with no delay (figure 3.14). This finding rules out the possibility that the lag phase is caused by a delay in the initiation of SNARE complex formation.

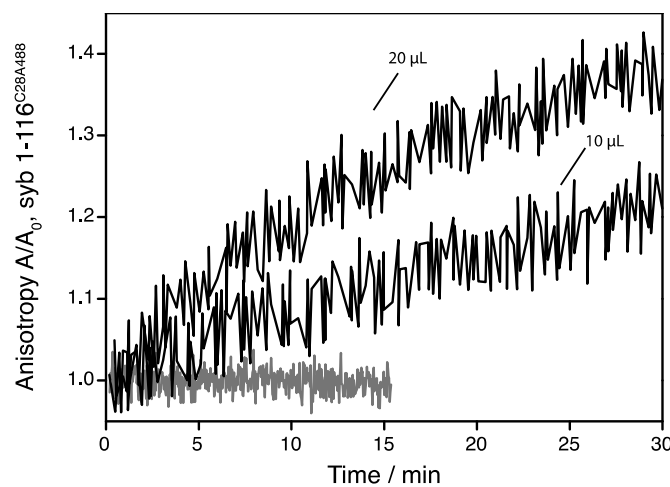


Figure 3.14: Kinetics of SNARE complex formation during a liposome fusion reaction monitored by anisotropy. Synaptobrevin 1-116 labeled at position 28 with an Alexa488 fluorophore was reconstituted in unlabeled large liposomes. ΔN syxH3-SN25 liposomes (10 and 20 μL) were added to Syb1-116^{28A488} liposomes (10 μL) both with nominal I/p of 500:1. The reaction was inhibited by excess unlabeled soluble syb (grey).

To confirm that liposomes were undergoing docking as would be expected during trans SNARE complex formation, FFF-MALLS was used to look at changes in the size distribution of the entire ensemble of SNARE-liposomes during the first minutes. For this a fusion reaction was quenched after 30 s by adding excess syb 1-96, effectively preventing new SNARE complexes from forming but allowing SNARE complexes that had already begun assembling to continue. Comparing the initial and quenched size distributions demonstrates a shift of the size distribution towards larger sizes (figure 3.15, left). Since no lipid-mixing signal was detectable prior to addition of syb 1-96 (figure 3.15, right), the increase in size strongly suggests

liposomes proceeded through a docked state for at least a few seconds before fusing.

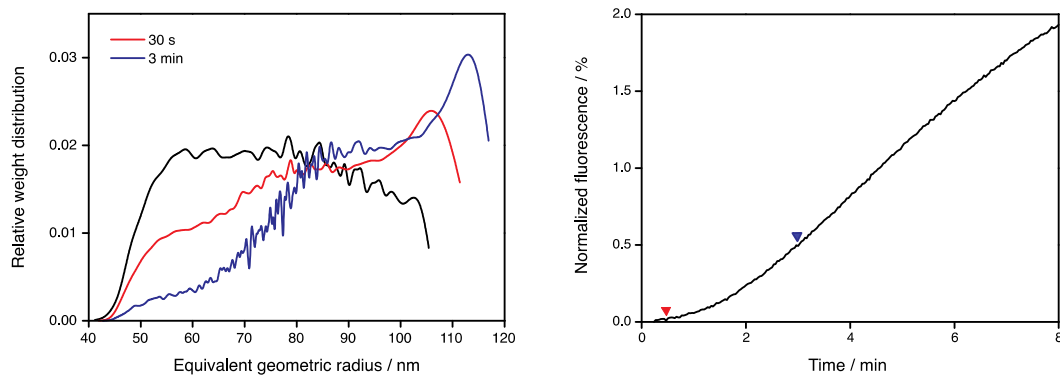


Figure 3.15: Size distributions of the first minutes of a liposome fusion reaction obtained by FFF-MALLS (section 2.4.4). The reaction consisted of syb RHO/NBD liposomes (10 μ L, nominal 1/p = 500:1) mixed with Δ N syxH3-SN25 liposomes (15 μ L, nominal 1/p = 500:1). Left: the starting weight size distribution (black) of both syb and Δ N syxH3-SN25 complex liposomes with pre-incubated syb 1-96 (2 μ M) and the arrested distributions quenched by syb 1-96 (2 μ M) at the indicated time points. Right: the lipid-mixing trace of the same reaction with the indicated points of addition of syb 1-96.

To determine what is the molecular cause of this prolonged docked state, both the binding of syb to the Δ N syxH3-SN25 complex and the displacement of the Δ N syb 49-96 fragment were postulated to be two steps that could slow down N to C-terminal nucleation of the SNARE complex and thus extend the docking lifetime. For this both steps were tested for how sensitive their kinetics were towards temperature to evaluate whether activation energies were comparable to thermal energies.

To assess syb binding, syb 1-96^{C28Alexa488} was added to Δ N syxH3-SN25 complex in solution and the anisotropy measured in the range 20-30 $^{\circ}$ C (figure 3.16). The kinetics remained unchanged with $t_{1/2} \approx 7$ s throughout this temperature range, showing that the activation energy for binding is below the surrounding thermal energy and therefore does not constitute a high-energy barrier.

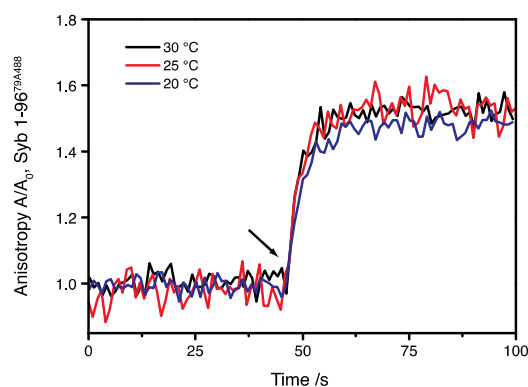


Figure 3.16: Effect of temperature on binding kinetics of syb to the ΔN syxH3-SN25 complex monitored by anisotropy. ΔN syxH3-SN25 acceptor complex (~ 400 nM) was added to soluble syb 1-96 labeled at position 28 with an Alexa488 fluorophore (~ 200 nM) at the indicated temperature. The addition point is marked and experiments were done in a 50 mM OG solution.

To assess displacement, a ΔN syxH3-SN25 complex containing a syb 49-96 fragment labeled at position 79 with Alexa488 (syb 49-96^{C79}Alexa488) was used to follow displacement kinetics, this time monitoring the decrease in anisotropy as the labeled fragment is removed from the complex. The reaction was started by adding 10-fold excess unlabeled syb 1-96, and the anisotropy immediately decreased with decay kinetics with a rate constant of 13.6 ± 0.9 s⁻¹ at 30 °C (figure 3.17, black curve). Unlike binding, displacement was considerably slowed down by temperature, suggesting this step comprises a significant energy barrier. An Arrhenius plot of the kinetic constants in the temperature range 15-30 °C reveals that the activation energy for displacement is in the range 57 - 78 kJ·mol⁻¹ (95 % confidence interval).

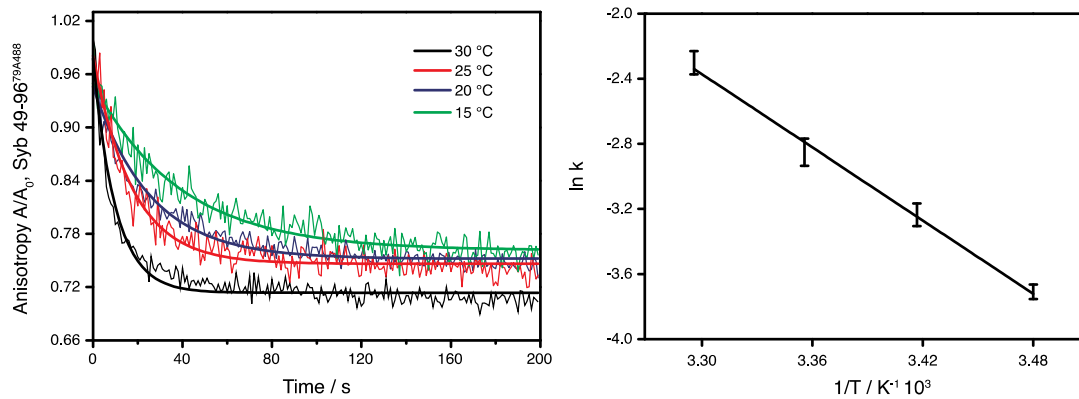


Figure 3.17: Temperature effect on the displacement kinetics of syb 49-96 from the ΔN syxH3-SN25 complex measured by anisotropy. Left: ΔN syxH3-SN25 complex (~ 200 nM in 50 mM OG solution) stabilized by a syb 49-96 fragment labeled at position 79 with an Alexa488 dye (syb 49-96^{79A488}) was displaced with ~ 10 -fold excess full-length syb at the indicated temperature. Curves were fitted with a mono-exponential decay function (solid lines). Right: Arrhenius plot of the 95 % confidence intervals of the decay rate constants (k) determined from the fittings.

To test the hypothesis that the high activation energy needed for syb 49-96 displacement prolongs the docking lifetime and consequently affects lipid-mixing kinetics, two experiments were designed. The first consisted of measuring lipid-mixing kinetics at different temperatures, the prediction being, given the high activation energy, that the kinetic profile should be considerably affected. This was indeed found to be the case, with the lag-phase in the lipid-mixing trace at 37 °C being approximately 1 min shorter than at 30 °C, while at 20 °C the lag phase was extended by ~ 4 min (figure 3.18).

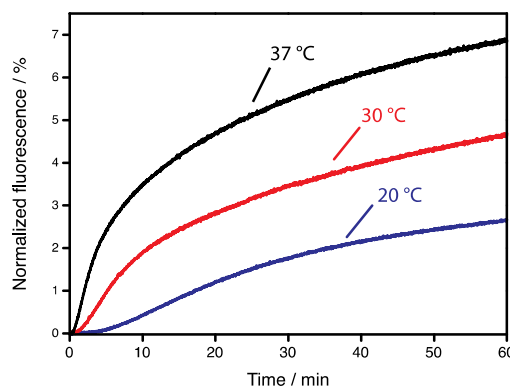


Figure 3.18: Effect of temperature on the lipid-mixing of large SNARE-liposomes. Lipid-mixing traces of syb RHO/NBD liposomes (10 μ L) mixed with ΔN syxH3-SN25 complex liposomes (10 μ L) at the indicated temperatures.

An additional and more definitive test consisted of evaluating the effect of varying ΔN syb fragment lengths on lipid-mixing kinetics

(figure 3.19). For this complexes stabilized by the C-terminal fragments syb 45-96, 49-96, and 53-96 were assembled and compared (syb 56-96 was initially included but was not able to form a complex probably because stabilization beyond the central 0 layer is required to lock the 1:1 syntaxin·SNAP-25 configuration). As would be expected based on thermodynamic considerations, the Q-SNARE acceptor complex stabilized by syb 53-96, which contains one less stacked layer than syb 49-96 (section 1.3.2), exhibited a substantially shorter lag phase (< 30 s). Conversely, adding an extra layer of stability to the ΔN syxH3·SN25 complex prolongs the lag phase (> 1.5 min), although not as substantially as the effect produced by shortening it.

To discard the possibility that the different lag phases are due to acceptor complexes binding to syb with different kinetics, syb 1-96^{C28Alexa488} binding to the four complexes was measured (figure 3.19, right). Although some variability in the kinetics was observed (the difference between the fastest and slowest being $t_{1/2} \approx 8$ s), the disparate lipid-mixing traces of the complexes are unlikely to be explained by these minor differences in syb binding.

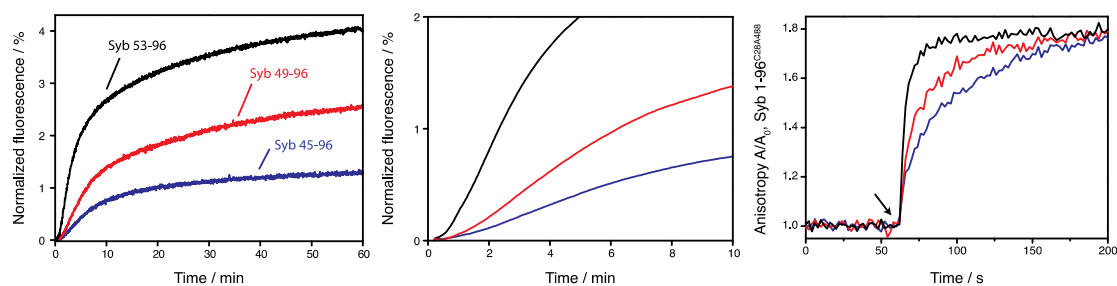


Figure 3.19: Effect of fragment displacement length on the lipid-mixing of large SNARE-liposomes. Left: lipid-mixing traces of syb RHO-PE/NBD-PS liposomes (15 μ L) mixed with ΔN syxH3·SN25 complex liposomes containing the indicated ΔN syb fragments (20 μ L). Center: close-up of the lipid-mixing traces showing the effect on the lag phase. Right: syb 1-96^{C28Alexa488} binding kinetics. ΔN syxH3·SN25 complex liposomes (20 μ L, estimated complex concentration ~ 60 nM) were added to syb 1-96^{C28Alexa488} (~ 40 nM). Color coding is the same as in the lipid-mixing traces and nominal l/p were 500:1 for all liposomes used.

3.3 Visualization and analysis of putative products and intermediates in the SNARE-mediated fusion pathway

The results presented in section 3.2 support the view that the stabilization of the Q-SNARE complex into a 1:1 configuration is essential for

SNARE complex formation and lipid-mixing of large liposomes. Furthermore, several lines of evidence implicates the displacement of the ΔN syb fragment from the ΔN syxH3-SN25 as an energetically costly step that gives rise to a transient meta-stable docking state which delays the initiation of fusion.

The effect of displacement on lipid-mixing kinetics is substantial and can be appreciated by modeling lipid-mixing kinetics with a simple two-step sequential model (figure 3.20). Although the model does not describe the lipid-mixing profile exactly, it can be fitted in a way that qualitatively describes its biphasic character, and reveals a long-lived docking step ($\tau_{\text{dock}} \approx 200$ s) and a fusion step ($\tau_{\text{fusion}} \approx 800$ s). Thus, docking and fusion in this system can be kinetically resolved, and can be exploited to investigate transitions from docking to fusion. In the following sections experiments are devised to take advantage of this property and gain novel insights on putative fusion intermediates.

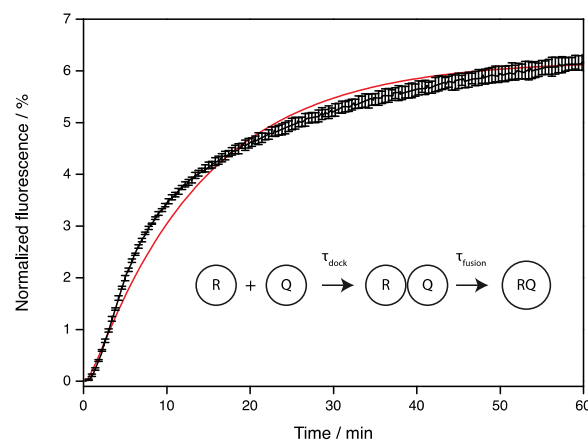


Figure 3.20: Kinetic modeling of lipid-mixing kinetics based on a two-step mechanism. Same lipid-mixing profile from figure 3.13 (black, average of three traces) and best fit line (red) derived from the phenomenological kinetic model shown using numerical integration. Best-fit parameters were found to be $\tau_{\text{dock}} \approx 200$ s and $\tau_{\text{fusion}} \approx 800$ s.

3.3.1 Ultrastructural identification of docked and hemifused liposomes

A first attempt at looking at fusion intermediates was done with negative staining electron microscopy (appendix 6.4). Although these images initially showed the first visual evidence for docking, it was difficult to reproduce the quality and consistency of the staining, preventing the application of appropriate controls.

To overcome these issues, rapid plunge freezing in liquid ethane and cryo-EM analysis was attempted. As predicted, many liposomes captured during the first three minutes of the reaction were found to be in a docked state (figure 3.21). Docking could be broadly distinguished by three ultrastructural criteria: 1) a proximity criteria where two membranes in the planar projection were separated by 8 nm or less; 2) by a contact criteria where opposing bilayers clearly appeared tightly or loosely juxtaposed onto one another and 3) by an extended contact criteria where lumina appeared connected via a flat constricted perimeter whose bilayer(s) could not be clearly distinguished without enhanced magnification (figure 3.22).

In some cases, juxtaposed bilayers appeared slightly bent or flattened onto each other, suggesting a pulling force was being exerted on them (figure 3.21, B-C and F). Contact between membranes was not always a strict requirement for bending; it could also be seen occurring between two liposomes within ~2-4 nm of each other (figure 3.21, D-E). Docked liposomes were considerably more difficult to find in the presence of excess amounts of syb 1-96 or when only R or Q-SNARE liposomes alone were analyzed, suggesting that docking was a result of a specific SNARE-mediated action.

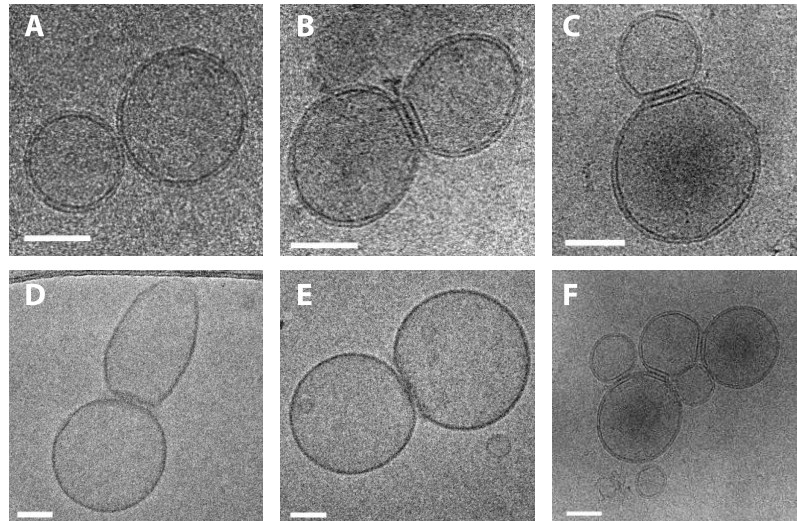


Figure 3.21: Ultrastructural identification and classification of docked SNARE-liposomes according to proximity and bilayer contact criteria. Syb and ΔN syxH3-SN25 complex liposomes (nominal $l/p = 500:1$) were mixed and plunge frozen in liquid ethane within the first 3 min. Liposomes were seen docked as evidenced by small (A) and extended (B and C) contact regions. Occasionally, closely opposed liposomes exhibited bending despite the fact a water cleft separated the membranes (D and E). Multiple-docked liposomes were also observed (F). Bar = 50 nm. Images taken by Dr. Dietmar Riedel and Elmar Behrmann.

Closer inspection of the ring-like membranous structure at its projected vertices reveals that its thickness is identical to that of the bilayers of the constituent liposomes, demonstrating that the lumina are separated by only one bilayer and therefore that they are not strictly docked but are actually in a hemifused state (figure 3.22 A-C).

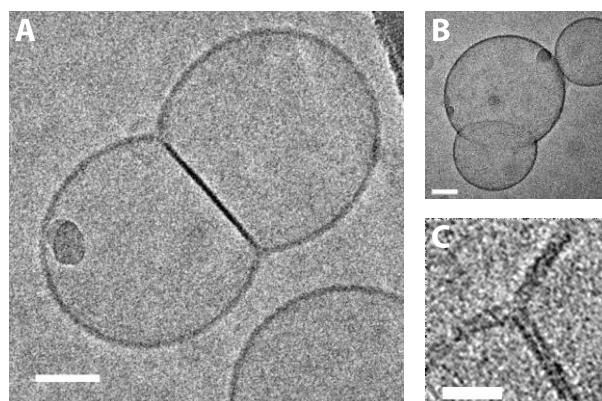


Figure 3.22: Ultrastructural identification of hemifused SNARE-liposomes during the initial stages of a fusion reaction. Syb and ΔN syxH3-SN25 complex liposomes (nominal $l/p = 500:1$) connected by a ring-like membranous structure as seen from a side-on (A) or tilted (B) view were found to be in a hemifused state, as judged by closer magnification of the vertices (C) depicting only one bilayer separating both lumina. Bar = 50 nm except for C which is 20 nm. Images taken by Dr. Dietmar Riedel.

To evaluate the abundance of free, docked and hemifused liposomes at the different stages of a fusion reaction, snapshots were taken by rapid-freezing samples at ~1, 3 and 60 min and the different states counted (figure 3.23, left). Additionally, the proportion of liposomes that were docked according to a proximity criteria (< 8 nm) or by bilayer-bilayer contact was accounted for (figure 3.23, right). This qualitative analysis reveals an ever-increasing presence of docked liposomes with bilayer-bilayer contacts during the reaction; a rather surprising result given the expectation that fused liposomes would drive the population of docked liposomes to progressively decline.

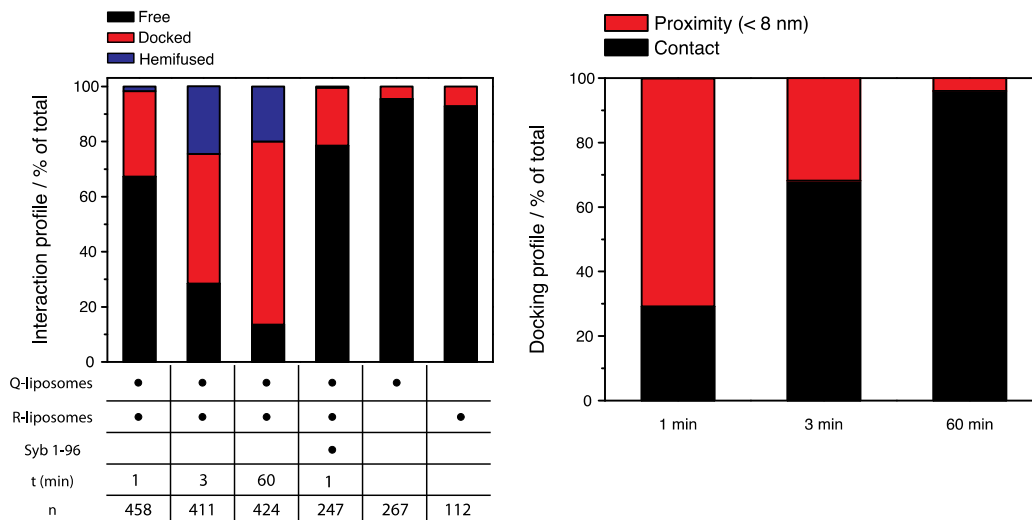


Figure 3.23: Time-dependent statistical counting of the interaction profile of large SNARE-liposomes constructed from cryo-EM. Syb and ΔN syxH3-SN25 complex liposomes (nominal l/p = 500:1) were mixed and samples plunge-frozen at 1, 3 and 60 min. Left: the proportion of free, docked or hemifused liposomes were counted together with appropriate controls. Right: docked liposomes were further classified according to a proximity or bilayer contact criteria.

3.3.2 Hemifusion as an alternative outcome to fusion

The high levels of hemifusion observed by cryo-EM after 60 min give rise to the question of whether they constitute an on-pathway intermediate or if they represent an alternative outcome to fusion caused by a yet unknown mechanism. At a first glance, the comparable levels of hemifusion at 3 and 60 min may suggest they constitute an off-pathway dead-end that accumulates during the reaction. However, it must be noted that cryo-EM analysis provides only a snapshot of the reaction for a given time, the absence

of dynamic information preventing a sequence of temporal events to be accurately made. The *proportion* of hemifused liposomes at any given time is determined both by its rate of formation and depletion (i.e. lifetime), but also indirectly by the amount of undocked/free liposomes which in turn is affected by fusion. In the absence of further knowledge on how these processes affect the proportion of hemifusion, it is not possible to ascertain precisely whether hemifused liposomes observed during the lag phase are genuine on-pathway intermediates caught in the act of fusion or whether they represent dead-end products which accumulate and are later observed at 60 min.

To clarify and understand the nature of the hemifusion state, the reducing agent dithionite was used to discriminate between total and inner leaflet lipid-mixing. Dithionite reduces the nitro functional group of NBD into an amine derivative that interrupts the conjugated electron ring, eliminating all fluorescence [185]. To ensure that the dequenching signal of dithionite-treated NBD-labeled liposomes truly reflects the mixing of the inner leaflet during fusion, the NBD-lipid probe must have a very low rate of translocation or “flip-flop” across the membrane bilayer. Because of this NBD-labeled PS is preferred over NBD-PE, owing to its 100-fold slower rate of translocation in PC membranes [186]. In order to find the right conditions and optimize the use of dithionite, syb RHO-PE/NBD-PS liposomes were prepared and a range of concentrations of dithionite tested.

As can be seen in figure 3.24, a sudden drop in NBD fluorescence is seen at the moment of dithionite addition. As the fluorescence signal declined to ~50 % of the initial value, the rate of dequenching rapidly plateaued out, indicating reduction of NBD was approaching completion (figure 3.24, left, black curve). The exact amount of dithionite used was found to be critical for the stability of NBD signal, as relatively small variations caused the signal to decrease rapidly towards zero probably due to inward leakage of dithionite (figure 3.24, left, red curve). Dithionite concentration was therefore optimized for each separate experiment. Confirmation of complete reduction of outer

leaflet NBD-PS was checked by using the membrane pore-forming peptide melittin [156], which demonstrates that enough dithionite is added to reduce both outer and inner leaflet NBD (figure 3.24, right).

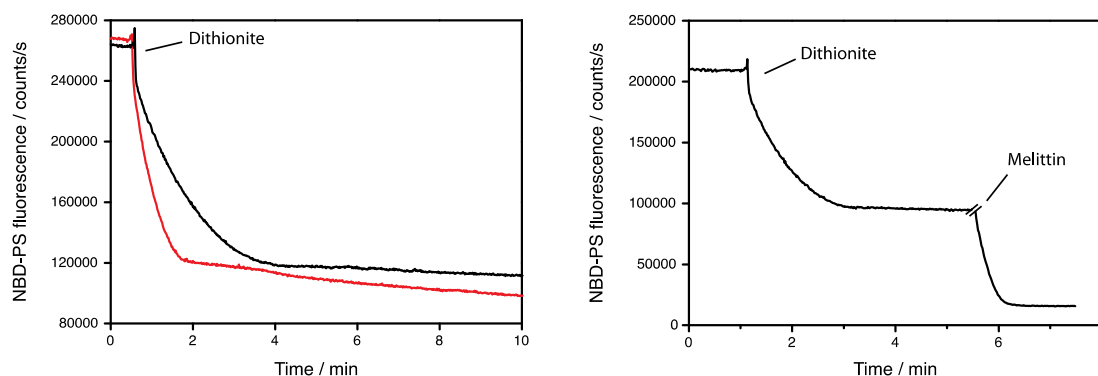


Figure 3.24: Quenching of outer monolayer NBD fluorescence on large syb RHO-PE/NBD-PS liposomes by dithionite. Left: a freshly-prepared dithionite solution was added to syb RHO-PE/NBD-PS liposomes (total lipid concentration $\sim 60 \mu\text{M}$). At concentrations of 1 mM dithionite (red) fast quenching of NBD fluorescence is observed but its signal is unstable after reaching a plateau at ~ 2 min, indicating that too much dithionite was added. Reducing the dithionite amounts by $\sim 20\%$ translates into a more stable fluorescence signal (black). Right: after addition of dithionite and a few minutes after fluorescence stabilization, melittin ($\sim 1.8 \mu\text{M}$) was added at the indicated point. The formation of pores on the membrane bilayer by melittin causes dithionite to diffuse through to the lumen and quench NBD fluorescence on the inner leaflet monolayer, confirming that saturating levels of dithionite were used.

To obtain both the total and the inner leaflet mixing profiles of a reaction, the total lipid-mixing profile was first measured using the standard procedure. For inner leaflet mixing, a previously optimized amount of dithionite was added to a separate reaction to quench outer leaflet fluorescence. After a 30 min signal stabilization period the reaction was initiated by adding unlabeled ΔN syxH3-SN25 complex liposomes. The inner leaflet lipid-mixing trace was normalized to the maximum fluorescence signal of the total lipid-mixing trace, and both profiles compared on the same graph (figure 3.25, left). The first derivative of these curves revealed both total and inner leaflet lipid-mixing shared similar mechanistic features and were mostly synchronized, indicating an intermediate involving a sequential merging of outer and then inner leaflets could not be resolved within the time resolution of the measurement (figure 3.25, middle).

Assuming the total amount of lipid-mixing is a result of full fusion, the expected amount of inner leaflet mixing was calculated by multiplying the

total lipid-mixing curve by the ratio between the fluorescence signal before and after dithionite addition (~42 %, figure 3.25, dashed curve). The difference between expected and actual inner leaflet mixing diverged during the course of the reaction until inner leaflet approached ~70 % of the expected assuming full fusion conditions. The remaining 30 % of the “lost” signal corresponds to liposomes that encountered lipid-mixing only on the outer leaflet, an operational definition of hemifusion. The increasing difference between expected and observed inner leaflet lipid-mixing throughout the reaction is interpreted as an accumulation of hemifused liposomes, supporting the view hemifusion constitutes a dead-end and is an alternative outcome to fusion (~figure 3.25, right).

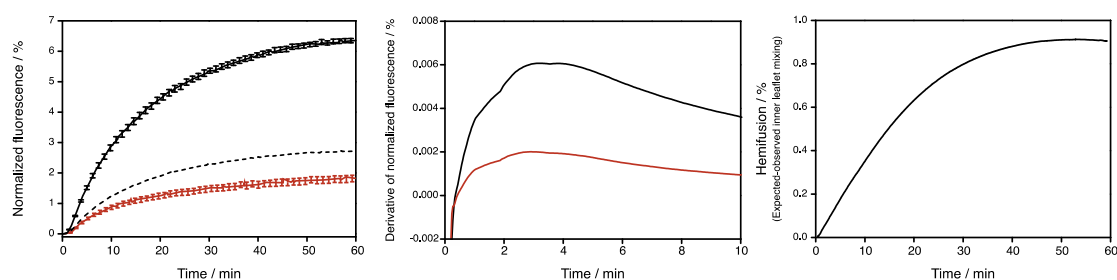


Figure 3.25: Total and inner leaflet lipid-mixing of large SNARE-liposomes reveals a net accumulation of hemifused liposomes. Left: syb RHO-PE/NBD-PS liposomes and ΔN syxH3-SN25 complex liposomes (both at nominal $l/p = 500:1$) were mixed and total (black) and inner (red) leaflet lipid-mixing measured as described in the text. Assuming full fusion conditions (i.e. no hemifusion), the expected amount of inner leaflet lipid-mixing is shown (dashed line, see text for details). Averages and standard deviations are from three traces. Middle: first derivative from the first 10 min of the lipid-mixing traces from the left, showing there is no lag between inner leaflet and outer leaflet lipid-mixing. Right: the difference between expected and observed inner leaflet lipid-mixing from the left graph reflects liposomes undergoing outer but no inner leaflet lipid-mixing i.e. hemifusion. The trace is thus proportional to the net amount of hemifused liposomes, revealing an accumulation.

3.3.3 Arrest at the bilayer-bilayer contact stage

A recurrent strategy in identifying intermediates in any chemical reaction commonly involves the ability to arrest them by changing chemical conditions. By definition, intermediates constitute local minima in a reaction coordinate, and thus they can be kinetically trapped if not enough energy is available for the reaction to proceed further. To evaluate intermediates in SNARE-mediated fusion between large liposomes, different approaches were considered.

A classic approach to trap intermediates is to lower the reaction temperature. Although temperature does lower the extent of lipid-mixing due to the high energy barrier for ΔN syb displacement (figure 3.18), there is also the possible effect that temperature may simultaneously alter the physical properties of the membrane through phase transitions. Low temperatures (~ 4 °C) have been used as a pre-incubation phase prior to SNARE-mediated liposome fusion, supposedly because liposomes are arrested at a docked state [12]. Because of the poorly understood relation between low temperature effects on membrane physical properties and SNARE assembly, this approach was not pursued.

Another approach consists of producing a mutation that impairs SNAREs with the ability to fuse liposomes without affecting its ability to dock them. This requires prior knowledge of key residues that are not essential for SNARE-complex assembly but that weaken it enough to prevent fusion. It is well known that alterations such as substitutions and deletions on the N-terminal portion of the SNARE complex are detrimental to assembly, whereas C-terminal modifications, including the linker region, tend not to disrupt assembly but impair fusogenic activity, as concluded in some studies [94, 150].

The finding that single C-terminal deletions in the SNARE motif of syb partially impairs fusion of small liposomes but not SNARE complex assembly constituted a starting point for investigating deletions that could arrest a putative docked intermediate [94]. These mutants exhibited between 40 to 60 % less fusion compared to wild-type, and although the term “docking” was not explicitly mentioned, the implication is that liposomes that do not fuse become trapped at a stable intermediate state.

Taking advantage of the observations from this study, wild-type and $\Delta 84$ syb, a mutation that abolishes the last +8 layer of the SNARE complex, were reconstituted into large liposomes and their lipid-mixing kinetics compared (figure 3.26, left). Surprisingly, in contrast to what has been reported in small liposomes, the mutant did not exhibit any measurable amount of lipid-mixing. To discard the possibility that $\Delta 84$ syb is unable to

mediate lipid-mixing because it cannot displace the ΔN syb fragment from the ΔN syxH3-SN25 complex, displacement kinetics from an acceptor complex containing labeled syb 49-96^{C79Alexa488} was measured (figure 3.26, right). No differences with wild-type syb were observed, indicating the mutant variant can displace syb 49-96 and hence form fully assembled ternary SNARE complexes as readily as the wild-type.

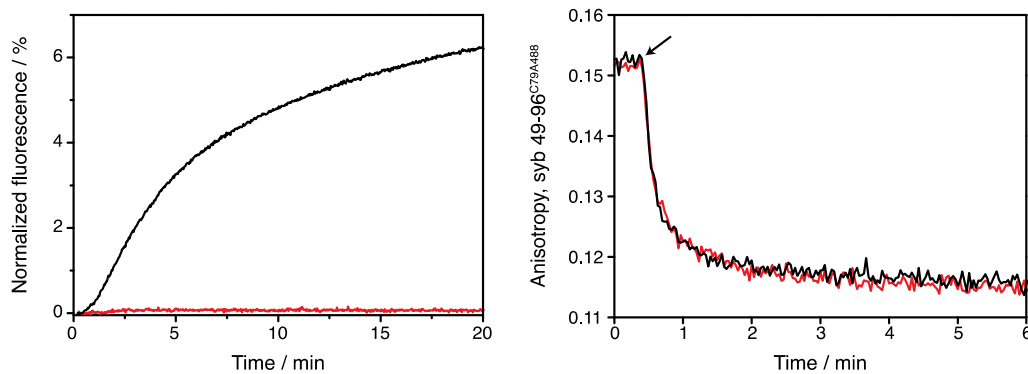


Figure 3.26: A syb deletion mutant $\Delta 84$ cannot mediate lipid-mixing but can readily displace syb 49-96 from a ΔN syxH3-SN25 complex. Left: lipid-mixing between large RHO-PE/NBD-PS liposomes containing full-length wild-type syb (black) and $\Delta 84$ syb (red) and unlabeled liposomes containing ΔN (53-96) syxH3-SN25 complex (nominal 1/p = 500:1). Right: displacement kinetics of syb 49-96^{C79Alexa488} from ΔN syxH3-SN25 complex (~ 200 nM) by full-length wild-type syb (black) and $\Delta 84$ syb (red) (both at ~ 2 μ M) in a 50 mM OG solution measured by anisotropy. Reaction starting point is marked by an arrow.

To explicitly compare the kinetics and extent of docking of wild-type $\Delta 84$ syb, single-particle FCCS analysis was used to monitor the degree of cross-correlated particles, which showed only slight differences between the two (figure 3.27, red curves). On the other hand, no considerable fluorescence lifetime changes were observed for $\Delta 84$ syb liposomes, whereas wild-type syb portrayed similar kinetics to lipid-mixing measured by NBD dequenching (figure 3.27, black curves).

By determining the differences between changes in cross-correlation and lifetime, the evolution of docked liposomes can be tracked [175], revealing that docking levels mediated by wild-type syb reaches its highest value at ~ 4 min and then plateaus out (figure 3.27, bottom left). In contrast, $\Delta 84$ syb liposomes exhibit an increasing amount of docking until saturation is

reached after ~20 min, strongly supporting and consistent with the earlier prediction of a stable intermediate docked state (figure 3.27, bottom right).

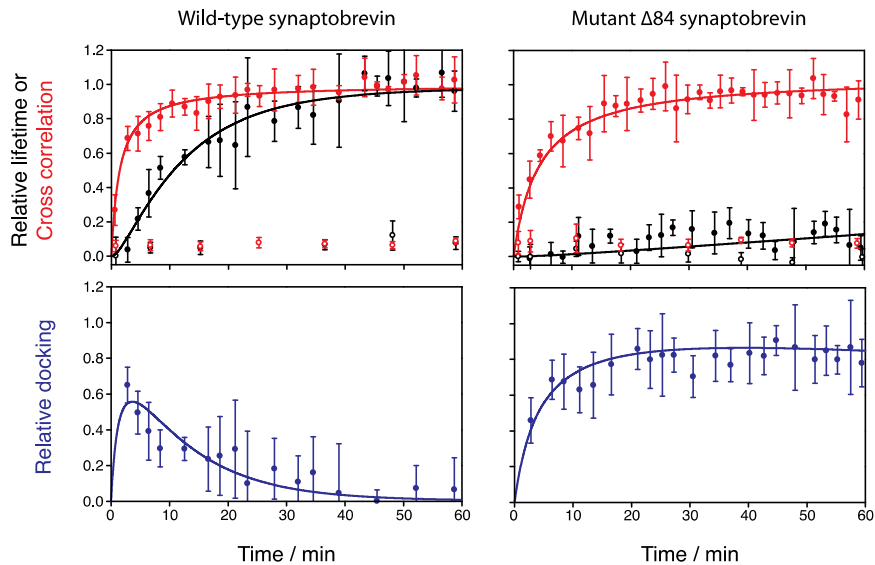


Figure 3.27: Discrimination between docking and fusion mediated by wild-type and $\Delta 84$ syb determined by fluorescence cross-correlation spectroscopy (FCCS). Large wild-type and $\Delta 84$ syb Texas Red liposomes (nominal 1/p = 500:1) and large ΔN syxH3-SN25 complex Oregon Green liposomes (nominal 1/p = 500:1) were mixed and the degree of particle cross correlation (filled red circles) and change in donor lifetime (filled black circles) were measured. Controls with excess syb 1-96 showed both cross correlation and lifetime changes were SNARE-mediated (open circles). Standard deviations correspond to six measurements. The difference between cross correlation and donor lifetime changes reflects relative populations of docked liposomes (filled blue circles), confirming $\Delta 84$ syb is arrested at a docked stage. Data was fitted (solid line) with the kinetic model presented in figure 3.20. Measurements made by Dr. Anna Cypionka.

A different way of comparing docking behavior is by evaluation of size distribution changes obtained by FFF-MALLS. Although both wild-type and $\Delta 84$ syb liposomes mediate substantial size changes, the former almost doubles in size while the latter increases by ~50 % (figure 3.28). Since the mutant is not capable of mediating lipid-mixing, the extent of the size change represents the maximum possible change produced by docking in the absence of fusion. Interestingly, the greater size change incurred by wild-type syb liposomes is probably reminiscent of multiple rounds of fusion combined with late-stage docking as observed by cryo-EM (figure 3.23).

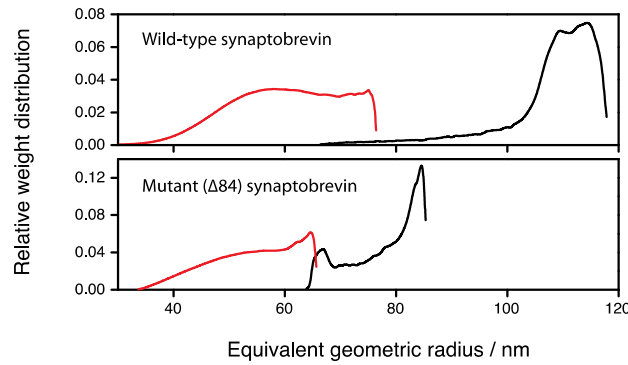


Figure 3.28: Comparison of size distribution changes induced by wild-type and $\Delta 84$ syb. Wild-type and $\Delta 84$ syb liposomes ($10 \mu\text{L}$, nominal $1/p = 500:1$) were mixed with ΔN (53-96) syxH3-SN25 complex liposomes ($10 \mu\text{L}$, $1/p = 500:1$) in a total reaction volume of $300 \mu\text{L}$ and after 60 min placed on ice. Samples were then analyzed with FFF-MALLS (black). Control and reference distributions (red) were obtained by including syb 1-96 ($\sim 6 \mu\text{M}$).

To directly confirm the existence of an arrested docked state, samples from reactions between $\Delta 84$ syb and ΔN syxH3-SN25 complex liposomes were plunge frozen for cryo-EM analysis. During the first 1-3 min many liposomes appeared docked at a bilayer-bilayer contact state (figure 3.29, A-E). After ~ 60 min, most liposomes were seen engaged in multiple-docking at the bilayer-bilayer contact stage, suggesting the system had reached its final state (figure 3.29, F). Hemifused liposomes were extremely rare, with only a handful being sighted in three independent experiments ($< 0.1\%$).

The ultrastructural features of the bilayer-bilayer contact interface resemble those observed in the docking mediated by wild-type syb during the lag phase (figure 3.21), strongly suggesting this state is an intermediate in the SNARE-mediated fusion pathway. The extent of the contact interface portrayed a wide range of diameters depicting the same strained ring pattern alluding to a strong pulling force. Occasionally this force was able to bend a membrane, usually towards the one with higher curvature (figure 3.29 D). In what may have been a bilayer-bilayer contact caught in the act of lateral expansion, no clear ultrastructural evidence for a stalk-like structure was visible within the resolution limits of the set-up (figure 3.29 E).

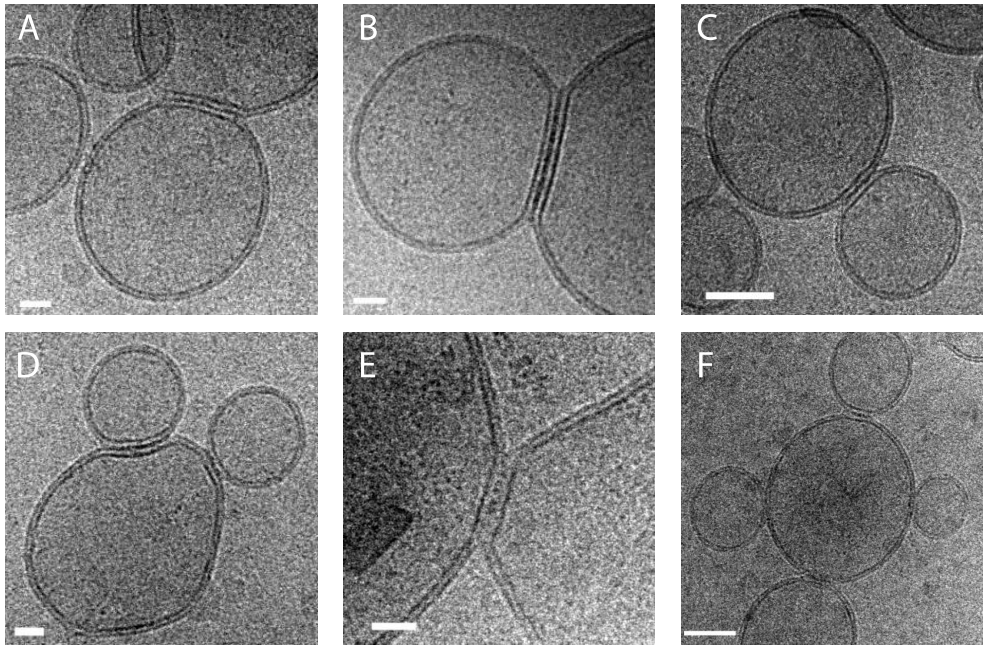


Figure 3.29: Arrest of a putative fusion intermediate at the bilayer-bilayer contact stage by $\Delta 84$ syb. Large $\Delta 84$ syb liposomes (nominal $l/p = 500:1$) were mixed to ΔN syxH3-SN25 complex liposomes (nominal $l/p = 500:1$) and samples plunge frozen during the first 3 min (A-E) and 60 min (F). Docking was almost completely abolished in the presence of excess syb 1-96, suggesting a SNARE-mediated process. Interpretation and description can be found in the text. Bar = 20 nm except for E and F for which bar = 50 nm. Images taken by Elmar Behrmann.

These results together show the presence of a stable docked state that is an intermediate in the SNARE-mediated fusion pathway of large liposomes. Although it is expected that such a state would also exist for small liposomes, the previous finding that $\Delta 84$ syb can still mediate lipid-mixing between small liposomes, in contrast to no lipid-mixing in the larger liposomes used here, suggests a possible linkage between membrane curvature and the ability for a weakened SNARE-complex to mediate fusion [94].

To test this hypothesis, small and large SNARE-liposomes containing wild-type and $\Delta 84$ syb were prepared and their lipid-mixing profiles compared (figure 3.30). Furthermore, reactions between small and large liposome populations were set up to evaluate whether curvature effects were R or Q-SNARE specific. Surprisingly, $\Delta 84$ syb was able to mediate high levels of lipid-mixing (~60 % of wild-type) only for the fusion reaction between two small SNARE-liposomes, while reactions between small and large liposomes had only lipid-mixing 5-10 % that of wild-type levels. Reactions between large liposomes had no measurable amount of lipid-mixing. This strongly

suggests that membrane curvature plays a role in the energetics of membrane fusion and has profound mechanistic implications on how SNAREs mediate fusion.

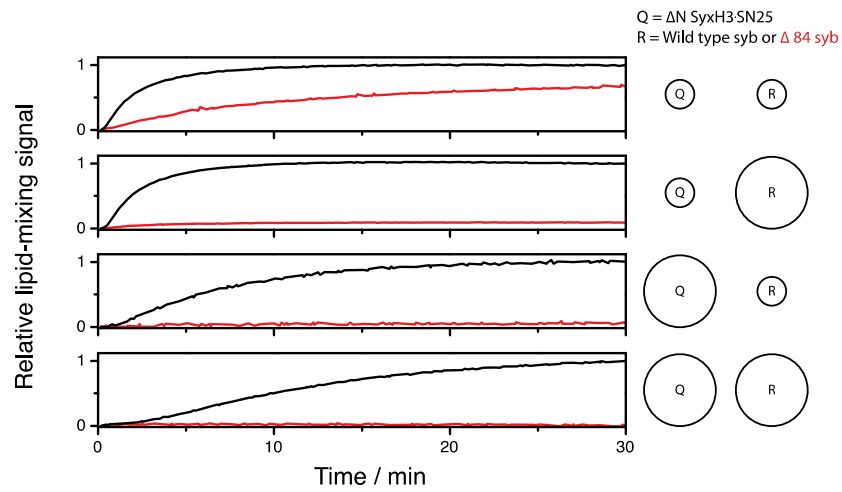


Figure 3.30: Mutant $\Delta 84$ syb is able to mediate lipid-mixing only between two small (<60 nm) liposomes. ΔN syxH3-SN25 complex was reconstituted into small and large RHO/NBD-PS liposomes at similar density ($l/p = 200:1$), while wild-type and $\Delta 84$ syb was reconstituted in small and large unlabeled liposomes ($l/p = 500:1$). Lipid-mixing kinetics were measured for both wild-type (black) and $\Delta 84$ syb (red) according to the different liposome size combinations depicted on the right. The size of liposomes was checked by FFF-MALLS and reactions were performed in 0.6 mL volumes.

4 Discussion

4.1 Reconstitution properties of large SNARE-liposomes

This study has attempted to address mechanistic questions regarding the ability of SNAREs to fuse liposomes, with a specific focus on large liposomes. Although the reconstitution approach for investigating SNARE-mediated fusion is widely applied, a few relatively recent studies have explored the relationship between the reconstitution method of SNAREs and the properties of the resulting proteoliposomes and have expressed reservations regarding the reliability and usefulness of these approaches [145, 154]. These concerns require attention and have in part provided motivation for this work to extend their findings and to try to reach a more complete understanding of why liposome fusion results vary widely among different studies and indeed within the same study [145, 164, 166].

The direct method for reconstitution of transmembrane proteins is in principle an attractive procedure for reconstituting SNAREs due to the asymmetric right side-out orientation of reconstituted proteins. This property can be said to be its defining feature, whereas symmetric distributions are generally reminiscent of reconstitutions via co-micellization. Several labs have employed OG to reconstitute SNAREs into preformed liposomes stating that reconstitution was performed according to the direct method [145, 164, 166] (see also table 3.1). However, only one of these studies has fully characterized the resulting SNARE-liposomes according to size, orientation and insertion efficiency, and none have explored how these depend on the detergent concentration.

The results presented in this study demonstrate that optimal insertion of SNAREs is critically dependent on OG concentration and that this occurs during a sharp transition in the interaction between OG and liposomes. Syb is quantitatively incorporated above a certain OG concentration of $R \approx 1-1.5$, a

range that agrees well with the reported direct reconstitution of Ca^{2+} -ATPase at $R = 1.3$ [170, 182]. However, quantitative incorporation of binary Q-SNARE complexes was achieved only for N-terminally truncated complexes, highlighting that the same reconstitution parameters are not universally applicable even to closely related proteins (figure 3.9).

Another difference between reconstitution of syb and the syntaxin-SNAP-25 complex is the random orientation of the former and a much more correctly orientated insertion of the latter. Although the asymmetric insertion of all N-terminally truncated complexes tested in this study has the features of a protein reconstituted by the direct mechanism, it does not necessarily mean it was reconstituted according this mechanism. In fact, cytochrome-*c* oxidase reconstituted by the co-micellization method has features which resemble proteins reconstituted by the direct method, with its orientation depending on the electrostatic interactions between the protein and negatively-charged phospholipids [187].

At all the reconstitution conditions tested, size distributions of resulting SNARE-liposomes were smaller than the original distribution of the template liposomes, the only exception being when a large amount ($R > 3$) of detergent is used, which exhibited a dramatic increase in size probably due to unspecific fusion of liposomes during reconstitution. This systematic decrease in size, even though it is minor, argues against a direct reconstitution mechanism. Taken together with all observations mentioned above regarding the differential properties of the SNAREs used here, these findings suggest the exact mechanism of reconstitution may be more complex than originally thought and seems to contain features of both direct and co-micellization methods, illustrating the still largely empirical nature of reconstitution models.

In light of this characterization, it is worthwhile to ask whether some conclusions from previous reconstituted liposome fusion studies may be explained by sub-optimal reconstitution procedures. The optimal OG-mediated reconstitution of syb in this study was at $R \approx 1-1.5$, which agrees

well with the high (> 90 %) insertion efficiency of syb of a different study which used $R = 1.1$ [145]. It is tempting to speculate whether the very low SNARE-mediated liposome fusion levels observed in some studies [154, 164], and on which important mechanistic conclusions were made, could be explained in part by sub-optimal reconstitution protocols at R -values close to zero. Furthermore, some protocols include a centrifugation or a density gradient flotation step for purifying SNARE-liposomes after reconstitution; however, these purification steps remove precisely those SNAREs which do not become inserted, it is therefore not possible to assess and compare the true insertion efficiency in these studies [12, 164, 166].

It is unlikely that the specific parameters optimized in this study are relevant to the specific model systems preferred by other research groups, since optimal conditions are very likely to be dependent on factors such as the SNARE fragments used and the lipid composition of the liposomes. Finding the right conditions for quantitative incorporation of SNAREs is crucial for making correct mechanistic conclusions of SNARE function and would facilitate comparison and repeatability among different studies.

4.2 Fusogenic properties of large SNARE-liposomes

A concern previously raised with respect to the ability of SNAREs to fuse liposomes was the presence of sub-populations of very small liposomes (diameters of 15-30 nm) in the preparation of SNARE-liposomes using the standard co-micellization method (discussed in section 3.1.2) [145]. Fusion of these liposomes was proposed to be driven by the high degree of curvature stress, which would make them more prone to forming stalks and to spontaneously fuse as has been observed in several *in vitro* systems [20, 138]. In contrast, SNARE-liposomes prepared by the direct method at comparable densities but containing larger diameters were not fusogenic, further validating their concern about the presence of highly fusogenic small SNARE-liposomes [145].

This work has tried to address this issue by thoroughly characterizing the size of the SNARE-liposomes. The absence of liposomes with very small diameters was confirmed by FFF-MALLS, a fractionation-light scattering based technique, and by electron microscopy. Thus, all fusion-related properties can safely be attributed to a relatively homogenous population of liposomes with diameters that are approximately twice as large compared to the more traditionally prepared liposomes (figure 3.6).

Lipid-mixing and size distribution data suggests the nature of the Q-SNARE acceptor complex is the determining biochemical factor for mediating membrane fusion (section 3.2.1). Stabilization of a Q-SNARE complex that stabilizes the syntaxin·SNAP-25 into a 1:1 configuration (ΔN syxH3·SN25 or ΔN syxFL·SN25 complexes) was essential for lipid-mixing and for mediating changes in the size distribution of liposomes. The Habc domain of syntaxin was shown to be inhibitory to fusion, even though syb binding is not compromised, suggesting steric factors may be at play and may required regulation by other proteins in order make fusion more efficient. The novel interaction between Munc-18 and the syntaxin N-peptide might be an important aspect of this regulation, as suggested recently by liposome fusion experiments [159].

Relatively efficient lipid-mixing was observed throughout a wide range of SNARE densities, similar to what has been recently reported but employing smaller liposomes (30-50 nm) [166, 188]. In contrast, no lipid-mixing or changes in liposome size distribution were detected with spontaneously formed Q-SNARE acceptor complexes (syxH3·SN25 and syxH3·SN25), a rather surprising result given that several studies have reported some degree of lipid-mixing on small liposomes [12, 94, 103, 151]. However, this observation is in agreement with a previous study employing SNARE-liposomes whose size distribution contained large liposomes and which were prepared with a reconstitution protocol similar to the one used here [145].

These fusogenic properties of large SNARE-liposomes come hand-in-hand and are strongly correlated with syb binding kinetics to these complexes (figure 3.11), a finding which is also seen with small SNARE-liposomes prepared with the co-micellization method [94, 103]. Together with these studies, the results presented here strongly indicate that the determining factor for liposome fusion is the formation of a stable N-terminal Q-SNARE binding region which is freely available for syb to engage in trans SNARE complex formation, and not physical factors such the liposome size.

A characteristic feature of these large SNARE-liposomes was the presence of an unusually long lag phase in the lipid-mixing profile. These phases had been observed in small liposomes, although they were considerably less pronounced and its mechanistic significance was not fully understood at the time [162]. A wealth of data supports the view that the long delay in the initiation of lipid-mixing reflects a long-lived docked state, a proposition ultimately confirmed by direct visualization of abundant docking by electron microscopy. Given that previous attempts at visualizing intermediate docking states by electron microscopy have been unsuccessful [145, 151, 153], it is worthwhile to discuss why docking appears so abundantly in this particular reconstitution system.

In order to readily observe docking with single particle techniques such as electron microscopy, two conditions need to be satisfied: docking must be an efficient process which occurs frequently, and the docking state must exhibit a lifetime which ensures it can be observed or captured once docking has been established. If only one of these conditions holds true, it would be extremely difficult to see widespread and abundant docking; thus, irrespective of the molecular details behind SNARE complex assembly which lead to fusion, it is evident that the molecular machinery underlying docking and fusion in these large SNARE-liposomes must entail an efficient (and therefore fast) docking reaction but a long (and therefore slow) transition from docking to fusion.

The results presented in section 3.2.2 show that the ΔN syb fragment present in the ΔN syxH3-SN25 complex is responsible for this dual behavior: it stabilizes the N-terminal portion of the three-helix bundle formed by syntaxin and SNAP-25, allowing efficient and fast nucleation of syb in trans (figures 3.11, 3.16 and 3.19), but delays the transition to a fully zippered cis complex since the fragment must first be displaced (figure 3.17). Thus, the predominant effect of the ΔN syxH3-SN25 complex on liposome fusion is the enhancement of high levels of efficient docking; once trans SNARE complex is established, the high activation energy for displacement ensures the docking state is long-lived and is likely to be rate-limiting for fusion (figure 3.17). Thus, fast fusion in this system is not driven by a fast fusion step per se, but rather indirectly by fast docking.

These results suggest slow or negligible lipid-mixing rates reported from previous liposome fusion experiments using spontaneously assembled Q-SNARE acceptor complexes could be explained by inefficient docking. As discussed in section 1.4.2, productive trans SNARE complex formation is rate-limited by the dissociation of a dead-end 2:1 syntaxin-SNAP-25 complex into a transient on-pathway 1:1 complex intermediate. For docking to occur in this case, two liposomes have to first collide and then a transient 1:1 complex be present at the docking site at the precise instant of the collision. On a single liposome basis, docking would be a rare event, but in an ensemble this can be artificially enhanced by performing liposome fusion experiments at very high concentrations of liposomes.

The majority of liposome fusion studies are done at liposome concentrations about 20-50 fold higher than here, which translates approximately to a 400-2500-fold increase in collisional frequency; thus, lipid-mixing in these systems appear to be primarily collision-driven. Even so, fusion is still a relatively slow process in these studies, as judged by modest size shifts, proportionally few rounds of fusion being completed and slow lipid-mixing kinetics in comparison with results presented in this study [12, 148, 149, 151, 189]. In fact, the low concentration regime of liposome fusion

reactions in this study is probably the reason why no lipid-mixing was observed for liposomes reconstituted with unstabilized binary acceptor complexes.

In essence, stabilization of a 1:1 syntaxin:SNAP-25 complex with a ΔN syb fragment replaces the rate-limiting step that occurs at the initial formation of trans SNARE complex assembly that establishes docking, to a step immediately after docking. Thus, a bimolecular rate-limiting docking step is replaced by a unimolecular rate-limiting displacement step. Recognizing and understanding this dramatic change in kinetic behavior is vital for correctly interpreting liposome fusion experiments. An important implication of this is that, given the high activation energy for fragment displacement from the ΔN syxH3·SN25 complex, the rates of lipid-mixing kinetics should be largely insensitive to the density of SNAREs. This has indeed been observed in small SNARE-liposomes containing the ΔN syxH3·SN25 complex and also here in large liposomes (figure 3.13), where it is seen that the extents of lipid-mixing vary with density, but not its rate [157, 188]. This has previously been interpreted as evidence for lack of kinetic cooperativity in SNARE-mediated fusion [188]; however, a much more plausible and simple explanation is that the unimolecular displacement reaction determines the rate by which lipid-mixing can occur, hiding faster steps that may occur downstream from fragment displacement.

The slowing down effect of ΔN syb displacement may be seen as an inconvenient limitation to the model system, since it places restrictions on how fast lipid-mixing kinetics can occur (ultimately, to a few seconds). The timescale of the fastest lipid-mixing reactions observed with large SNARE-liposomes exhibit half-time constants of ~ 5 min (see for instance appendix 6.6), and in small liposomes they can approach ~ 0.5 min [103]. These timescales are still 5 orders of magnitude slower than that observed during neurotransmitter release. Recently, however, SNARE-mediated liposome-planar bilayer fusion using the ΔN syxH3·SN25 complex has corroborated

SNARE-mediated fusion with millisecond kinetics [165, 190]. The reasons for the disparate kinetics between liposome-liposome fusion and liposome-planar bilayer fusion are not fully established, but one important difference is that liposome-liposome fusion kinetics corresponds to an ensemble, whereas the kinetics observed in liposome-planar bilayer fusion corresponds to a single fusion event; thus, the rates are not directly comparable.

Interestingly, *in vitro* the syb 1-84 fragment is slower at displacing the ΔN syb 49-96 fragment from the ΔN syxH3·SN25 complex than the syb 1-96 fragment used in many of the binding measurements in this work. This suggests the fragment is bound to the complex at the linker region proximal to the membrane, delaying N to C-terminal zippering not just throughout the SNARE motif regions of the complex, but further down towards the TMDs. It is tempting to speculate whether the extremely fast fusion rates recorded in the liposome-planar bilayer fusion reactions mediated by the ΔN syxH3·SN25 complex captures the very instant after removal of the ΔN syb fragment and therefore reflects only the relevant membrane-merging step [190].

4.3 Bilayer-bilayer contact as an on-pathway intermediate mediated by a partially assembled SNARE complex

The observation of widespread docking by electron microscopy revealed a few different forms of putative docking intermediates (figures 3.21 and 3.22). Since these images were taken after a few minutes upon starting the reaction and when lipid-mixing had just begun, it was initially thought that docked liposomes were at an intermediate step just prior to fusion. However, many docked liposomes were also observed at the end of the reaction when lipid-mixing became saturated (~60 min), a rather surprising finding since if fusion represented the end-point of the reaction then liposomes would be expected to be predominantly in a free state. An alternative interpretation is therefore possible suggesting docked liposomes observed during the lag phase were not actually undergoing fusion but are instead arrested.

Several lines of evidence point out that at least a proportion of liposomes fuse. This is supported by dithionite-based experiments revealing lipid-mixing occurring in the inner leaflet monolayer, and also by FCCS analysis (figure 3.27, left) which shows that the docking profile consists of an initial accumulation of docked liposomes which peaks at 3-4 min and then declines as a result of liposomes fusing (if not docking levels would increase until saturation, as in the $\Delta 84$ syb docking mutant). Furthermore, large size shifts are observed by FFF-MALLS that is compatible with several rounds of fusion (figures 3.10 and 3.28). Thus, these results inevitably indicate that at least some of the docked liposomes observed during the lag phase must have fused and therefore are found at an intermediate step just prior to fusion.

On the other hand, the arrest at the bilayer-bilayer contact state by $\Delta 84$ syb suggests that the close opposition of two bilayers can be arrested if not enough force is provided, indicating the bilayer-bilayer contact state represents a local minimum in the energy reaction coordinate; hence, it cannot be ruled out that some of the docked liposomes observed during the lag phase are kinetically trapped in that local minimum of energy as well.

Two factors are probably determine how liposomes reconstituted with wild-type SNAREs may not have the energy available to overcome the energy barrier to proceed past the bilayer-bilayer contact state and remain trapped or arrested at that state. One factor appears evident upon consideration of the energy required to displace the ΔN syb fragment from the ΔN syxH3·SN25 complex. Isothermal titration calorimetry measurements show that syb 1-52 can bind to the ΔN (syb 49-96) syxH3·SN25 complex without ΔN syb displacement and provides ~ 44 kJ·mol⁻¹ of free energy at 25 °C [191]. In turn, the activation energy for displacement of syb 49-96 from the ΔN syxH3·SN25 complex was estimated to be in the range 57 - 78 kJ·mol⁻¹ (figure 3.17, right); thus, it is conceivable that the free energy gained during assembly of the first N-terminal layers of the SNARE complex will not always be sufficient to

displace the C-terminal ΔN syb fragment, and further suggests full displacement and fusion might in fact be a stochastic process.

Consistent with this thermodynamic picture is the finding that displacement kinetics is very sensitive to temperature (figure 3.17, left), and in liposome fusion experiments this is reflected in a substantial prolongation of the lag phase and also in a reduction of the extent of lipid-mixing as temperatures are decreased i.e. the conversion efficiency from docking to fusion is reduced and more liposomes remained trapped at a docked state (figure 3.18). The same pattern of behavior is seen by alterations of complex stabilization by the ΔN syb fragment, where addition of a single layer of stabilization has a similar effect to decreasing the temperature. The existence of a partially assembled SNARE complex which is unable to mediate fusion is thus inferred. This partially assembled state has been recently proposed based on assembly studies of soluble SNARE fragments [191]; the present study extends this finding to suggest that a partially assembled SNARE complex can mediate and stabilize a kinetically-trapped docked state, most likely at the bilayer-bilayer contact state.

The proposed stochastic nature and high energetic barrier of ΔN syb displacement cannot be the only factor preventing docked liposomes to fuse, however. The second factor is readily deduced from the observation that $\Delta 84$ syb can mediate some fusion of small liposomes, strongly suggesting the energetics of membrane curvature contributes towards the barrier which prevents the bilayer-bilayer contact state to proceed to fusion.

It is possible that the more stringent energy requirements for fusing large liposomes may need the combined energies from more than one SNARE complex, and this may also account for the observation of high levels of arrested docking after 60 min. In this scenario, liposomes may fuse and dock several times, but at some point towards the end of the reaction liposomes will have most of their SNAREs consumed and present in cis SNARE complexes. The last freely available SNAREs would then engage in the last rounds of trans complex formation, but would not be able to mediate fusion

from the energy of a single SNARE complex. Thus, the end-state of the ensemble may not necessarily be fusion as more commonly envisaged, but late-stage docking resulting from previous multiple rounds of fusion. This scenario is not contradictory to FCCS analysis which shows that docking steadily declines after reaching a maximum peak, since FCCS measures the first full round of fusion and docking but cannot detect docking and fusion between liposomes that are already double-labeled (i.e. have already fused).

A more rigorous and systematic analysis to determine the number of SNARE complexes required to fuse two large SNARE-liposomes is needed to confirm this interpretation; however, the observations that fusion between two small liposomes can be mediated by a weakened SNARE complex and that a single SNARE complex appears to suffice for their fusion [188] make this a feasible scenario.

4.4 Extended hemifusion as a sidetracked off-pathway state

The net accumulation of hemifused liposomes during the course of the reaction inferred by an increasing difference between expected and observed inner leaflet lipid-mixing, suggests that hemifusion in this system represents an alternative outcome to fusion (figure 3.25). Inner leaflet lipid-mixing did not lag behind total lipid-mixing and shared a very similar kinetic profile, suggesting liposomes that fused did so via an intermediate whose lifetime was too short to be captured by electron microscopy. Thus, hemifused liposomes with expanded diaphragms identified by electron microscopy are most likely to originate from a parallel mechanism that constitutes an alternative outcome to fusion. A similar conclusion has already been made based on an *in vitro* system using cells expressing flipped-SNAREs on their surfaces, where approximately one-third of liposomes end up in a hemifused state [143].

However, the interpretation that these hemifused liposomes represent an alternative outcome to fusion is in disagreement with conclusions from two bulk liposome fusion studies using a similar dithionite-based approach

[141, 192]; in particular, these studies observed that inner-leaflet kinetics lags by several minutes behind total lipid-mixing, suggesting a slow conversion of hemifusion to fusion was taking place. This would imply that hemifusion is an intermediate that is part of a sequential pathway for fusion. Unfortunately, no visual confirmation of hemifused liposomes with such long lifetimes was provided. Moreover, neither study presented a thorough characterization of the reduction of outer leaflet NBD, and it is noted that lipid-mixing experiments started 10-15 min after dithionite reduction. In this study, as well as elsewhere [88], it took at least 30 min for dithionite present at saturating levels to be completely inactivated (appendix 6.5); thus, it cannot be safely excluded that small amounts of active dithionite could have leaked into the liposomes during fusion in those experiments, which would have reduced NBD fluorescence on the inner leaflet side and altered the inner leaflet lipid-mixing profile.

Hemifused liposomes with expanded diaphragms identified here probably represent what has been identified before in viral hemagglutinin-mediated fusion as unrestricted hemifusion, which is a state where outer leaflet lipid-mixing occurs unimpeded [48]. No ultrastructural topological features of these hemifused liposomes seen here suggest that lipids are unable to freely diffuse throughout the merged outer monolayers. This type of hemifusion appears to be an alternative final state, although the diaphragm is able to break under certain conditions [48].

A second type of hemifusion has been described referred to as restricted hemifusion, where only localized portions of proximal monolayer leaflets are merged and where lipid-mixing is topologically restricted. This hemifusion appears to constitute an intermediate leading towards fusion pore opening in hemagglutinin-mediated liposome fusion [48]. Interestingly, a similar state has been observed in SNARE-mediated fusion by detecting discrete lipid-mixing intermediate FRET states of single fusion events between liposomes [142]. The state is relatively short-lived (~10-20 s) and appears to be a genuine intermediate in the fusion pathway. Despite this, a

hemifusion state with these characteristic could not be identified by cryo electron microscopy, although it is also not possible to discard that in this system such a state could have had a shorter lifetime than reported and therefore not easy to observe. Nevertheless, this elusive fast intermediate may be the missing link between the bilayer-bilayer contact state and fusion, although more supporting evidence, such as a mutation that arrests this state, would be needed to confirm this.

If the unrestricted hemifused liposomes in this study represent an off-pathway product, are they generated from a completely different and alternative SNARE-mediated pathway, or does it share a common pathway with fusion that later sidetracks at an intermediate step? The answer to this crucial question is provided by the $\Delta 84$ syb deletion mutant. No hemifusion is observed during $\Delta 84$ syb-mediated docking, strongly suggesting hemifusion sidetracks from the fusion pathway after this intermediate step. Furthermore, the absence of both fusion and hemifusion in large $\Delta 84$ syb-liposomes suggests both processes actively require efficient mechanical coupling between the SNARE motif and the linker region connecting the TMDs, in accordance with helical extension into the membrane as revealed by the SNARE complex structure [75].

The molecular process that determines whether a docked liposome will proceed to fusion or hemifusion is not clear and requires further investigation. Preliminary experiments suggest when the SNARE density is reduced, the accumulation of hemifusion is substantially lowered (appendix 6.6). Thus, it would appear as if a high number of SNARE complexes promotes hemifusion by exerting either too much or an uneven distribution of force between membranes. However, this finding has yet to be confirmed with electron microscopy. Alternatively, SNARE-mediated hemifusion and fusion may occur stochastically, requiring additional correcting or stabilization factors such as has already been proposed for complexin [130].

4.5 Towards a mechanistic understanding of SNARE-mediated fusion

Despite thousands of analyzed liposomes, an intermediate structure resembling an hourglass shaped stalk could not be found. Instead, many docked liposomes were seen with their bilayers tightly pressed onto one another covering extensive contact zones. This bilayer-bilayer contact state could be arrested by a single deletion affecting the last +8 layer of the SNARE complex. Ultrastructural imaging of liposomes docked by this weakened complex showed that membranes were still strained, revealing that SNARE complexes were exerting a pulling force across the membranes, albeit not strong enough to fuse them (figure 3.29).

It is not clear from the images if a thin water layer is present in between the tightly opposed membranes and whether this could be the final barrier for the formation of a lipidic connection between the proximal leaflets. However, the force generated by the weakened complex is partially sufficient to fuse two small liposomes, which argues against a water layer being a barrier for fusion initiation. Instead, it suggests that a weakened SNARE complex may still be able to mediate fusion if the membrane is already prone to fuse, which in the case of a highly curved membrane probably means that the energetic penalty for lipid bending or splaying is reduced and is compensated by release in curvature stress, facilitating lipidic connections between closely-opposed proximal monolayers. Thus, it appears that SNARE-mediated fusion proceeds via intermediate lipid-structures that are consistent with a stalk.

In contrast to the more commonly conceived hourglass-shaped stalk, however, the ultrastructural data suggests SNARE-mediated fusion proceeds according to a geometrically different stalk-like configuration but which is functionally equivalent. The strong pulling force inferred from the highly pressed bilayer-bilayer contact structure observed by cryo EM (figure 3.21) shows that it generates positive curvature at the edges of a docking interface conformed by a ring. It is precisely at these ring edges where lipids would be expected to be most stressed and likely to bend outwards or splay their

hydrophobic tails and form a stalk-like connection. Such asymmetric stalks and their formation along ring-like edges have been observed in simulations, and so they are at least thermodynamically conceivable [193]. The role of SNAREs in fusion would be, according to this model, to pull the membranes as close together as possible to minimize the energy associated with bending and exposure of hydrophobic lipid tails to the aqueous solvent.

A relevant question for biological vesicle fusion, in particular for regulated fusion of synaptic vesicles, is whether this pulling can be controlled in a way that allows vesicles to remain docked in a tight association with the plasma membrane, perhaps in a bilayer-bilayer contact state such as observed here, but without fusing until an influx of Ca^{2+} arrives. In this *in vitro* system, the force transduction of SNAREs is altered, either by a mutation or by introducing an artificial barrier in the SNARE assembly process which delays zippering. This has been essential for being able to arrest novel putative intermediate states in this study, and the question lingers as to what are the biological mechanisms (if any) which can accomplish this *in vivo*. In this regard, the clamp mechanism proposed for complexin or synaptotagmin discussed in section 1.3.3.3 is a particularly attractive model, since it proposes a way in which full SNARE complex assembly is prevented in much the same way as the ΔN syb appears to be doing. However, the biochemical evidence for a clamp-like mechanism of these proteins remains weak, and structures of trapped complexes have not been reported.

Alternative models on how SNARE-complexes might be able to arrest a vesicle in a readily releasable state may include a type of regulation that involves controlling the number of SNARE complexes formed. The energy required to fuse a synaptic vesicle to a plasma membrane is likely to be considerably greater than that required to fuse two small liposomes, and so a scenario could be envisaged where one or two SNARE complexes may form to bring the two membranes in a tight bilayer-bilayer contact state. Upon an influx of Ca^{2+} other SNARE complexes would then form and mediate fusion. In this scenario, Ca^{2+} binding to synaptotagmin must be rapidly coupled to

SNARE complex formation, a proposal that has been biochemically observed, albeit with kinetics that is probably too slow for being relevant [156].

A slight variation of this mechanism involves the formation of a small number of SNARE complexes that are not able to mediate fusion but can do so once the energy barrier for fusion is reduced. This hypothesis has emerged from the various observations that synaptotagmin binds to membranes in a Ca^{2+} -dependent manner that can either stabilize certain fusion intermediates or induce structural defects to make the plasma membrane more prone for fusion [157]. In one proposal, synaptotagmin generates positive curvature by inserting parts of its amphiphilic helices into the lipid bilayer in order to bend membranes. Such a mechanism would further reduce the activation energy for bending or splaying at the edges of the docking bilayer-bilayer contact surface as proposed above, and tests are underway to see if the arrested docking state stabilized by $\Delta 84$ syb can be “relieved” and proceed to fusion by the action of synaptotagmin [160, 161].

In an attempt to rationalize the present findings, a pathway for SNARE-mediated fusion depicting fusion intermediates is presented in figure 4.1 which includes an energy landscape. Although the model relies in part on some intuitive thinking, it is based on the various types of kinetic analysis and ultrastructural information gathered during the entire length of this work and also from others [142].

Fusion is depicted beginning with docking (1) between two liposomes, which constitutes the first energy barrier needed to overcome electrostatic and hydration forces. Docking mediated by one SNARE complex will bring the two membranes closer together (2a), but assembly of additional SNARE complexes would result in a tighter and more extended bilayer-bilayer contact surface (2b). This state constitutes a local minimum in the energy landscape. The strain produced at the edges of this contact promotes the formation of stalk-like lipid connections, which are depicted as a transition state (3) (inset). Once a stalk has been formed, it propagates asymmetrically. What happens at this point is critical for the fate of the entire process: rapid propagation of the

stalk could be quickly followed by an opening or breaking of the transient hemifusion diaphragm (4), leading to fusion (6). Alternatively, for reasons that are not yet clear, stalk propagation may be vast and extended and give rise to an expanded hemifusion diaphragm that is stable and likely constitutes an alternative end-state (5).

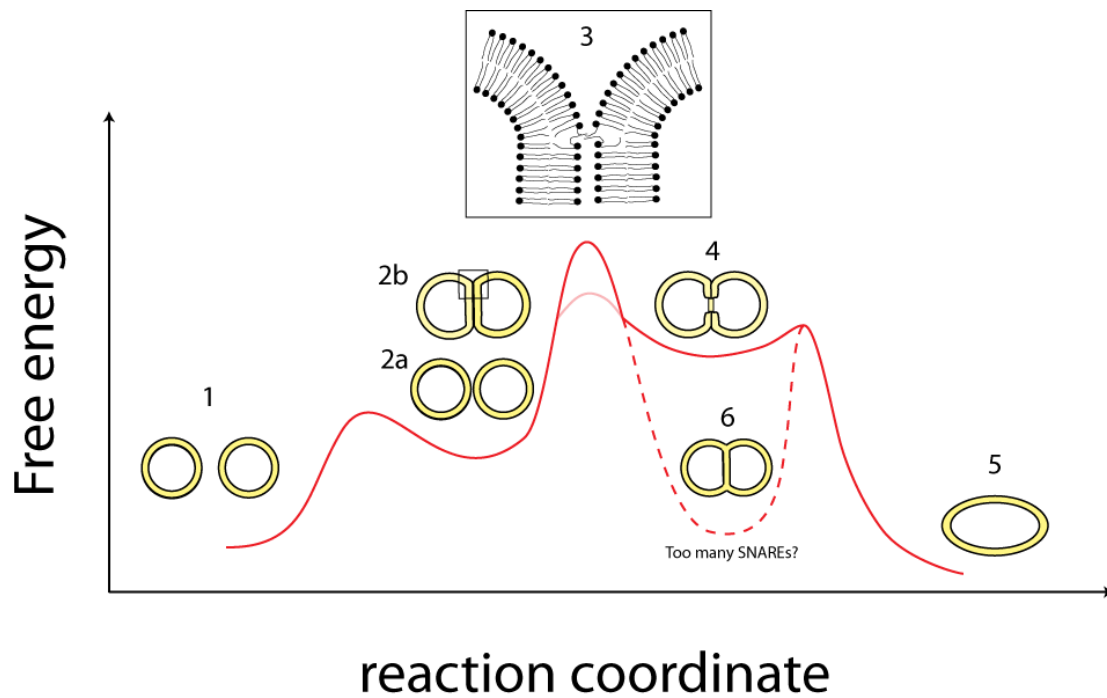


Figure 4.1: A proposal for an energy landscape for SNARE-mediated fusion based on analysis and experiments from this work. A description of the landscape is provided in the text. The red solid line is the proposed on-pathway sequence for fusion. The dashed line denotes an alternative pathway that is projected behind the plane of the paper. The light-colored solid line denotes the energy barrier for a fusion involving highly curved membranes.

5 Conclusions

The development of a novel fusion model system has been described and a detailed analysis has been presented regarding mechanistic aspects of SNARE-mediated fusion. One of the aims of this study was to see whether SNAREs were able to fuse large liposomes that were in the 80-120 nm range. By and large, and under certain biochemical requirements, SNAREs do seem to fuse large liposomes, as ultimately evidenced by the measurement of inner-leaflet lipid-mixing. However, a more rigorous analysis waits to establish whether SNAREs can also mediate content-mixing.

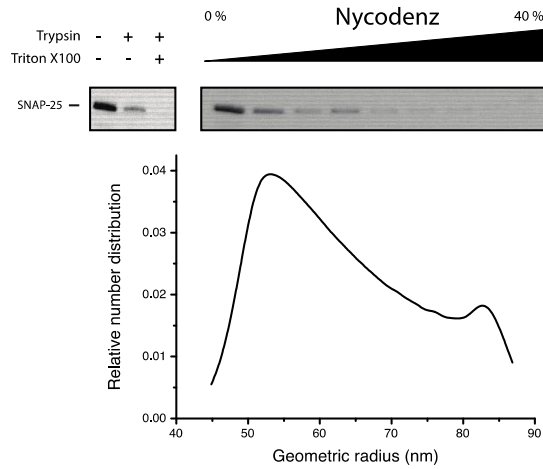
Surprisingly, the use of large SNARE-liposomes has led to unexpected avenues of research; most notably it has opened new possibilities to investigate intermediates in the SNARE-mediated fusion pathway that have lifetimes that make them amenable for direct visualization. Such long-lived intermediates have so far been extremely challenging to observe and represent a complementary approach to single particle studies where intermediates are short-lived [142]. Although the displacement from a Q-SNARE binary complex of a C-terminal synaptobrevin fragment is mainly responsible for allowing to see these intermediates, the large size of the liposomes was found to have an inhibitory effect on fusion and constitutes an additional barrier which may have helped to prolong their lifetime.

By using a combination of tools, an important conclusion is that a bilayer-bilayer contact docking state represents an on-pathway intermediate located on a local minima of the reaction coordinate, and that hemifusion seems to be an alternative outcome to fusion. Furthermore, an interpretation of kinetic and ultrastructural data suggests that the bilayer-bilayer contact state is mediated and stabilized by a partially-assembled complex which is prevented from fully zippering by a C-terminal synaptobrevin which has to be displaced at high energetic costs and from the reduced curvature of the

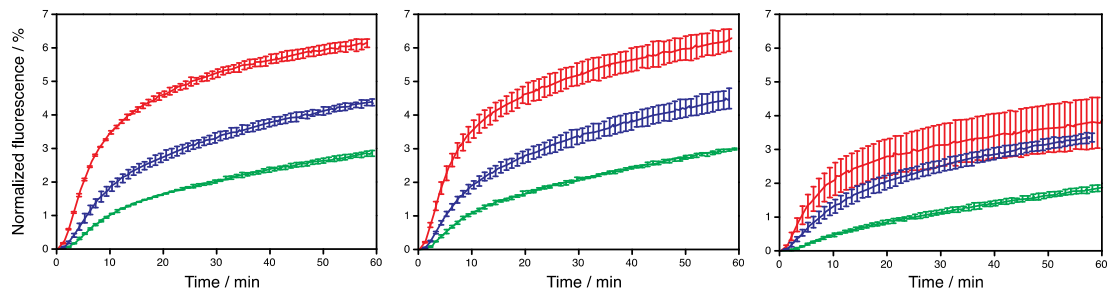
large liposomes. Thus, an inference has been made regarding the state of assembly of a SNARE complex and the state of interaction of the liposomes.

The physiological relevance of this finding, as well as the proposed energetic landscape for SNARE-mediated fusion, are not yet clear, but it provides a roadmap that can be used as a guide for studying SNARE-mediated fusion *in vivo*. At the very least, these results tell us what SNAREs are able to do and what membrane structures SNAREs are able to stabilize, and this already constitutes a step forward towards a mechanistic understanding of SNARE-mediated fusion.

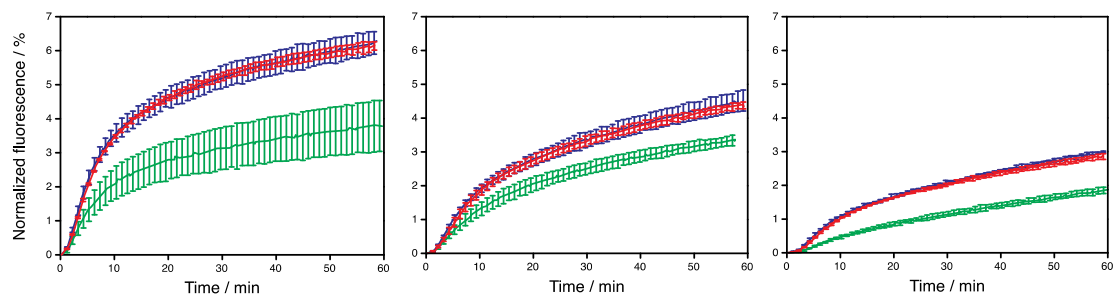
6 Appendix



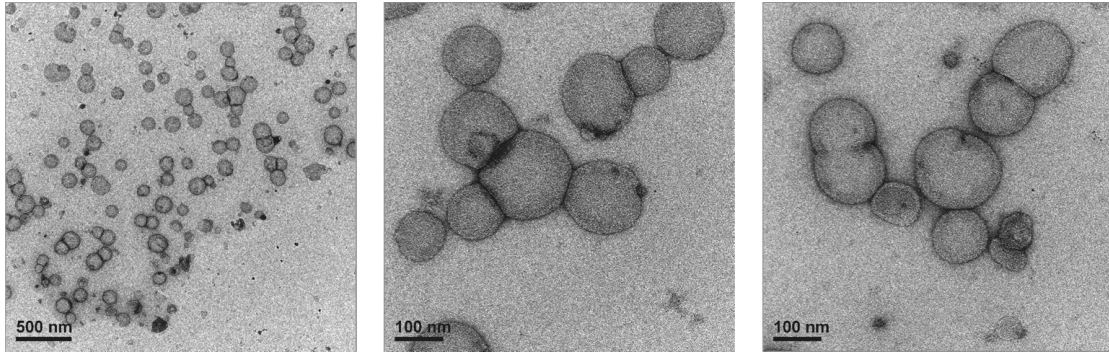
Appendix 6.1: Characterization of ΔN syxH3-SN25 liposomes (nominal l/p = 500:1) reconstituted at $R \approx 2$. Reconstitution was done as described in section 2.3.



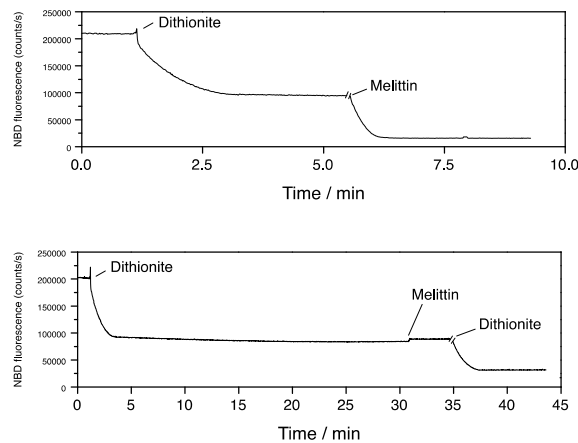
Appendix 6.2: Lipid-mixing kinetics of large SNARE-liposomes at varying syb density. Kinetic profiles of ΔN syxH3-SN25 complex liposomes (10 μ L) at l/p of 250:1 (300:1) (left), 500:1 (600:1) (middle), and 1500:1 (1750:1) (right) mixed with syb RHO/NBD liposomes (10 μ L) with l/p of 250:1 (450:1) (red), 500:1 (1050:1) (blue) and 1500:1 (2950:1) (green). L/p values in brackets are estimates of the density of active SNAREs taking into account phospholipid loss and protein orientation.



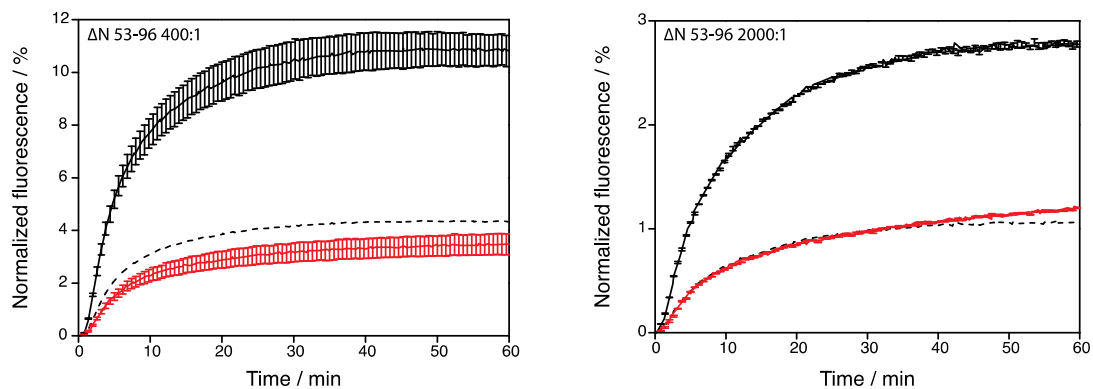
Appendix 6.3: Lipid-mixing kinetics of large SNARE-liposomes at varying density of ΔN syxH3-SN25 complex. Kinetic profiles of syb RHO/NBD liposomes (10 μ L) at l/p of 250:1 (450:1) (left), 500:1 (1050:1) (middle), and 1500:1 (2950:1) (right) mixed with ΔN syxH3-SN25 complex liposomes (10 μ L) with l/p of 250:1 (300:1) (red), 500:1 (600:1) (blue) and 1500:1 (1750:1) (green). L/p values in brackets are estimates of the density of active SNAREs taking into account phospholipid loss and protein orientation.



Appendix 6.4: Syb NBD/RHO liposomes and unlabeled ΔN syxH3-SN25 complex liposomes (both with total lipid content of $\sim 40 \mu\text{M}$ and nominal $l/p = 500:1$) were mixed and after ~ 1.5 min the reaction was fixed and stained with uranyl acetate. Electron microscopy imaging revealed the presence of docking as evidenced by electron dense regions in between closely apposed liposomes. Images taken by Dr. Dietmar Riedel.



Appendix 6.5: Time-dependent aqueous decomposition of dithionite. Top: exactly the same NBD-PS quenching curve as shown in figure 3.24. Pore-forming melittin was added ~ 4 min after addition of dithionite. Bottom: melittin was added ~ 30 min after addition of dithionite, revealing that by this point dithionite had decomposed. A few minutes later extra freshly prepared dithionite was added to show melittin had formed pores on the membrane.



Appendix 6.6: Accumulation of hemifusion of SNARE-liposomes appears to depend on the SNARE density. Total (black) and inner (red) leaflet lipid-mixing profiles of large ΔN (53-96) syxH3-SN25 complex liposomes ($12 \mu\text{L}$) at $l/p = 400:1$ (left) and $l/p = 2000:1$ (right) mixed to large syb RHO-PE/NBD-PS liposomes ($l/p = 500:1$). Expected inner leaflet lipid-mixing expecting full fusion conditions are depicted as dashed lines. At a high ΔN (53-96) syxH3-SN25 complex density, the difference between expected and observed increases during the course of the reaction, whereas at lower density no detectable difference is seen, suggesting off-pathway hemifusion is not taking place at lower SNARE densities. Traces represent three runs.

7 References

1. Bonifacino, J.S. and B.S. Glick, *The mechanisms of vesicle budding and fusion*. Cell, 2004. **116**(2): p. 153-166.
2. Jahn, R., T. Lang, and T.C. Sudhof, *Membrane fusion*. Cell, 2003. **112**(4): p. 519-533.
3. Martens, S. and H.T. McMahon, *Mechanisms of membrane fusion: disparate players and common principles*. Nature Reviews Molecular Cell Biology, 2008. **9**(7): p. 543-556.
4. White, J.M., et al., *Structures and mechanisms of viral membrane fusion proteins: Multiple variations on a common theme*. Critical Reviews in Biochemistry and Molecular Biology, 2008. **43**(3): p. 189-219.
5. Jahn, R. and R.H. Scheller, *SNAREs - engines for membrane fusion*. Nature Reviews Molecular Cell Biology, 2006. **7**(9): p. 631-643.
6. Cai, H.Q., K. Reinisch, and S. Ferro-Novick, *Coats, tethers, Rabs, and SNAREs work together to mediate the intracellular destination of a transport vesicle*. Developmental Cell, 2007. **12**(5): p. 671-682.
7. Luzio, J.P., P.R. Pryor, and N.A. Bright, *Lysosomes: fusion and function*. Nature Reviews Molecular Cell Biology, 2007. **8**(8): p. 622-632.
8. Wickner, W., *Yeast vacuoles and membrane fusion pathways*. Embo Journal, 2002. **21**(6): p. 1241-1247.
9. Chen, E.H. and E.N. Olson, *Unveiling the mechanisms of cell-cell fusion*. Science, 2005. **308**(5720): p. 369-373.
10. Bansal, D. and K.P. Campbell, *Dysferlin and the plasma membrane repair in muscular dystrophy*. Trends in Cell Biology, 2004. **14**(4): p. 206-213.
11. Cervený, K.L., et al., *Regulation of mitochondrial fusion and division*. Trends in Cell Biology, 2007. **17**(11): p. 563-569.
12. Weber, T., et al., *SNAREpins: Minimal machinery for membrane fusion*. Cell, 1998. **92**(6): p. 759-772.
13. Rand, R.P., *Interacting Phospholipid-Bilayers - Measured Forces and Induced Structural-Changes*. Annual Review of Biophysics and Bioengineering, 1981. **10**: p. 277-314.
14. Wilschut, J., et al., *Studies on the Mechanism of Membrane-Fusion - Kinetics of Calcium-Ion Induced Fusion of Phosphatidylserine Vesicles Followed by a New Assay for Mixing of Aqueous Vesicle Contents*. Biochemistry, 1980. **19**(26): p. 6011-6021.
15. Bentz, J., N. Duzgunes, and S. Nir, *Kinetics of Divalent-Cation Induced Fusion of Phosphatidylserine Vesicles - Correlation between Fusogenic Capacities and Binding Affinities*. Biochemistry, 1983. **22**(14): p. 3320-3330.
16. Bentz, J., N. Duzgunes, and S. Nir, *Temperature-Dependence of Divalent-Cation Induced Fusion of Phosphatidylserine Liposomes - Evaluation of the Kinetic Rate Constants*. Biochemistry, 1985. **24**(4): p. 1064-1072.

17. Wu, J.R. and B.R. Lentz, *Mechanism of Poly(Ethylene Glycol)-Induced Lipid Transfer between Phosphatidylcholine Large Unilamellar Vesicles - a Fluorescent-Probe Study*. *Biochemistry*, 1991. **30**(27): p. 6780-6787.
18. Kuvichkin, V.V., et al., *DNA-Induced Aggregation and Fusion of Phosphatidylcholine Liposomes in the Presence of Multivalent Cations Observed by the Cryo-TEM Technique*. *Journal of Membrane Biology*, 2009. **227**(2): p. 95-103.
19. Nir, S., J. Wilschut, and J. Bentz, *The Rate of Fusion of Phospholipid-Vesicles and the Role of Bilayer Curvature*. *Biochimica Et Biophysica Acta*, 1982. **688**(1): p. 275-278.
20. Talbot, W.A., L.X. Zheng, and B.R. Lentz, *Acyl chain unsaturation and vesicle curvature alter outer leaflet packing and promote poly(ethylene glycol)-mediated membrane fusion*. *Biochemistry*, 1997. **36**(19): p. 5827-5836.
21. Pantazatos, D.P. and R.C. MacDonald, *Directly observed membrane fusion between oppositely charged phospholipid bilayers*. *Journal of Membrane Biology*, 1999. **170**(1): p. 27-38.
22. Lei, G.H. and R.C. MacDonald, *Lipid bilayer vesicle fusion: Intermediates captured by high-speed microfluorescence spectroscopy*. *Biophysical Journal*, 2003. **85**(3): p. 1585-1599.
23. Takiguchi, K., et al., *Liposomes possess drastic capabilities for topological transformation*. *Chemphyschem*, 2002. **3**(7): p. 571-574.
24. Verkley, A.J., et al., *The Lipidic Particle as an Intermediate Structure in Membrane-Fusion Processes and Bilayer to Hexagonal Hii Transitions*. *Biochimica Et Biophysica Acta*, 1980. **600**(3): p. 620-624.
25. Siegel, D.P., *Inverted Micellar Intermediates and the Transitions between Lamellar, Cubic, and Inverted Hexagonal Lipid Phases .1. Mechanism of the L-Alpha[--]Hii Phase-Transitions*. *Biophysical Journal*, 1986. **49**(6): p. 1155-1170.
26. Hui, S.W., et al., *Membrane-Fusion through Point-Defects in Bilayers*. *Science*, 1981. **212**(4497): p. 921-923.
27. Kozlov, M.M. and V.S. Markin, *Possible Mechanism of Membrane-Fusion*. *Biofizika*, 1983. **28**(2): p. 242-247.
28. Siegel, D.P., *Energetics of Intermediates in Membrane-Fusion - Comparison of Stalk and Inverted Micellar Intermediate Mechanisms*. *Biophysical Journal*, 1993. **65**(5): p. 2124-2140.
29. Kozlovsky, Y. and M.M. Kozlov, *Stalk model of membrane fusion: Solution of energy crisis*. *Biophysical Journal*, 2002. **82**(2): p. 882-895.
30. Rizo, J., X.C. Chen, and D. Arac, *Unraveling the mechanisms of synaptotagmin and SNARE function in neurotransmitter release*. *Trends in Cell Biology*, 2006. **16**(7): p. 339-350.
31. Knecht, V. and S.J. Marrink, *Molecular dynamics simulations of lipid vesicle fusion in atomic detail*. *Biophysical Journal*, 2007. **92**(12): p. 4254-4261.
32. Kasson, P.M. and V.S. Pande, *Control of membrane fusion mechanism by lipid composition: Predictions from ensemble molecular dynamics*. *Plos Computational Biology*, 2007. **3**(11): p. 2228-2238.

33. Smeijers, A.F., et al., *A detailed look at vesicle fusion*. Journal of Physical Chemistry B, 2006. **110**(26): p. 13212-13219.
34. Yang, L. and H.W. Huang, *Observation of a membrane fusion intermediate structure*. Science, 2002. **297**(5588): p. 1877-1879.
35. Lee, J. and B.R. Lentz, *Evolution of lipidic structures during model membrane fusion and the relation of this process to cell membrane fusion*. Biochemistry, 1997. **36**(21): p. 6251-6259.
36. Chernomordik, L.V. and M.M. Kozlov, *Membrane hemifusion: Crossing a chasm in two leaps*. Cell, 2005. **123**(3): p. 375-382.
37. Kemble, G.W., T. Danieli, and J.M. White, *Lipid-Anchored Influenza Hemagglutinin Promotes Hemifusion, Not Complete Fusion*. Cell, 1994. **76**(2): p. 383-391.
38. Qiao, H., et al., *A specific point mutant at position 1 of the influenza hemagglutinin fusion peptide displays a hemifusion phenotype*. Molecular Biology of the Cell, 1999. **10**(8): p. 2759-2769.
39. Melikyan, G.B., J.M. White, and F.S. Cohen, *Gpi-Anchored Influenza Hemagglutinin Induces Hemifusion to Both Red-Blood-Cell and Planar Bilayer-Membranes*. Journal of Cell Biology, 1995. **131**(3): p. 679-691.
40. Nikolaus, J., et al., *Direct Visualization of Large and Protein-Free Hemifusion Diaphragms*. Biophysical Journal, 2010. **98**(7): p. 1192-1199.
41. Chernomordik, L.V. and M.M. Kozlov, *Protein-lipid interplay in fusion and fission of biological membranes*. Annual Review of Biochemistry, 2003. **72**: p. 175-207.
42. Siegel, D.P. and M.M. Kozlov, *The Gaussian curvature elastic modulus of N-monomethylated dioleoylphosphatidylethanolamine: Relevance to membrane fusion and lipid phase behavior*. Biophysical Journal, 2004. **87**(1): p. 366-374.
43. Haque, M.E., T.J. McIntosh, and B.R. Lentz, *Influence of lipid composition on physical properties and PEG-mediated fusion of curved and uncurved model membrane vesicles: "Nature's own" fusogenic lipid bilayer*. Biochemistry, 2001. **40**(14): p. 4340-4348.
44. Chernomordik, L.V., et al., *Lysolipids Reversibly Inhibit Ca²⁺-Dependent, Gtp-Dependent and Ph-Dependent Fusion of Biological-Membranes*. Febs Letters, 1993. **318**(1): p. 71-76.
45. Chernomordik, L., M.M. Kozlov, and J. Zimmerberg, *Lipids in Biological Membrane-Fusion*. Journal of Membrane Biology, 1995. **146**(1): p. 1-14.
46. Chernomordik, L., et al., *The Hemifusion Intermediate and Its Conversion to Complete Fusion - Regulation by Membrane-Composition*. Biophysical Journal, 1995. **69**(3): p. 922-929.
47. Melikyan, G.B., et al., *Inner but not outer membrane leaflets control the transition from glycosylphosphatidylinositol-anchored influenza hemagglutinin-induced hemifusion to full fusion*. Journal of Cell Biology, 1997. **136**(5): p. 995-1005.
48. Chernomordik, L.V., et al., *The pathway of membrane fusion catalyzed by influenza hemagglutinin: Restriction of lipids, hemifusion, and lipidic fusion pore formation*. Journal of Cell Biology, 1998. **140**(6): p. 1369-1382.

49. Muller, M., K. Katsov, and M. Schick, *New mechanism of membrane fusion*. *Journal of Chemical Physics*, 2002. **116**(6): p. 2342-2345.
50. Palade, G., *Intracellular Aspects of Process of Protein-Synthesis*. *Science*, 1975. **189**(4200): p. 347-358.
51. Balch, W.E., et al., *Reconstitution of the transport of protein between successive compartments of the Golgi measured by the coupled incorporation of N-acetylglucosamine*. *Cell*, 1984. **39**(2 Pt 1): p. 405-16.
52. Balch, W.E. and J.E. Rothman, *Characterization of Protein-Transport between Successive Compartments of the Golgi-Apparatus - Asymmetric Properties of Donor and Acceptor Activities in a Cell-Free System*. *Archives of Biochemistry and Biophysics*, 1985. **240**(1): p. 413-425.
53. Block, M.R., et al., *Purification of an N-Ethylmaleimide-Sensitive Protein Catalyzing Vesicular Transport*. *Proceedings of the National Academy of Sciences of the United States of America*, 1988. **85**(21): p. 7852-7856.
54. Malhotra, V., et al., *Role of an N-Ethylmaleimide-Sensitive Transport Component in Promoting Fusion of Transport Vesicles with Cisternae of the Golgi Stack*. *Cell*, 1988. **54**(2): p. 221-227.
55. Clary, D.O., I.C. Griff, and J.E. Rothman, *Snaps, a Family of Nsf Attachment Proteins Involved in Intracellular Membrane-Fusion in Animals and Yeast*. *Cell*, 1990. **61**(4): p. 709-721.
56. Weidman, P.J., et al., *Binding of an N-Ethylmaleimide Sensitive Fusion Protein to Golgi Membranes Requires Both a Soluble Protein(S) and an Integral Membrane-Receptor*. *Journal of Cell Biology*, 1989. **108**(5): p. 1589-1596.
57. Wilson, D.W., et al., *A Multisubunit Particle Implicated in Membrane-Fusion*. *Journal of Cell Biology*, 1992. **117**(3): p. 531-538.
58. Sollner, T., et al., *Snap Receptors Implicated in Vesicle Targeting and Fusion*. *Nature*, 1993. **362**(6418): p. 318-324.
59. Blasi, J., et al., *Botulinum Neurotoxin-C1 Blocks Neurotransmitter Release by Means of Cleaving Hpc-1/Syntaxin*. *Embo Journal*, 1993. **12**(12): p. 4821-4828.
60. Schiavo, G., et al., *Tetanus and Botulinum-B Neurotoxins Block Neurotransmitter Release by Proteolytic Cleavage of Synaptobrevin*. *Nature*, 1992. **359**(6398): p. 832-835.
61. Sollner, T., et al., *A Protein Assembly-Disassembly Pathway in-Vitro That May Correspond to Sequential Steps of Synaptic Vesicle Docking, Activation, and Fusion*. *Cell*, 1993. **75**(3): p. 409-418.
62. Broadie, K., et al., *Syntaxin and Synaptobrevin Function Downstream of Vesicle Docking in Drosophila*. *Neuron*, 1995. **15**(3): p. 663-673.
63. Hunt, J.M., et al., *Post-Docking Role for Synaptobrevin in Synaptic Vesicle Fusion*. *Neuron*, 1994. **12**(6): p. 1269-1279.
64. Mayer, A., W. Wickner, and A. Haas, *Sec18p (NSF)-driven release of sec17p (alpha-SNAP) can precede docking and fusion of yeast vacuoles*. *Cell*, 1996. **85**(1): p. 83-94.
65. Hanson, P.I., et al., *Structure and conformational changes in NSF and its membrane receptor complexes visualized by quick-freeze/deep-etch electron microscopy*. *Cell*, 1997. **90**(3): p. 523-535.

66. Otto, H., P.I. Hanson, and R. Jahn, *Assembly and disassembly of a ternary complex of synaptobrevin, syntaxin, and SNAP-25 in the membrane of synaptic vesicles*. Proceedings of the National Academy of Sciences of the United States of America, 1997. **94**(12): p. 6197-6201.
67. Fasshauer, D., et al., *Structural changes are associated with soluble N-ethylmaleimide-sensitive fusion protein attachment protein receptor complex formation*. Journal of Biological Chemistry, 1997. **272**(44): p. 28036-28041.
68. Hanson, P.I., J.E. Heuser, and R. Jahn, *Neurotransmitter release - four years of SNARE complexes*. Current Opinion in Neurobiology, 1997. **7**(3): p. 310-315.
69. Gonzalez, L.C., W.I. Weis, and R.H. Scheller, *A novel SNARE N-terminal domain revealed by the crystal structure of Sec22b*. Journal of Biological Chemistry, 2001. **276**(26): p. 24203-24211.
70. Yamaguchi, T., et al., *Sly1 binds to Golgi and ER syntaxins via a conserved N-terminal peptide motif*. Developmental Cell, 2002. **2**(3): p. 295-305.
71. Burri, L. and T. Lithgow, *A complete set of SNAREs in yeast*. Traffic, 2004. **5**(1): p. 45-52.
72. Burkhardt, P., et al., *Munc18a controls SNARE assembly through its interaction with the syntaxin N-peptide*. Embo Journal, 2008. **27**(7): p. 923-933.
73. Hayashi, T., et al., *Synaptic Vesicle Membrane-Fusion Complex - Action of Clostridial Neurotoxins on Assembly*. Embo Journal, 1994. **13**(21): p. 5051-5061.
74. Fasshauer, D., et al., *Identification of a minimal core of the synaptic SNARE complex sufficient for reversible assembly and disassembly*. Biochemistry, 1998. **37**(29): p. 10354-10362.
75. Stein, A., et al., *Helical extension of the neuronal SNARE complex into the membrane*. Nature, 2009. **460**(7254): p. 525-U105.
76. Sutton, R.B., et al., *Crystal structure of a SNARE complex involved in synaptic exocytosis at 2.4 angstrom resolution*. Nature, 1998. **395**(6700): p. 347-353.
77. Ossig, R., et al., *The Yeast Sly Gene-Products, Suppressors of Defects in the Essential Gtp-Binding Ypt1 Protein, May Act in Endoplasmic Reticulum-to-Golgi Transport*. Molecular and Cellular Biology, 1991. **11**(6): p. 2980-2993.
78. Zwilling, D., et al., *Early endosomal SNAREs form a structurally conserved SNARE complex and fuse liposomes with multiple topologies*. Embo Journal, 2007. **26**(1): p. 9-18.
79. Antonin, W., et al., *Crystal structure of the endosomal SNARE complex reveals common structural principles of all SNAREs*. Nature Structural Biology, 2002. **9**(2): p. 107-111.
80. Bock, J.B., et al., *A genomic perspective on membrane compartment organization*. Nature, 2001. **409**(6822): p. 839-841.
81. Fasshauer, D., et al., *Conserved structural features of the synaptic fusion complex: SNARE proteins reclassified as Q- and R-SNAREs*. Proc Natl Acad Sci U S A, 1998. **95**(26): p. 15781-6.

82. Ossig, R., et al., *Exocytosis requires asymmetry in the central layer of the SNARE complex*. *Embo Journal*, 2000. **19**(22): p. 6000-6010.
83. Graf, C.T., et al., *Identification of functionally interacting SNAREs by using complementary substitutions in the conserved 'O' layer*. *Molecular Biology of the Cell*, 2005. **16**(5): p. 2263-2274.
84. Yang, B., et al., *SNARE interactions are not selective - Implications for membrane fusion specificity*. *Journal of Biological Chemistry*, 1999. **274**(9): p. 5649-5653.
85. Fasshauer, D., et al., *Mixed and non-cognate SNARE complexes - Characterization of assembly and biophysical properties*. *Journal of Biological Chemistry*, 1999. **274**(22): p. 15440-15446.
86. Fasshauer, D., et al., *SNARE assembly and disassembly exhibit a pronounced hysteresis*. *Nature Structural Biology*, 2002. **9**(2): p. 144-151.
87. Hohl, T.M., et al., *Arrangement of subunits in 20 S particles consisting of NSF, SNAPs, and SNARE complexes*. *Molecular Cell*, 1998. **2**(5): p. 539-548.
88. Mima, J., et al., *Reconstituted membrane fusion requires regulatory lipids, SNAREs and synergistic SNARE chaperones*. *Embo Journal*, 2008. **27**(15): p. 2031-2042.
89. Sieber, J.J., et al., *Anatomy and dynamics of a supramolecular membrane protein cluster*. *Science*, 2007. **317**(5841): p. 1072-1076.
90. Lang, T., et al., *SNAREs are concentrated in cholesterol-dependent clusters that define docking and fusion sites for exocytosis*. *Embo Journal*, 2001. **20**(9): p. 2202-2213.
91. Lang, T., et al., *SNAREs in native plasma membranes are active and readily form core complexes with endogenous and exogenous SNAREs*. *Journal of Cell Biology*, 2002. **158**(4): p. 751-760.
92. Edelmann, L., et al., *Synaptobrevin Binding to Synaptophysin - a Potential Mechanism for Controlling the Exocytotic Fusion Machine*. *Embo Journal*, 1995. **14**(2): p. 224-231.
93. Kweon, D.H., C.S. Kim, and Y.K. Shin, *Regulation of neuronal SNARE assembly by the membrane*. *Nature Structural Biology*, 2003. **10**(6): p. 440-447.
94. Siddiqui, T.J., et al., *Determinants of synaptobrevin regulation in membranes*. *Molecular Biology of the Cell*, 2007. **18**(6): p. 2037-2046.
95. Nicholson, K.L., et al., *Regulation of SNARE complex assembly by an N-terminal domain of the t-SNARE Sso1p*. *Nature Structural Biology*, 1998. **5**(9): p. 793-802.
96. Munson, M., et al., *Interactions within the yeast t-SNARE Sso1p that control SNARE complex assembly*. *Nature Structural Biology*, 2000. **7**(10): p. 894-902.
97. Margittai, M., et al., *Single-molecule fluorescence resonance energy transfer reveals a dynamic equilibrium between closed and open conformations of syntaxin 1*. *Proceedings of the National Academy of Sciences of the United States of America*, 2003. **100**(26): p. 15516-15521.

98. Verhage, M., et al., *Synaptic assembly of the brain in the absence of neurotransmitter secretion*. *Science*, 2000. **287**(5454): p. 864-869.
99. Toonen, R.F.G. and M. Verhage, *Munc18=1 in secretion: lonely Munc joins SNARE team and takes control*. *Trends in Neurosciences*, 2007. **30**(11): p. 564-572.
100. Misura, K.M.S., R.H. Scheller, and W.I. Weis, *Three-dimensional structure of the neuronal-Sec1-syntaxin 1a complex*. *Nature*, 2000. **404**(6776): p. 355-362.
101. Gulyas-Kovacs, A., et al., *Munc18-1: Sequential interactions with the fusion machinery stimulate vesicle docking and priming*. *Journal of Neuroscience*, 2007. **27**(32): p. 8676-8686.
102. Deak, F., et al., *Munc18-1 binding to the neuronal SNARE complex controls synaptic vesicle priming*. *Journal of Cell Biology*, 2009. **184**(5): p. 751-764.
103. Pobbati, A.V., A. Stein, and D. Fasshauer, *N- to C-terminal SNARE complex assembly promotes rapid membrane fusion*. *Science*, 2006. **313**(5787): p. 673-676.
104. Fasshauer, D. and M. Margittai, *A transient N-terminal interaction of SNAP-25 and syntaxin nucleates SNARE assembly*. *Journal of Biological Chemistry*, 2004. **279**(9): p. 7613-7621.
105. Parlati, F., et al., *Topological restriction of SNARE-dependent membrane fusion*. *Nature*, 2000. **407**(6801): p. 194-198.
106. Fiebig, K.M., et al., *Folding intermediates of SNARE complex assembly*. *Nature Structural Biology*, 1999. **6**(2): p. 117-123.
107. Fasshauer, D., *Structural insights into the SNARE mechanism*. *Biochimica Et Biophysica Acta-Molecular Cell Research*, 2003. **1641**(2-3): p. 87-97.
108. Margittai, M., et al., *Homo- and heterooligomeric SNARE complexes studied by site-directed spin labeling*. *Journal of Biological Chemistry*, 2001. **276**(16): p. 13169-13177.
109. Weninger, K., et al., *Accessory proteins stabilize the acceptor complex for synaptobrevin, the 1 : 1 syntaxin/SNAP-25 complex*. *Structure*, 2008. **16**(2): p. 308-320.
110. Xiao, W.Z., et al., *The neuronal t-SNARE complex is a parallel four-helix bundle*. *Nature Structural Biology*, 2001. **8**(4): p. 308-311.
111. Misura, K.M.S., R.H. Scheller, and W.I. Weis, *Self-association of the H3 region of syntaxin 1A - Implications for intermediates in snare complex assembly*. *Journal of Biological Chemistry*, 2001. **276**(16): p. 13273-13282.
112. Hua, S.Y. and M.P. Charlton, *Activity-dependent changes in partial VAMP complexes during neurotransmitter release*. *Nature Neuroscience*, 1999. **2**(12): p. 1078-1083.
113. Stevens, C.F. and T. Tsujimoto, *Estimates for the Pool Size of Releasable Quanta at a Single Central Synapse and for the Time Required to Refill the Pool*. *Proceedings of the National Academy of Sciences of the United States of America*, 1995. **92**(3): p. 846-849.
114. Xu, T., et al., *Inhibition of SNARE complex assembly differentially affects kinetic components of exocytosis*. *Cell*, 1999. **99**(7): p. 713-722.

115. Xu, T., et al., *Multiple kinetic components of exocytosis distinguished by neurotoxin sensitivity*. *Nature Neuroscience*, 1998. **1**(3): p. 192-200.
116. Sorensen, J.B., *Conflicting Views on the Membrane Fusion Machinery and the Fusion Pore*. *Annual Review of Cell and Developmental Biology*, 2009. **25**: p. 513-537.
117. Sorensen, J.B., et al., *Sequential N- to C-terminal SNARE complex assembly drives priming and fusion of secretory vesicles*. *Embo Journal*, 2006. **25**(5): p. 955-966.
118. Sudhof, T.C. and J.E. Rothman, *Membrane Fusion: Grappling with SNARE and SM Proteins*. *Science*, 2009. **323**(5913): p. 474-477.
119. Brose, N., et al., *Synaptotagmin - a Calcium Sensor on the Synaptic Vesicle Surface*. *Science*, 1992. **256**(5059): p. 1021-1025.
120. Fernandez-Chacon, R., et al., *Synaptotagmin I functions as a calcium regulator of release probability*. *Nature*, 2001. **410**(6824): p. 41-49.
121. Sorensen, J.B., et al., *The SNARE protein SNAP-25 is linked to fast calcium triggering of exocytosis*. *Proceedings of the National Academy of Sciences of the United States of America*, 2002. **99**(3): p. 1627-1632.
122. Gerona, R.R.L., et al., *The C terminus of SNAP25 is essential for Ca²⁺-dependent binding of synaptotagmin to SNARE complexes*. *Journal of Biological Chemistry*, 2000. **275**(9): p. 6328-6336.
123. Broadie, K., et al., *Absence of Synaptotagmin Disrupts Excitation-Secretion Coupling during Synaptic Transmission*. *Proceedings of the National Academy of Sciences of the United States of America*, 1994. **91**(22): p. 10727-10731.
124. Littleton, J.T., et al., *Mutational Analysis of Drosophila Synaptotagmin Demonstrates Its Essential Role in Ca²⁺-Activated Neurotransmitter Release*. *Cell*, 1993. **74**(6): p. 1125-1134.
125. Chen, X.C., et al., *Three-dimensional structure of the complexin/SNARE complex*. *Neuron*, 2002. **33**(3): p. 397-409.
126. Reim, K., et al., *Complexins regulate a late step in Ca²⁺-dependent neurotransmitter release*. *Cell*, 2001. **104**(1): p. 71-81.
127. Cai, H.J., et al., *Complexin II plays a positive role in Ca²⁺-triggered exocytosis by facilitating vesicle priming*. *Proceedings of the National Academy of Sciences of the United States of America*, 2008. **105**(49): p. 19538-19543.
128. Brose, N., *For better or for worse: Complexins regulate SNARE function and vesicle fusion*. *Traffic*, 2008. **9**(9): p. 1403-1413.
129. Huntwork, S. and J.T. Littleton, *A complexin fusion clamp regulates spontaneous neurotransmitter release and synaptic growth*. *Nature Neuroscience*, 2007. **10**(10): p. 1235-1237.
130. Schaub, J.R., et al., *Hemifusion arrest by complexin is relieved by Ca²⁺-synaptotagmin I*. *Nature Structural & Molecular Biology*, 2006. **13**(8): p. 748-750.
131. Giraudo, C.G., et al., *A clamping mechanism involved in SNARE-dependent exocytosis*. *Science*, 2006. **313**(5787): p. 676-680.

132. Giraudo, C.G., et al., *Distinct domains of complexins bind SNARE complexes and clamp fusion in vitro*. *Journal of Biological Chemistry*, 2008. **283**(30): p. 21211-21219.
133. Giraudo, C.G., et al., *Alternative Zippering as an On-Off Switch for SNARE-Mediated Fusion*. *Science*, 2009. **323**(5913): p. 512-516.
134. Maximov, A., et al., *Complexin Controls the Force Transfer from SNARE Complexes to Membranes in Fusion*. *Science*, 2009. **323**(5913): p. 516-521.
135. Tang, J., et al., *A complexin/syntaxin 1 switch controls fast synaptic vesicle exocytosis*. *Cell*, 2006. **126**(6): p. 1175-1187.
136. Bullough, P.A., et al., *Structure of Influenza Hemagglutinin at the Ph of Membrane-Fusion*. *Nature*, 1994. **371**(6492): p. 37-43.
137. Melikyan, G.B., et al., *A point mutation in the transmembrane domain of the hemagglutinin of influenza virus stabilizes a hemifusion intermediate that can transit to fusion*. *Molecular Biology of the Cell*, 2000. **11**(11): p. 3765-3775.
138. Razinkov, V.I., et al., *Effects of spontaneous bilayer curvature on influenza virus-mediated fusion pores*. *Journal of General Physiology*, 1998. **112**(4): p. 409-422.
139. Lee, J. and B.R. Lentz, *Secretory and viral fusion may share mechanistic events with fusion between curved lipid bilayers*. *Proceedings of the National Academy of Sciences of the United States of America*, 1998. **95**(16): p. 9274-9279.
140. Zampighi, G.A., et al., *Conical electron tomography of a chemical synapse: Vesicles docked to the active zone are hemi-fused*. *Biophysical Journal*, 2006. **91**(8): p. 2910-2918.
141. Lu, X.B., et al., *Membrane fusion induced by neuronal SNAREs transits through hemifusion*. *Journal of Biological Chemistry*, 2005. **280**(34): p. 30538-30541.
142. Yoon, T.Y., et al., *Multiple intermediates in SNARE-induced membrane fusion*. *Proceedings of the National Academy of Sciences of the United States of America*, 2006. **103**(52): p. 19731-19736.
143. Giraudo, C.G., et al., *SNAREs can promote complete fusion and hemifusion as alternative outcomes*. *Journal of Cell Biology*, 2005. **170**(2): p. 249-260.
144. Melia, T.J., et al., *Lipidic antagonists to SNARE-mediated fusion*. *Journal of Biological Chemistry*, 2006. **281**(40): p. 29597-29605.
145. Chen, X.C., et al., *SNARE-mediated lipid mixing depends on the physical state of the vesicles*. *Biophysical Journal*, 2006. **90**(6): p. 2062-2074.
146. Engel, A. and P. Walter, *Membrane lysis during biological membrane fusion: collateral damage by misregulated fusion machines*. *Journal of Cell Biology*, 2008. **183**(2): p. 181-186.
147. Nickel, W., et al., *Content mixing and membrane integrity during membrane fusion driven by pairing of isolated v-SNAREs and t-SNAREs*. *Proceedings of the National Academy of Sciences of the United States of America*, 1999. **96**(22): p. 12571-12576.
148. Parlati, F., et al., *Rapid and efficient fusion of phospholipid vesicles by the alpha-helical core of a SNARE complex in the absence of an N-terminal*

- regulatory domain*. Proceedings of the National Academy of Sciences of the United States of America, 1999. **96**(22): p. 12565-12570.
149. McNew, J.A., et al., *The length of the flexible SNAREpin juxtamembrane region is a critical determinant of SNARE-dependent fusion*. Molecular Cell, 1999. **4**(3): p. 415-421.
 150. McNew, J.A., et al., *Close is not enough: SNARE-dependent membrane fusion requires an active mechanism that transduces force to membrane anchors*. Journal of Cell Biology, 2000. **150**(1): p. 105-117.
 151. Schuette, C.G., et al., *Determinants of liposome fusion mediated by synaptic SNARE proteins*. Proceedings of the National Academy of Sciences of the United States of America, 2004. **101**(9): p. 2858-2863.
 152. Hu, K., et al., *Vesicular restriction of synaptobrevin suggests a role for calcium in membrane fusion*. Nature, 2002. **415**(6872): p. 646-650.
 153. Holt, M., et al., *Synaptic vesicles are constitutively active fusion machines that function independently of Ca²⁺*. Current Biology, 2008. **18**(10): p. 715-722.
 154. Dennison, S.M., et al., *Neuronal SNAREs do not trigger fusion between synthetic membranes but do promote PEG-mediated membrane fusion*. Biophysical Journal, 2006. **90**(5): p. 1661-1675.
 155. Chicka, M.C., et al., *Synaptotagmin arrests the SNARE complex before triggering fast, efficient membrane fusion in response to Ca²⁺*. Nature Structural & Molecular Biology, 2008. **15**(8): p. 827-835.
 156. Bhalla, A., et al., *Ca²⁺-synaptotagmin directly regulates t-SNARE function during reconstituted membrane fusion*. Nature Structural & Molecular Biology, 2006. **13**(4): p. 323-330.
 157. Xue, M.S., et al., *The Janus-faced nature of the C2B domain is fundamental for synaptotagmin-1 function*. Nature Structural & Molecular Biology, 2008. **15**(11): p. 1160-1168.
 158. Tareste, D., et al., *SNAREpin/Munc18 promotes adhesion and fusion of large vesicles to giant membranes*. Proceedings of the National Academy of Sciences of the United States of America, 2008. **105**(7): p. 2380-2385.
 159. Shen, J.S., et al., *SNARE bundle and syntaxin N-peptide constitute a minimal complement for Munc18-1 activation of membrane fusion*. Journal of Cell Biology, 2010. **190**(1): p. 55-63.
 160. Martens, S., M.M. Kozlov, and H.T. McMahon, *How synaptotagmin promotes membrane fusion*. Science, 2007. **316**(5828): p. 1205-1208.
 161. Hui, E.F., et al., *Synaptotagmin-Mediated Bending of the Target Membrane Is a Critical Step in Ca²⁺-Regulated Fusion*. Cell, 2009. **138**(4): p. 709-721.
 162. Stein, A., et al., *Synaptotagmin activates membrane fusion through a Ca²⁺-dependent trans interaction with phospholipids*. Nature Structural & Molecular Biology, 2007. **14**: p. 904-911.
 163. Chicka, M.C. and E.R. Chapman, *Concurrent Binding of Complexin and Synaptotagmin to Liposome-Embedded SNARE Complexes*. Biochemistry, 2009. **48**(4): p. 657-659.
 164. Stroupe, C., et al., *Minimal membrane docking requirements revealed by reconstitution of Rab GTPase-dependent membrane fusion from purified*

- components. Proceedings of the National Academy of Sciences of the United States of America, 2009. **106**(42): p. 17626-17633.
165. Domanska, M.K., V. Kiessling, and L.K. Tamm, *Docking and Fast Fusion of Synaptobrevin Vesicles Depends on the Lipid Compositions of the Vesicle and the Acceptor SNARE Complex-Containing Target Membrane*. Biophysical Journal, 2010. **99**(9): p. 2936-2946.
 166. Ji, H., et al., *Protein Determinants of SNARE-Mediated Lipid Mixing*. Biophysical Journal, 2010. **99**(2): p. 553-560.
 167. Stein, A., *Untersuchungen zur Rekonstitution der SNARE-vermittelten Membranfusion*, in *Fachbereich Biologie, Chemie und Pharmazie 2007*, Freien Universität Berlin: Berlin.
 168. Bradford, M.M., *Rapid and Sensitive Method for Quantitation of Microgram Quantities of Protein Utilizing Principle of Protein-Dye Binding*. Analytical Biochemistry, 1976. **72**(1-2): p. 248-254.
 169. Duzgunes, N., *Preparation and quantitation of small unilamellar liposomes and large unilamellar reverse-phase evaporation liposomes*, in *Liposomes, Pt A2003*, Academic Press Inc: San Diego. p. 23-27.
 170. Rigaud, J.L. and D. Levy, *Reconstitution of membrane proteins into liposomes*. Liposomes, Pt B, 2003. **372**: p. 65-86.
 171. Rouser, G., Fleische, S, and A. Yamamoto, *2 Dimensional Thin Layer Chromatographic Separation of Polar Lipids and Determination of Phospholipids by Phosphorus Analysis of Spots*. Lipids, 1970. **5**(5): p. 494-&.
 172. Gibson, G.A. and L.M. Loew, *Phospholipid Vesicle Fusion Monitored by Fluorescence Energy-Transfer*. Biochemical and Biophysical Research Communications, 1979. **88**(1): p. 135-140.
 173. Hoekstra, D., N. Duzgunes, and D. Nejat, *Lipid mixing assays to determine fusion in liposome systems*, in *Methods in Enzymology 1993*, Academic Press. p. 15-32.
 174. Lakowicz, J.R., *Principles of fluorescence spectroscopy*. 2nd ed 1999, New York ; London: Kluwer Academic/Plenum. xxiii, 698 p.
 175. Cypionka, A., et al., *Discrimination between docking and fusion of liposomes reconstituted with neuronal SNARE-proteins using FCS*. Proc Natl Acad Sci U S A, 2009. **106**(44): p. 18575-80.
 176. Giddings, J.C., *Field-Flow Fractionation - Analysis of Macromolecular, Colloidal, and Particulate Materials*. Science, 1993. **260**(5113): p. 1456-1465.
 177. Wyatt, P.J., *Light-Scattering and the Absolute Characterization of Macromolecules*. Analytica Chimica Acta, 1993. **272**(1): p. 1-40.
 178. Korgel, B.A., J.H. van Zanten, and H.G. Monbouquette, *Vesicle size distributions measured by flow field-flow fractionation coupled with multiangle light scattering*. Biophysical Journal, 1998. **74**(6): p. 3264-3272.
 179. Schagger, H., *Tricine-SDS-PAGE*. Nat. Protocols, 2006. **1**(1): p. 16-22.
 180. Towbin, H., T. Staehelin, and J. Gordon, *Electrophoretic Transfer of Proteins from Polyacrylamide Gels to Nitrocellulose Sheets - Procedure and Some Applications*. Proceedings of the National Academy of Sciences of the United States of America, 1979. **76**(9): p. 4350-4354.

181. Rigaud, J.L., B. Pitard, and D. Levy, *Reconstitution of Membrane-Proteins into Liposomes - Application to Energy-Transducing Membrane-Proteins*. *Biochimica Et Biophysica Acta-Bioenergetics*, 1995. **1231**(3): p. 223-246.
182. Levy, D., et al., *Reconstitution of the Sarcoplasmic-Reticulum Ca²⁺-Atpase - Mechanisms of Membrane-Protein Insertion into Liposomes During Reconstitution Procedures Involving the Use of Detergents*. *Biochimica Et Biophysica Acta*, 1992. **1107**(2): p. 283-298.
183. Lichtenberg, D., R.J. Robson, and E.A. Dennis, *Solubilization of Phospholipids by Detergents - Structural and Kinetic Aspects*. *Biochimica Et Biophysica Acta*, 1983. **737**(2): p. 285-304.
184. Lopez, O., et al., *Octyl glucoside-mediated solubilization and reconstitution of liposomes: Structural and kinetic aspects*. *Journal of Physical Chemistry B*, 2001. **105**(40): p. 9879-9886.
185. McIntyre, J.C. and R.G. Sleight, *Fluorescence Assay for Phospholipid Membrane Asymmetry*. *Biochemistry*, 1991. **30**(51): p. 11819-11827.
186. Meers, P., et al., *Novel inner monolayer fusion assays reveal differential monolayer mixing associated with cation-dependent membrane fusion*. *Biochimica Et Biophysica Acta-Biomembranes*, 2000. **1467**(1): p. 227-243.
187. Steverding, D., et al., *Influence of Surface-Charge on the Incorporation and Orientation of Cytochrome-C Oxidase in Liposomes*. *Febs Letters*, 1989. **257**(1): p. 131-133.
188. van den Bogaart, G., et al., *One SNARE complex is sufficient for membrane fusion*. *Nature Structural & Molecular Biology*, 2010. **17**(3): p. 358-U129.
189. Tucker, W.C., T. Weber, and E.R. Chapman, *Reconstitution of Ca²⁺-regulated membrane fusion by synaptotagmin and SNAREs*. *Science*, 2004. **304**(5669): p. 435-438.
190. Domanska, M.K., et al., *Single Vesicle Millisecond Fusion Kinetics Reveals Number of SNARE Complexes Optimal for Fast SNARE-mediated Membrane Fusion*. *Journal of Biological Chemistry*, 2009. **284**(46): p. 32158-32166.
191. Wiederhold, K. and D. Fasshauer, *Is Assembly of the SNARE Complex Enough to Fuel Membrane Fusion?* *Journal of Biological Chemistry*, 2009. **284**(19): p. 13143-13152.
192. Xu, Y.B., et al., *Hemifusion in SNARE-mediated membrane fusion*. *Nature Structural & Molecular Biology*, 2005. **12**(5): p. 417-422.
193. Stevens, M.J., J.H. Hoh, and T.B. Woolf, *Insights into the molecular mechanism of membrane fusion from simulation: Evidence for the association of splayed tails*. *Physical Review Letters*, 2003. **91**(18).

Summary

A novel and well-characterized model system has been developed and used in order to extract mechanistic insights on the SNARE-mediated fusion process. The reconstitution of SNAREs onto large liposomes mediated by *n*-octyl- β -D-glucoside (OG) was characterized according to size, protein orientation and insertion efficiency. This resulted in SNARE-liposomes with good reconstitution properties that were in the 100 nm range. To induce relatively fast lipid-mixing and observe substantial size increments, it was found essential to stabilize a 1:1 syntaxin·SNAP-25 acceptor complex with a C-terminal synaptobrevin fragment (denoted Δ N syb), which provided a fast nucleation site for trans SNARE complex formation.

The kinetics of lipid-mixing was found to be governed by the displacement of Δ N syb from the syntaxin·SNAP-25 acceptor complex, which gave rise to a transient but long-lived docking state which could be kinetically resolved from fusion. The ability for Δ N syb to delay and slow-down N to C-terminal nucleation, or zippering, was exploited to capture and arrest putative fusion intermediates. This led to the ultrastructural identification of hemifused liposomes exhibiting extended diaphragms and also to a docked intermediate that consisted of a tight bilayer-bilayer contact interaction. Using a bulk assay to discriminate inner leaflet-lipid mixing from outer leaflet lipid-mixing it was possible to conclude that hemifusion in this system constitutes an alternative end-state to fusion.

The bilayer-bilayer contact state could be arrested by introducing a deletion mutation on synaptobrevin (Δ 84) which interrupted the +8 layer of the SNARE complex, suggesting that a SNARE complex requires efficient mechanical transduction from the SNARE complex to the transmembrane domains in order to mediate fusion. Furthermore, the mutant could not mediate hemifusion, suggesting hemifusion side tracked from fusion at a step posterior to bilayer-bilayer contact. However, Δ 84 synaptobrevin was found to mediate fusion between two small

liposomes, revealing that curvature stress does play a role in SNARE-mediated fusion and was interpreted as being consistent with the stalk mechanism of membrane fusion.

Based on these findings and on the ability to slow down and arrest putative fusion intermediates, a SNARE-mediated fusion reaction pathway was proposed.

Curriculum Vitae

PERSONAL INFORMATION

Name: Javier Matias Hernandez Amezquita

Address: Johannisstrasse 2, 37077 Göttingen, Germany

E-mail: mhernan@gwdg.de

Nationality: Chilean

Date of birth: 10 December, 1983

Place of birth: Antofagasta, Chile

EDUCATION

Max Planck Institute for Biophysical Chemistry 4/2007– present

Department of Neurobiology, Göttingen, Germany

Candidate for Doctor of Philosophy

- Doctoral candidate in final year of research as part of the Göttingen Graduate School for Neurosciences and Molecular Biosciences (GGNB), Georg-August-Universität Göttingen
- Supervisor: Reinhard Jahn
- Research topic: biochemistry of neuronal membrane fusion
- Funded by a fellowship from the National Commission for Scientific and Technological Research, Chile

University of Sydney

3-12/2006

Department of Chemistry, Australia

Master of Science (Chemistry)

- Research topic: polymer chemistry of starch branching
- Supervisor: Robert Gilbert
- Recipient of an Australian Postgraduate Award (APA)

Bachelor of Science (Honours)

3/2002–11/2005

- Majors in Molecular Biotechnology and Chemistry
- Graduated with 1st Class Honours and the University Medal
- Awards: Sydney University International Merit Scholarships 2004 and 2005

Santiago College High School, Santiago, Chile

3/1999–12/2001

International Baccalaureate (IB)

- Bilingual Diploma (English and Spanish)

WORK EXPERIENCE

Scientific conference organizer

Encuentros 2010 Conference, Cambridge

9/2010

Co-organizer & logistics coordinator

- Was part of a 6-member organizing committee overseeing a budget of more than 60,000 £

Encuentros 2009 Conference, Göttingen

2/2009

Principal organizer

- Organizer of a Chilean scientific conference in collaboration with the Max Planck Society focusing on the creation

of an interactive networking platform between Chilean researchers working in Chile with those working overseas

Teaching and Supervision

Supervisor to master and undergraduate students 3/2009-present

- Responsible for supervision of Master student at the Department of Neurobiology, Max Planck Institute
- Mentoring and training of two undergraduate students as part of a lab rotation program

Laboratory demonstrator 4/2005–11/2006

- Teaching of laboratory techniques to first-year undergraduate students at the University of Sydney (10-20 students per class)

Research assistant 11/2003–3/2004

- Summer research internship at the Key Centre for Polymer Colloids; one-month stay at the Institute for Polymer Science at the University of Stellenbosch, South Africa

AWARDS

- Doctoral Fellowship from the Comisión Nacional para **2007**
Investigación Científica y Tecnológica (CONICYT), Chile
- Australian Postgraduate Award **2006**
- Bruce Veness Chandler Scholarship in Chemistry **2006**
- University Medal **2005**
- Faculty of Science International Merit Scholarship **2005**
- Faculty of Science International Merit Scholarship **2004**

CONFERENCE PRESENTATIONS

- Poster presented at the 23rd Symposium of the Protein Society, 25-29 July, 2009, Boston, USA. Award received for best poster
- Speaker, VIII European Symposium of the Protein Society, 14-18 June, 2009, Zurich, Switzerland
- Poster presented at the World Polymer Congress – Macro 2006, 16-21 July, 2006, Rio de Janeiro, Brazil

PUBLICATIONS

- Hernandez JM, et al. Arrest and visualization of fusion intermediates of model membranes. Manuscript currently in preparation.
- Cypionka A, et al. (2009). Discrimination between docking and fusion of liposomes reconstituted with neuronal SNARE-proteins using FCS. PNAS 106(44): 18575-80
- Hernandez JM, et al. (2008). Mechanistic investigation of a starch-branching enzyme using hydrodynamic volume SEC analysis. Biomacromolecules 9(3): 954-965
- Gaborieau M, Gilbert RG, et al. (2007). Theory of multiple-detection size-exclusion chromatography of complex branched polymers. Macromolecular Theory and Simulations 16(1): 13-28
- Hoang NL, et al. (2008). Toward a full characterization of native starch: separation and detection by size-exclusion chromatography. Journal of Chromatography A 1205(1-2): 60-70

